

國立交通大學

電信工程研究所

碩士論文

使用基底擴展模型實現 OFDM 通道估測之研究

Study of Channel Estimation in OFDM

Exploiting Basis-Expansion Model

研究生：張凱翔

指導教授：謝世福 教授

中華民國九十八年八月

使用基底擴展模型實現 OFDM 通道估測之研究

Study of Channel Estimation in OFDM

Exploiting Basis-Expansion Model

研究生：張凱翔

Student：Kai-Hsiang Chang

指導教授：謝世福

Advisor：Shih-Fu Hsieh

國立交通大學

電信工程研究所

碩士論文



Submitted to Institute of Communications Engineering

College of Electrical and Computer Engineering

National Chiao Tung University

in partial Fulfillment of the Requirements

for the Degree of

Master

in

Communications Engineering

August 2009

Hsinchu, Taiwan, Republic of China

中華民國九十八年八月

使用基底擴展模型實現 OFDM 通道估測之研究

學生：張凱翔

指導教授：謝世福

國立交通大學電信工程研究所碩士班



在無線通訊傳輸環境下，為了降低位元錯誤率，通道估測是一項重要的議題。在本篇論文中，我們採用了近年受到廣泛地使用的正交分頻多工(OFDM)系統，利用傑克模型來模擬雙重選擇通道環境，藉由基底擴展模型來實現通道估測的任務。我們將分析常見的基底擴展模型，並推導出理論的估測錯誤率，以及使用維納濾波器來提高已估測通道之訊雜比，可運用在不同的基底擴展模型上。同時也考慮了實際環境中，載波頻率偏移以及相位雜訊的影響，我們提出改善的模型藉此降低其效應。另外，為了降低運算複雜度以及提高收斂速率，我們提出了具有不同調整步伐的最小均方演算法(LMS)以及遞迴最小平方演算法(RLS)，理論分析出最佳的非時變調整步伐，在不同的投影係數上，其調整步伐將會與其基底的重要性呈現正比關係。此外。如果當都普勒頻率在低頻區間改變的情況下，基底也將隨之改變，我們則提出藉由少量的參數記憶以及冪法演算法來模擬追蹤出改變後的基底，可有效節省運算複雜度或記憶空間的使用。

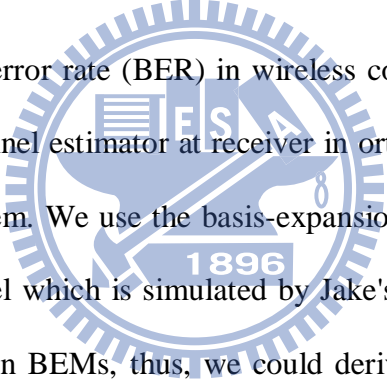
Study of Channel Estimation in OFDM Exploiting Basis-Expansion Model

Student: Kai-Hsiang Chang

Advisor: Dr. Shih-Fu Hsieh

Institute of Communications Engineering
National Chiao Tung University

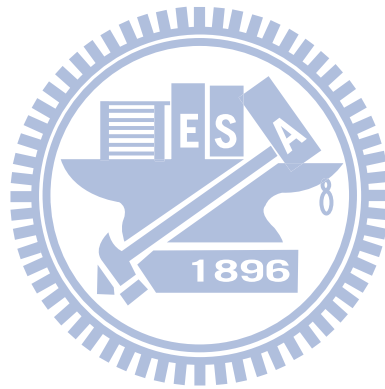
Abstract



For reducing the bit-error rate (BER) in wireless communication systems, it is important to provide a channel estimator at receiver in orthogonal frequency-division multiplexing (OFDM) system. We use the basis-expansion model (BEM) to estimate the doubly-selective channel which is simulated by Jake's model. We would analyze and discuss some often seen BEMs, thus, we could derive the theoretical MSE and apply the Wiener filter to enhance the signal-to-noise ratio (SNR) for estimated channel. The carrier frequency offset (CFO) and phase noise (PHN) issues are also considered in our proposed scheme. Moreover, for reduce complexity, we update the BEM coefficients by different weighting corresponding to the significance of basis, which could be verify by the theoretic derivation. Besides, when Doppler frequency changes, we propose two methods to obtain the new bases, these two schemes use Power method and asymptotic sinusoidal function that need only few parameters and computation than conventional methods.

Acknowledgment

很高興能在這裡完成了碩士班的求學生涯，回顧這兩年來的日子，必須要十分感謝我的指導老師謝教授，不厭其煩的耐心以及深刻巧妙的解說，讓我能在陷入研究的瓶頸當下能當頭棒喝、如獲甘霖、醍醐灌頂，將來對於工作或是追求學問上想必都是相當受用。另外，也要感謝我的家人父母、兄弟姐妹、女友、實驗室的夥伴和學弟妹、大學的好友們以及任何給我幫助的朋友，在這兩年的生活中帶來了歡樂和鼓勵，使我研究更加順利，讓我能在水深火熱後終於完成了學業。



Contents

中文摘要.....	i
English Abstract.....	ii
Acknowledgement.....	iii
Contents.....	iv
List of Tables.....	vii
List of Figures.....	viii
1. Introduction.....	1
2. OFDM System Basics.....	5
2.1 OFDM system description.....	6
2.2 Carrier frequency offset and phase noise.....	7
2.3 Time-invariant channel estimation.....	8
2.3.1 Time domain approach.....	9
2.3.2 Frequency domain approach.....	10
2.4 Time-varying channel model.....	13
2.4.1 Doubly selective channel.....	14
2.4.2 Doppler frequency effect.....	14
2.4.3 Jake's model and channel statistics.....	15
2.4.4 Problems from time-varying channel.....	16
2.4.5 Data detection.....	17
3. Basis Expansion Model for Channel Estimation Schemes.....	19
3.1 Introduction of basis expansion model.....	20

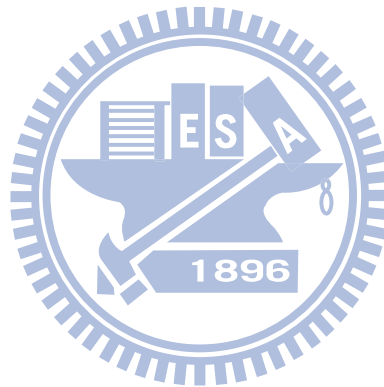
3.2	Complex exponential basis expansion model.....	23
3.2.1	Oversampling approach CE-BEM.....	24
3.2.2	Non-uniform sampling approach CE-BEM.....	25
3.3	SVD basis expansion model.....	26
3.4	Slepian basis expansion model.....	28
3.5	Basis expansion model analysis.....	30
3.5.1	Derivation of the theoretical MSE.....	30
3.5.2	Wiener filter.....	33
3.5.3	Comparison of UB-BEM.....	34
3.5.4	Complexity comparison with the conventional method.....	36
3.6	Consideration of CFO and PHN.....	37
3.6.1	Mixed channel in the presence of PHN.....	37
3.6.2	The CFO estimation scheme.....	38
4.	Adaptive BEM Estimation.....	40
4.1	BEM parameters tracking.....	41
4.1.1	Adaptive algorithms.....	41
4.1.2	Derivation of the theoretical MSE and the optimum time-variant stepsize matrix.....	43
4.1.3	Eigen weighted for adaptive algorithms.....	46
4.2	BEM bases tracking.....	48
4.2.1	Principle eigenvalues adaptive.....	48
4.2.2	Principle eigenvectors adaptive.....	53
5.	Computer Simulations.....	59
5.1	Simulation parameters.....	60
5.2	Time-invariant channel estimation.....	61
5.3	CE-BEM.....	66

5.4 SVD and Slepian BEM.....	67
5.5 Consideration of CFO and PHN.....	70
5.6 EW-RLS with eigen weighting.....	73
5.7 BEM bases tracking.....	85
6. Conclusions.....	90
Bibliography.....	92



List of Tables

3.1 λ for different length of sequence and Doppler frequency.....	30
4.1 The power method algorithm.....	52
4.2 Complexity and memory needed for four methods.....	57
5.1 CFO estimation MSE in different SNR.....	71
5.2 Three fitting methods for principle eigenvalues variation.....	86



List of Figures

1.1 The structure of OFDM system.....	3
2.1 OFDM system block diagram.....	6
2.2 Cyclic prefix schematic.....	7
2.3 OFDM system and PHN/CFO channel model.....	8
2.4 Comb-type pilot arrangement.....	11
2.5 Interpolation example (linear interpolation).....	11
2.6 Block-type pilot arrangement.....	12
2.7 Multipath and mobility.....	13
2.8 Channel vector in different Doppler frequency (10,100,300 Hz).....	15
2.9 Power spectral density of Jake's model.....	16
2.10 Packet transmission schematic.....	18
3.1 BEM for real time-varying channel.....	21
3.2 CE-BEM sampling in Jake's model PSD.....	24
3.3 Non-uniform sampling under Doppler PSD.....	25
3.4 Block diagram representation of the statistical filtering problem.....	34
3.5 (a) Universal power delay profile.....	35
(b) Particular power delay profile.....	35
3.6 The UB flowchart.....	36
3.7 OFDM system in the presence of phase noise.....	37
4.1 Eigenvalues variation under f_d changes in Slepian bases.....	49
4.2 Eigenvalues variation under f_d changes in Jake's bases.....	49
4.4 The principle bases waveform in different Doppler frequency.....	53

4.5 (a) $p_{2,1}$ versus Doppler frequency.....	55
(b) Linear fitting for $p_{2,1}$	55
4.6 $p_{3,2}$ versus Doppler frequency.....	56
4.7 Four methods to obtain the new bases after f_d changes.....	57
5.1 The power delay profile of the multi-path channel.....	61
5.2 Comparison of time and frequency domain channel estimation.....	62
5.3 Comparison of different interpolation methods of comb type.....	63
5.4 Received constellation with (*) and without (o) channel estimation (ZP).....	64
5.5 Comparison of different interpolation methods of comb type.....	64
5.6 Comparison of different pilot ratio in block type.....	65
5.7 Comparison of different CE-based methods.....	66
5.8 ACF of Jake's and Slepian basis ($f_d = 50, T_s = 0.001$).....	68
5.9 Principle basis for Slepian and Jake's model ($f_d = 18, T_s = 0.001$).....	68
5.10 Comparison of SVD-BEM and Wiener filter applied.....	69
5.11 Comparison of SVD and UB.....	69
5.12 The mixed PHN channel estimation performance.....	71
5.13 CFO estimation error in different SNR (a) SNR=10 (b) SNR=20 (dB).....	72
5.14 (a) CE-BEM coefficients changes in successive iteration.....	74
(b) SVD-BEM coefficients changes in successive iteration.....	74
5.15 (a) CE-BEM 1 st -coefficient tracking.....	75
(b) CE-BEM 2 nd -coefficient tracking.....	75
(c) CE-BEM 3 rd -coefficient tracking.....	76
(d) CE-BEM 4 th -coefficient tracking.....	76
(e) CE-BEM 5 th -coefficient tracking.....	77
(f) CE-BEM 6 th -coefficient tracking.....	77

(g) CE-BEM 7 th -coefficient tracking.....	78
(h) CE-BEM 8 th -coefficient tracking.....	78
(i) CE-BEM 9 th -coefficient tracking.....	79
5.16 (a) SVD-BEM 1 st -coefficient tracking.....	79
(b) SVD-BEM 2 nd -coefficient tracking.....	80
(c) SVD-BEM 3 rd -coefficient tracking.....	80
5.17 The weights of each basis in CE-BEM. (B=9)	81
5.18 (a) Learning curve of CE-BEM coefficients tracking.....	81
(b) Learning curve of Slepian-BEM coefficients tracking.....	82
(c) Learning curve of SVD-BEM coefficients tracking.....	82
(d) Comparison of three BEMs with eigen weighting.....	83
5.19 (a) SVD-BEM coefficients tracking in f_d changes with new bases.....	83
(b) SVD-BEM coefficients tracking in f_d changes without new bases.....	84
5.20 Three fitting methods for 1 st -eigenvalue variation in f_d changes.....	85
5.21 Eigenvalue estimated error between exponential and linear methods.....	86
5.22 Bases estimated RMSE under different Power method iteration times (fd=10)..	87
5.23 Bases estimated RMSE by way 3.....	87
5.24 Bases estimated RMSE by way 4.....	88
5.25 Example of basis estimation by the power method. (K=6 $\lambda_{1st}=29.2$ $f_d=13$).....	88
5.26 Example of basis estimation by directly eigenvector fitting. ($f_d=20$).....	89
5.27 Comparison of principle eigenvalues and eigenvectors tracking.....	89

Chapter 1

Introduction

For wireless communication systems, it is important to provide users a better quality and stable transmission. The OFDM system has recently been applied widely in wireless communication systems due to its high data rate transmission capability with high bandwidth efficiency and its robustness to multi-paths delay [20,28,43]. It has been used in wireless LAN standards such as American IEEE802.11a and the European equivalent HIPERLAN/2 [27] and in multimedia wireless services such as Japanese Multimedia Mobile Access Communications. [20]

Among many problems which degrade the performance in OFDM systems, frequency-selective channel is a major issue that leads to bad transmission quality. A channel estimator evaluating the wireless channel can offer an approximated channel for equalizer, and then the effect of the frequency-selective channel can be removed. Carrier frequency offset (CFO) and phase noise (PHN) are two serious problems in channel estimation which can fail to estimate the channel impulse response especially for pilot symbol assisted modulation [9,15,18-20,23-24,29-30,33-34,39,41].

An OFDM system with channel estimator is shown in figure 1.1 where $\hat{\mathbf{h}}$ is used to model the wireless channel \mathbf{h} between transmitter and receiver (users and base-station). Thus the replica transmitted signal $\hat{\mathbf{x}}$ is generated after equalizer, which is the result of the received signal \mathbf{y} divided by the estimated channel vector $\hat{\mathbf{h}}$. Then the original data could be decoded after the demodulator.

The implementation of such a system is not easy as it seems. Due to the performance of the channel estimation scheme will be affected by the time-varying statistics of the Rayleigh channels because of the Doppler effect, therefore, the orthogonality between the sub-carriers of OFDM systems is lost in case of time-varying channels, and thus, the system performance is degraded because of the resulting Inter-Carrier Interference (ICI) phenomenon [30-31].

Among all the estimation schemes to cope with this channel, the basis expansion model (BEM) is popular for their simplicity and robust behavior [32]. There are several often seen BEM methods (e.g. CE, Slepian and SVD-BEM) for time-variant channel estimation. In general, the Doppler spectrum is assumed to adhere to Jakes' model [13]. The Jakes' spectrum is valid for a dense scatterer model in the limit of an infinite number of scatterers around a linear omnidirectional antenna [49]. But this assumption is not fulfilled if a few dominant propagation paths are present only. It was shown by measurements in [17] that wireless channels at 5.3 GHz do not have a Jakes spectrum. Furthermore, the actual velocity of the user and the angles of arrival enter the autocorrelation as parameters and have to be estimated explicitly.

Important issues such as CFO and PHN, and the conventional estimation method for time-invariant channel, compare several interpolation methods based on the frequency domain pilot tones. Finally, we introduce the time-varying channel model which is not easy implemented as before, so we model the channel as the Jake's model [12-13], which the assumption is reasonable and often seen.

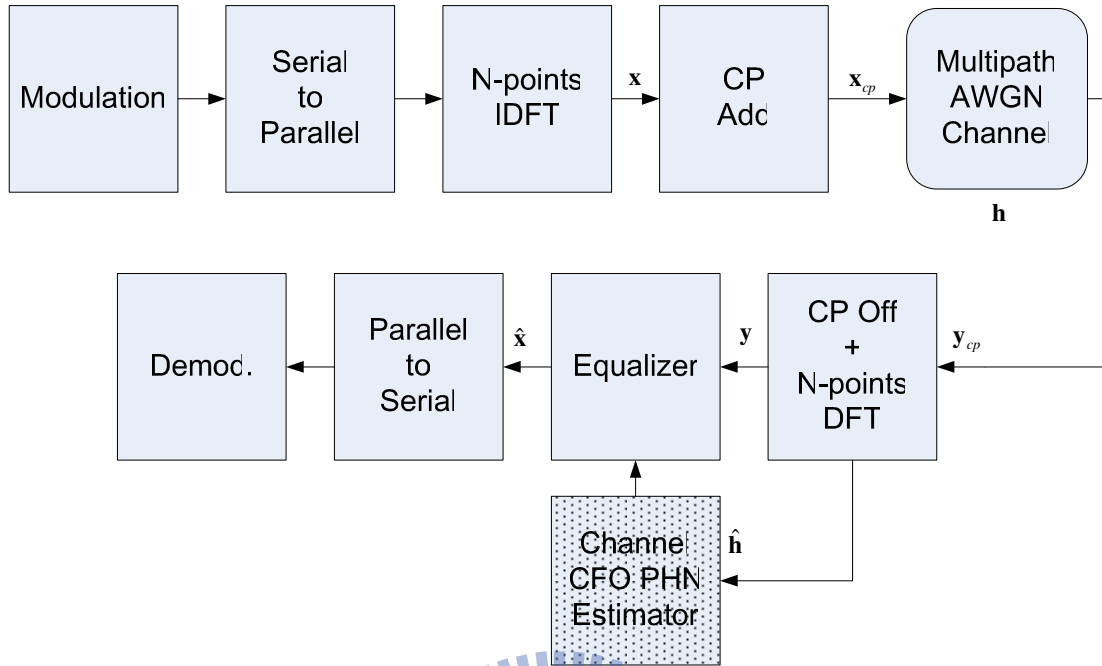


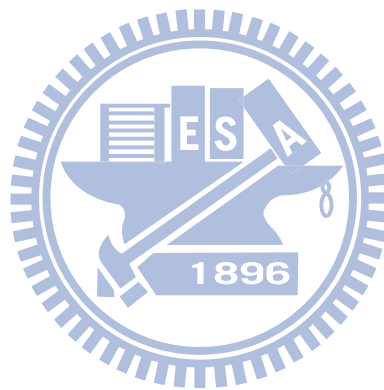
Figure 1.1 The structure of OFDM system

In Chapter 3, several BEM schemes are introduced and analyzed such as CE, Slepian and SVD-BEM. Moreover, we apply the Wiener filter after these BEMs channel estimation to enhance the SNR and improve channel MSE. Certainly, we derive the theoretical mean square error for these BEM methods. Moreover, we consider both CFO and PHN into the OFDM transmission, which are not rare and practical conditions.

In Chapter 4, in order to reduce the complexity, we would like to update the BEM parameters. First, we update the BEM coefficients using least mean squares (LMS) and exponentially-weighted recursive least square (EW-RLS) [33] algorithm, and we consider the significance of each BEM bases, which can improve the convergence rate. For the purpose to ensure the optimum stepsizes are proportional to the bases significance (eigenvalues), we derived the theoretical MSE for LMS and found the time-invariant stepsizes for each basis coefficient. Second, when the Doppler

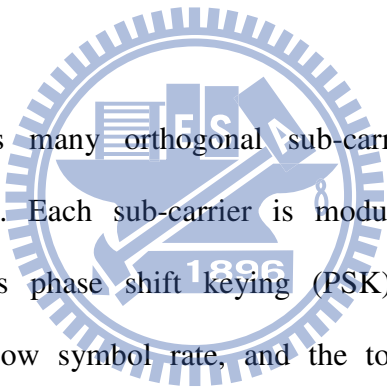
frequency is not always fixed, we propose two ways that can obtain the new bases, which are the asymptotic curve for the new bases directly and the approximated eigenvalues with power method to get new bases.

In Chapter 5, the simulations verify the result of our analysis in the Chapter 2-4 and the comparison between the proposed and other methods, and then the conclusions are in Chapter 6.



Chapter 2

OFDM System Basics



OFDM system exploits many orthogonal sub-carriers to transmit multiple sub-signals simultaneously. Each sub-carrier is modulated with a conventional modulation scheme such as phase shift keying (PSK) or quadrature amplitude modulation (QAM) at a low symbol rate, and the total data rate is similar to conventional single-carrier modulation schemes in the same bandwidth.

The features of OFDM comprises good spectral efficiency, orthogonality between sub-carriers, no inter-carrier guard band, easy implementation by fast Fourier transform, easy design for equalizer and is effective for multi-paths and frequency selective fading channel. Moreover, the key points for OFDM schemes are synchronization, carrier frequency offset, high PAPR (Peak to average power ratio) problem and sensitive to Doppler effect. [29,44-45]

OFDM has developed for wideband digital communication. The applications include digital television and audio broadcasting. [45-46]

2.1 OFDM system description

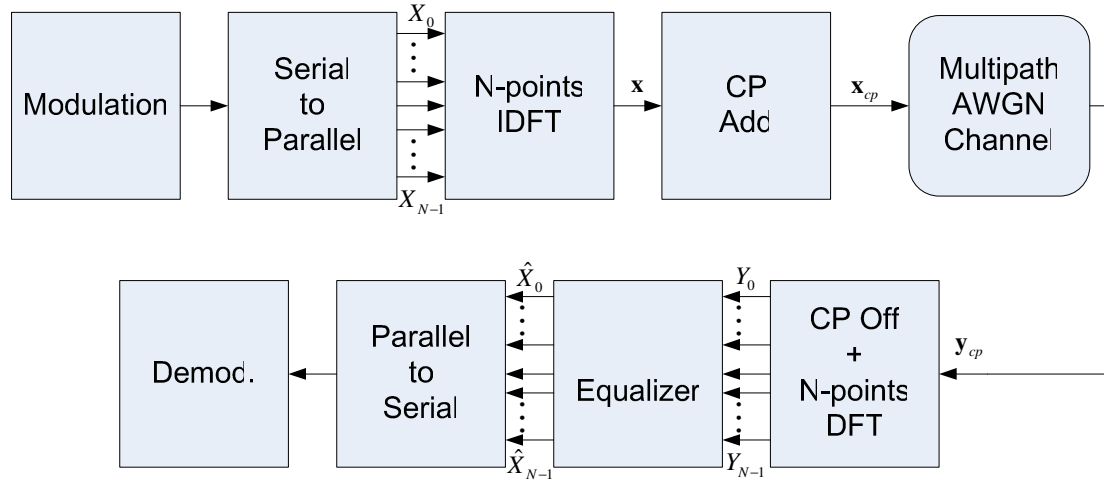


Figure.2.1 OFDM system block diagram

In fig.2.1, after QPSK, M-ary QAM modulation, the modulated data $\mathbf{X} = \{X_0, X_1, \dots, X_{N-1}\}^T$ is transferred into time domain signal vector \mathbf{x} by N-points inverse discrete Fourier transform (IDFT) that is represented as $\mathbf{x} = \mathbf{F}^H \mathbf{X}$, where N denotes the FFT length, and the matrix \mathbf{F} defines a DFT matrix with $\mathbf{F}^H \mathbf{F} = \mathbf{F} \mathbf{F}^H = \mathbf{I}_N$ [20]. Afterwards, the vector $\mathbf{x} = \{x_0, x_1, \dots, x_{N-1}\}^T$ adds the CP (cyclic prefix) which denotes a copy of tail part (Ng) of OFDM signal \mathbf{x} is attached to its front. (Figure 2.2), where Ng should not be less than length of channel impulse L . The CP is used to prevent intercarrier interference (ICI).

The multipath channel is assumed to be time-invariant during a data block transmission and the delay spread is L, in other hand, $h[l] \neq 0$ for $l \in [0, L-1]$. Therefore the effect of multipath ($\mathbf{h} = \{h[0], \dots, h[L-1]\}^T$) is linear convolution with transmitted signal, thanks to the cyclic prefix, the linear convolution can be replaced by circular convolution on account of that we only focus on the useful part of

complete OFDM signal.

The received complete signal:

$$\mathbf{y}_{cp} = \mathbf{x}_{cp} * \mathbf{h},$$

where $\mathbf{y}_{cp} : (N + Ng + L - 1) \times 1$. The received useful part signal (after CP removed):

$$\mathbf{y} = \mathbf{x} \otimes_N \mathbf{h},$$

where \otimes_N denotes N-points circular convolution. The detected symbol after DFT:

$$\mathbf{Y} = DFT(\mathbf{y}) = DFT(\mathbf{x} \otimes_N \mathbf{h}) = \mathbf{X}\mathbf{H},$$

where $\mathbf{H} = DFT(\mathbf{h})$.

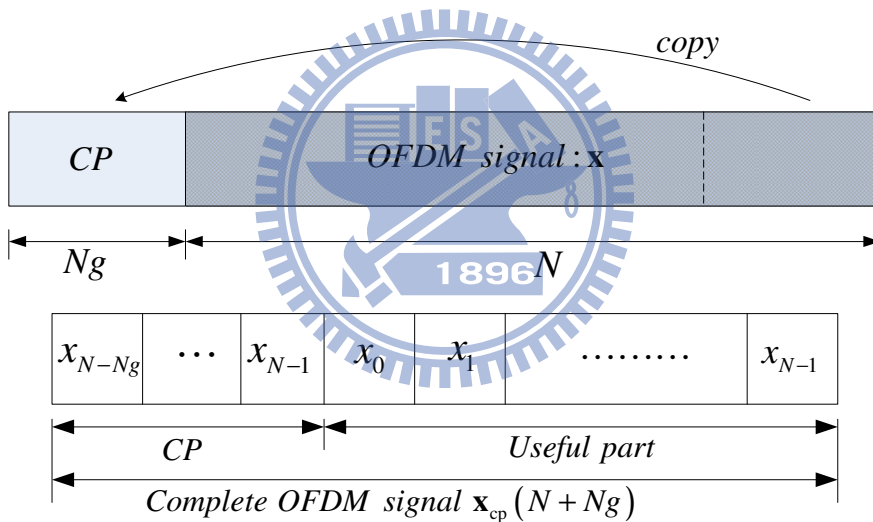


Figure 2.2 Cyclic prefix schematic

2.2 Carrier frequency offset and phase noise

The practical receiver encounters non-negligible phase noise (PHN) and carrier frequency offset (CFO), which result in substantial intercarrier interference that destroy the orthogonality of the system. The Tx/Rx structure and the channel model over a period of one OFDM symbol, taking into account the distortion caused by CFO and PHN, are illustrated in Figure 2.3

After CP is removed, we have the received OFDM symbol in time-domain as

$$\begin{aligned} \mathbf{y} &= e^{j(\frac{2\pi n\epsilon}{N} + \varphi)} (\mathbf{h} \otimes \mathbf{x}) + \boldsymbol{\omega} \\ &= e^{j(\frac{2\pi n\epsilon}{N} + \varphi)} \sum_{l=0}^L h_l[n]x[n-l] + \boldsymbol{\omega}[n] \end{aligned} \quad (2.2.1)$$

where \otimes denotes circular convolution, $\boldsymbol{\omega}$ is the AWGN, and ϵ is the normalized CFO within a packet. $\boldsymbol{\varphi} = [\varphi[0] \varphi[1], \dots, \varphi[N-1]]^T$ is the phase noise sequence which can be modeled as two kinds of processes. First, *Gaussian PHN*, which is zero-mean, stationary, finite-power Gaussian distributed random process [7], *i.e.*, $\boldsymbol{\varphi} \sim N(\mathbf{0}, \boldsymbol{\Phi})$. $\boldsymbol{\Phi}$ is the covariance matrix of $\boldsymbol{\varphi}$ and $\mathbf{0}$ is the zero vector. Second, *Wiener PHN*, and the discrete time equation can be written as $\varphi[n] = \varphi[n-1] + \xi[n]$, where $\xi[n] \sim N(0, 4\pi f_{3dB} T_s)$ is a Gaussian random variable [3].

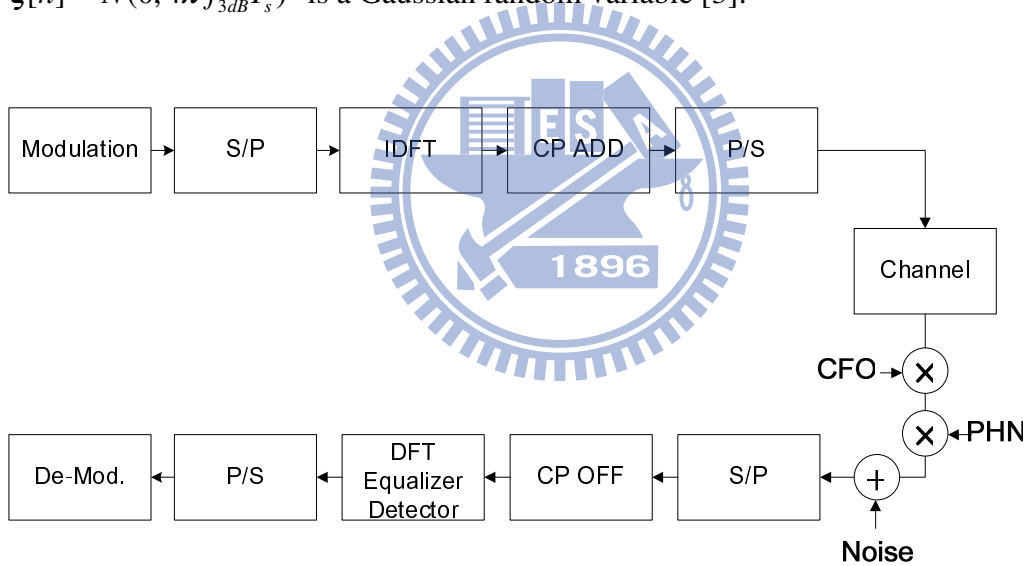


Fig.2.3 OFDM system and PHN/CFO channel model

2.3 Time-invariant channel estimation

A dynamic estimation of channel is necessary before the demodulation of OFDM signals since the radio channel is frequency selective and time-varying for wideband mobile communication systems [21]. In Section 2.3.1 we introduce the time domain approach for time-invariant channel estimation. Then in Section 2.3.2, we introduce

that the channel estimation scheme could be performed in frequency domain by either inserting pilot tones into all of the subcarriers of OFDM symbols with a specific period or inserting pilot tones into each OFDM symbol.

2.3.1 Time domain approach

In time-domain approach for channel estimation, we estimate the time-domain channel impulse response $h[l]$, where $l = 0, 1, \dots, L-1$.

The received signal during N_T training periods in time-domain can be represented as $y_m[n] = h[l] \otimes x[n] + \text{noise}$, where $m = 1, \dots, N_T$, and the matrix form

$$\mathbf{y}_m = \begin{bmatrix} y_m[0] \\ y_m[1] \\ \vdots \\ y_m[N-1] \end{bmatrix} = \mathbf{X}\mathbf{h} + \text{noise} \quad (2.3.1)$$

$\mathbf{h} = [h_0, h_1, \dots, h_{L-1}]^T$, and the circular convolution matrix form for training signal

$$\mathbf{X} = \begin{pmatrix} x[0] & x[N-1] & x[N-2] & \dots & x[N-L+1] \\ x[1] & x[0] & x[N-1] & \dots & \vdots \\ \vdots & x[1] & \vdots & \ddots & \vdots \\ \vdots & \vdots & \vdots & \ddots & \vdots \\ x[N-1] & x[N-2] & x[N-3] & \dots & x[N-L] \end{pmatrix}_{N \times L}$$

In (2.3.1), we can obtain the estimated channel estimation via LS approach

$$\begin{aligned} \hat{\mathbf{h}} &= \mathbf{X}^\dagger \left(\frac{1}{N_T} \sum_{m=1}^{N_T} \mathbf{y}_m \right) = \mathbf{X}^\dagger \left(\frac{1}{N_T} \sum_{m=1}^{N_T} \mathbf{X}\mathbf{h} + \text{noise} \right) \\ &= \mathbf{X}^\dagger \mathbf{X}\mathbf{h} + \text{noise term} \end{aligned} \quad (2.3.2)$$

Then we can obtain frequency response $\hat{\mathbf{H}}$ by applying the discrete Fourier transform of Eq. (2.3.2) with zero padding. Note that the noise effect would be smoothed out by time averaging.

The advantages of time-domain approach is fewer parameters are estimated given a fixed amount of data rather than frequency-domain approach, and leading to more accurate estimates. But there are more computations required for one estimation.

2.3.2 Frequency domain approach

In frequency-domain approach for channel estimation, we estimate $H[k]$, the Fourier transform of channel impulse response, where $k = 0, 1, \dots, N_p - 1$.

The channel estimation based on comb type pilot arrangement (Figure 2.4) is through different algorithms for both estimating channel at pilot frequencies and interpolating the channel. In comb-type pilot based channel estimation, the N_p pilot signals are uniformly inserted into according to the following equation:

$$X[k] = X[mL + l],$$

where L denotes the period of pilot inserting. We define $\{H_p[k], k = 0, 1, \dots, N_p\}$ as the frequency response of the channel at the pilot subcarriers. The estimated channel before interpolation is given by:

$$H_e[k] = \frac{Y_p[k]}{X_p[k]}, \quad k = 0, 1, \dots, N_p - 1,$$

where Y_p and X_p are output and input signal.

The estimation of channel at pilot frequencies is based on least-square (LS) while the channel interpolation is done using linear interpolation, second order interpolation, low-pass interpolation, spline cubic interpolation, and time domain interpolation (Figure 2.5). Time-domain interpolation is obtained by passing to time domain through IDFT, zero padding and going back to frequency domain through DFT. [REF papers]

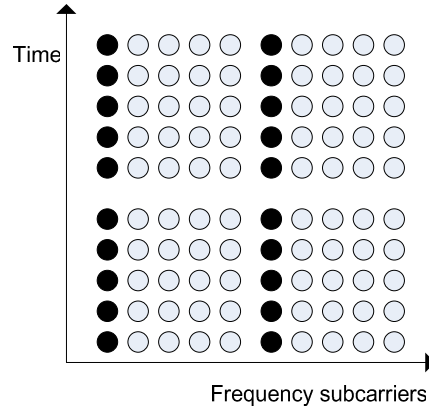


Figure 2.4 Comb-type pilot arrangement

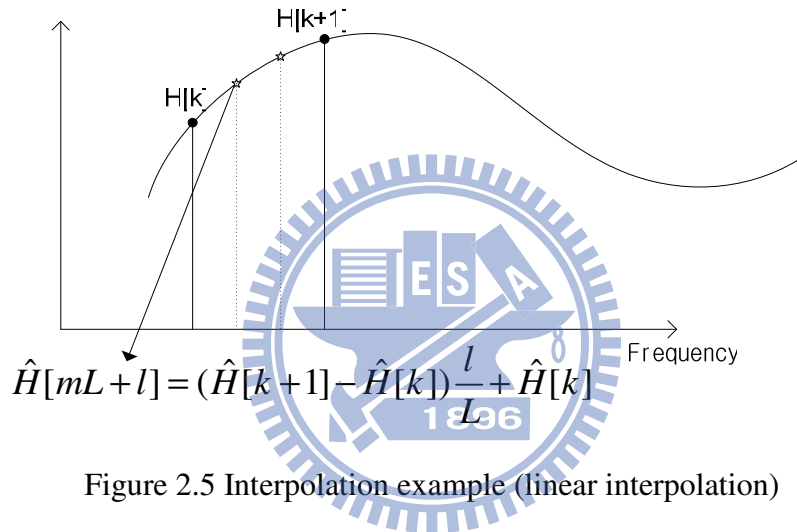


Figure 2.5 Interpolation example (linear interpolation)

In addition, the channel estimation based on block type pilot arrangement (Figure 2.6) is performed by sending pilots at every sub-channel and using this estimation for a specific number of following symbols.

In block-type pilot based channel estimation, OFDM channel estimation symbols are transmitted periodically, in which all subcarriers are used as pilots. If the channel is constant during the block, there will be no channel estimation error since the pilots are sent at all carriers. The estimation can be performed by using either LS or MMSE [18-19]. Given $Y = XFh + W$, where F denotes the DFT matrix.

$$H_{MMSE} = FR_{hY}R_{YY}^{-1}Y$$

where $R_{hY} = E\{hY\} = R_{hh}F^H X^H$ and $R_{YY} = E\{YY\} = XFR_{hh}F^H X^H + \sigma^2 I_N$ are the cross covariance matrix between h and Y and the auto-covariance matrix of Y . R_{hh} is the auto-covariance matrix of h and σ^2 represents the noise power. And the LS estimation can be represented as:

$$H_{LS} = X^{-1}Y \text{ which minimizes } (Y - XFh)^H (Y - XFh).$$

When the channel is slow fading, the channel estimation inside the block can be updated using the decision feedback equalizer at each sub-carrier.

- The estimated transmitted signal $X_e[k] = \frac{Y[k]}{H_e[k]}$
- $\{X_e\}$ de-map to binary data and then back map to $\{X_{pure}\}$
- The estimated channel $H_e[k] = \frac{Y[k]}{X_{pure}[k]}$

Since the decision feedback equalizer has to assume that the decisions are correct, the fast fading channel will cause the loss of estimated channel parameters. Therefore, as the channel fading becomes faster, there happens to be a compromise between the estimation error due to the interpolation and the error due to loss of channel tracking.

For fast fading channels, we will discuss in chapter 2.4 and chapter 3.

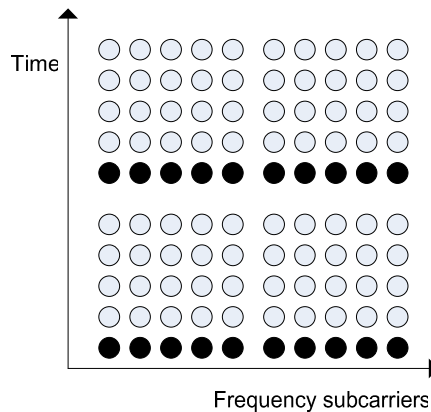


Figure 2.6 Block-type pilot arrangement

2.4 Time-varying channel model

In wireless communications such as satellite communication and cell-phones, the information signal is transmitted across free space. Two principal factors which influence the distortion of the signal transmitted across the wireless medium are multipath fading and mobility as illustrated in Fig. 2.7.

Multipath phenomenon means the transmitted signal arrives at the receiver via multiple propagation paths at different delays. As the matter of the fact, the multiple signals arriving at the receiver may add constructively or destructively resulting in wide variations in the signal strength.

Mobility is the phenomenon in which the relative positions of the different objects change with time, causing the nature of channel distortion to vary with time. It will be discussed in Section 2.4.2.

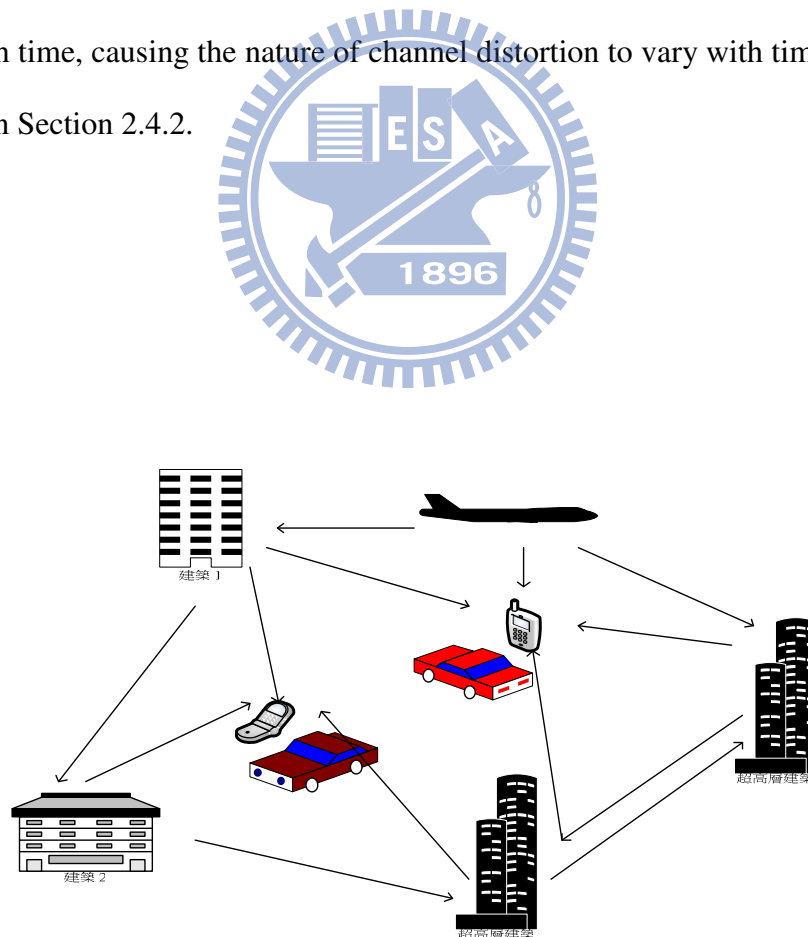


Figure 2.7 Multipath and mobility

2.4.1 Doubly-selective channel

All simple equalizers are based on the assumption that the channel is quasi-stationary which means that channel is time-invariant during a transmitted block. However, in wireless environment, the channel state may change within a transmitted block. This time-varying multipath indicates frequency-selective channel.

Under frequency-selective fading, the channel bandwidth and delay spread are smaller than the coherent bandwidth of signal and symbol period respectively, moreover, the different frequencies of transmitted subcarriers correspond to different channel frequency response.

Accordingly, we can denote the impulse response of time varying channel as $h_l[n]$, where n can be interpreted as time index and l as channel tap index and $l \in [0, L)$.

The received signal with Doppler effect corresponding to transmitted signal $x[n]$ (in the complex baseband) and can be represented as

$$y[n] = \sum_{l=0}^L h_l[n]x[n-l] + \omega[n] \quad (2.4.1)$$

Note that we usually use Jake's Model to describe $h_l[n]$ which will be introduced elaborately in section 2.4.3 and $\omega[n]$ is additive noise term. The time-selectivity due to Doppler effect and frequency-selectivity due to multipaths in the wireless channel, which is usually called doubly-selective channel. [2,9,11,16]

2.4.2 Doppler frequency effect

Since the relative motion of transmitter and receiver, the Doppler effect must be evaluated, and the corresponding mathematical equation can be represented [14] as

$$\tilde{f}_d = \frac{v f_c}{c T_s} = \frac{f_d}{T_s} \quad (2.4.2)$$

where \tilde{f}_d is the normalized Doppler frequency, with v (m/s) the speed of the mobile,

f_c the carrier frequency in Hz, c the speed of light, f_d the actual Doppler frequency, and T_s the subcarrier spacing.

The rate of variation of the channel response across time due to mobility is called the Doppler spread. If the channel response varies significantly in the signaling duration, it becomes time-selective. Note that channel are both time and frequency selective are doubly-selective channels.

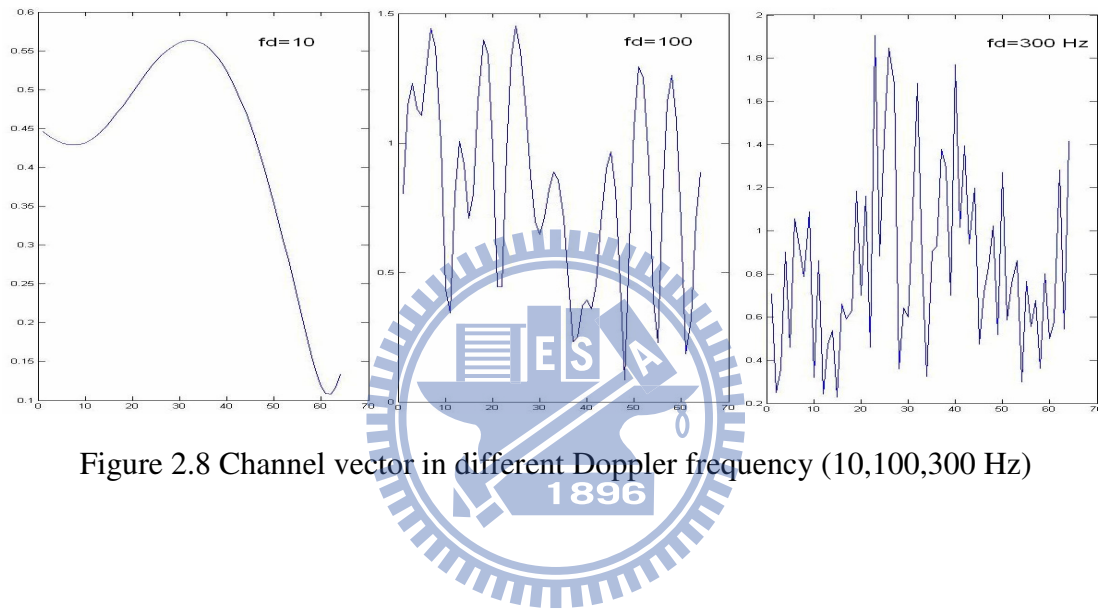


Figure 2.8 Channel vector in different Doppler frequency (10,100,300 Hz)

2.4.3 Jake's model and channel statistics

In wireless channel, there does not exist the LOS (line-of-sight) signal, thus the Rayleigh fading channel is always used to simulate the real channel. Moreover, if there is Doppler effect in the multipath channel simultaneously, it is generally believed that the Jake's model is very appropriate for time-varying channel discussed in Section 2.4.1.

Noted that the auto-correlation function [12-13]

$$r_l(\tau) = \sigma_l^2 \mathbf{J}_0(2\pi \tilde{f}_d \tau)$$

Where $\mathbf{J}_0(\cdot)$ denotes the zeroth-order Bessel function of first kind and σ_l^2 the power

of the l th channel tap. Therefore, we can obtain the auto-covariance matrix \mathbf{R}_l in dimension $N \times N$, whose (i, j) -th element is $r_l(i - j) = \sigma_l^2 \mathbf{J}_0(2\pi \tilde{f}_d(i - j))$.

The Doppler power spectral density

$$S(f) = \frac{1}{\pi f_d \sqrt{1 - \left(\frac{v}{f_d}\right)^2}} \quad (2.4.3)$$

which is illustrated in Fig. 2.9

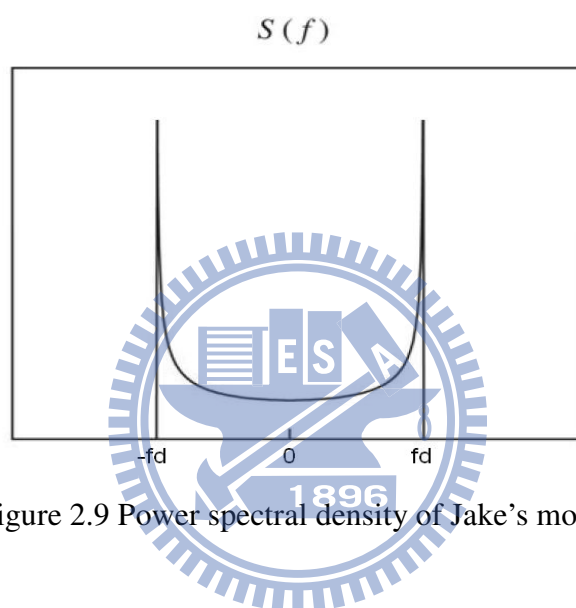


Figure 2.9 Power spectral density of Jake's model

2.4.4 Problems from Time-Varying Channel

When the transmitted signal goes through the time-varying channel, there are some crucial problems induced, two of which will be depicted as follows.

1. Channel estimation issue

We use pilot sequences to estimate the channel information in conventional time invariant channel, but doubly selective channel changes so fast that giving rise to two successive time-domain channel tap $h_l[k]$ and $h_l[k+1]$ are normally distinct.

Thanks to the estimation schemes of BEM, which is effective to be exploited to overcome the time-varying channel, and we will discuss the issue in Chapters 3 and 4.

Moreover, there are also some useful methods such as blind estimation scheme in [8-9].

2. Equalization issue

In a time-varying channel, the channel matrix H in Eq.(3.2.2) is not circulant, thus, the traditional equalizer [10] can not be applied. This problem is discussed in detail in [11].

2.4.5 Data detection

Due to the equalization issue in Section 2.4.4, the data transmitting method in doubly-selective channel is important. In [2], one data transmitting method will be introduced in the following paragraph.

The input is made by time-division multiplexing pilot and data symbols. The pilot symbols are known to the receiver, and the data symbols come from a finite alphabet. The system uses zero-padded block transmission, where each transmitted block, or packet, is made of alternating data/pilot sub-blocks. All pilot sub-blocks are assumed to be of length $\bar{N}_p = 2L + 1$ and of the form $[\mathbf{0}_L^T \ p \ \mathbf{0}_L^T]$. All data sub-blocks are of length \bar{N}_d . If the number of pilot/data sub-blocks in a packet is $Q + 1$ (for even Q) and the q -th data sub-block is denoted \mathbf{d}_q then the input is given by

$$\mathbf{s} = [\mathbf{d}_0 \mathbf{0}_L^T \ p \ \mathbf{0}_L^T \ \cdots \ \mathbf{d}_Q \mathbf{0}_L^T \ p \ \mathbf{0}_L^T]^T \text{ (as in [2]),}$$

the fact that the final L symbols are zeros guards against inter-block interference. The total number of pilot and data symbols is

$$N_p = (Q + 1) \bar{N}_p \text{ and } N_d = (Q + 1) \bar{N}_d \text{ respectively.}$$

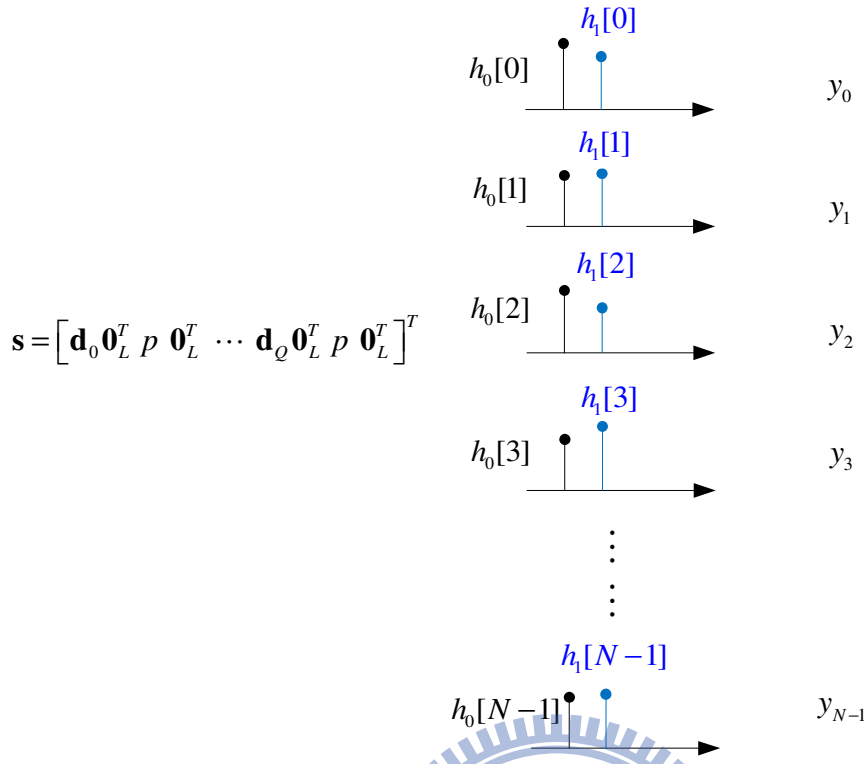


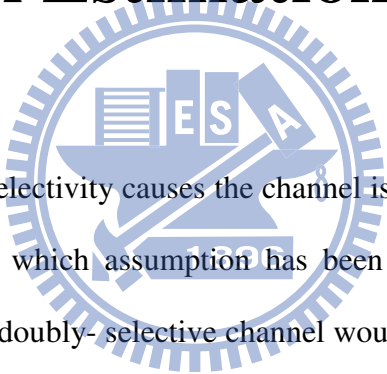
Figure 2.10 Packet transmission schematic

We have $Q+1$ received signal y^p to obtain $B \times L$ coefficients by exploiting the known bases (obtained from the channel statistics). Find the optimum combination of bases for \mathbf{h}^p as the whole channel vector $\mathbf{h}_i (N \times 1)$, thus the channel tap that data pass \mathbf{h}^d can be estimated. Since we also have the received signal resulted from data: y^d , thus the data detection can be accomplished.

To summarize this chapter, the OFDM and its main problems has been introduced. For the channel estimation in time-varying channel with Doppler effect, we discussed the issue in Section 2.4, which was prepared for Chapter 3, which will introduce and analyze some estimation schemes.

Chapter 3

Basis Expansion Model for Channel Estimation Schemes



In Section 2.4, the time selectivity causes the channel is time-invariant over a block assumption does not hold, which assumption has been adopted by many existing wireless environment. This doubly- selective channel would affect the communication performance critically. The issue of estimation of this channel is getting more attention due to the significance to the future wireless application.

Basis Expansion Model (BEM) is an effective scheme to overcome the difficulties with a few complex exponentials and low-cost. [2,4,22-23,25,35-38,39-42]

The BEM that is optimal in terms of the mean square error (MSE) is the discrete Karhuen–Loève BEM (DKL-BEM or SVD-BEM) [36-38], the problem though is that if the assumed channel statistics deviate from the true scenario, which is very likely in practice, the SVD-BEM will perform suboptimally.

As a compromise, one can derive a BEM that is based on a general approximation for all kinds of channel statistics. For instance, the discrete prolate spheroidal BEM

(Slepian-BEM) [22-23]. It is featured by a set of orthogonal spheroidal functions that are perfectly band-limited but have maximal time concentration within the considered interval.

Note that it is also possible to construct BEMs that are not dependent on the channel statistics like the complex-exponential BEM (CE-BEM) [35]. The CE-BEM introduced in Section 3.1 exploits the Fourier basis expansion gained a great deal of attention thanks to its algebraic ease [2,4,39-42], but fails to track the channel at the edges of the block resulting in much more modeling error [25]. As we understand, the CE-BEM can actually be viewed as a special SVD-BEM but based on a white spectrum.

At first, we introduce the essence of the basis expansion model in Section 3.1. Then we introduce some BEM methods including the CE-BEM in Section 3.2, and then the improvement by over-sampling and non-uniform sampling version in Section 3.2.1 and 3.2.2. In Section 3.3, we introduce the singular value decomposition basis expansion model, which exploits the principle eigen-vectors as the basis rather than CE-BEM. In the following Section 3.4, the Slepian BEM would also be introduced. In Section 3.5, we analyze the theoretical MSE of BEM and propose the Wiener filter methods for enhancement. Moreover, we also consider the phase noise and the carrier frequency offset problem in Section 3.6.

3.1 Introduction of basis expansion model

Rapidly time-varying channels may be normally encountered in highly mobile wireless environment. We approximate the time-varying channel using the basis expansion model (BEM) as a liner combination of finite number of complex coefficients (Fig. 3.1). That can reduce the computation complexity and diminish the

noise.

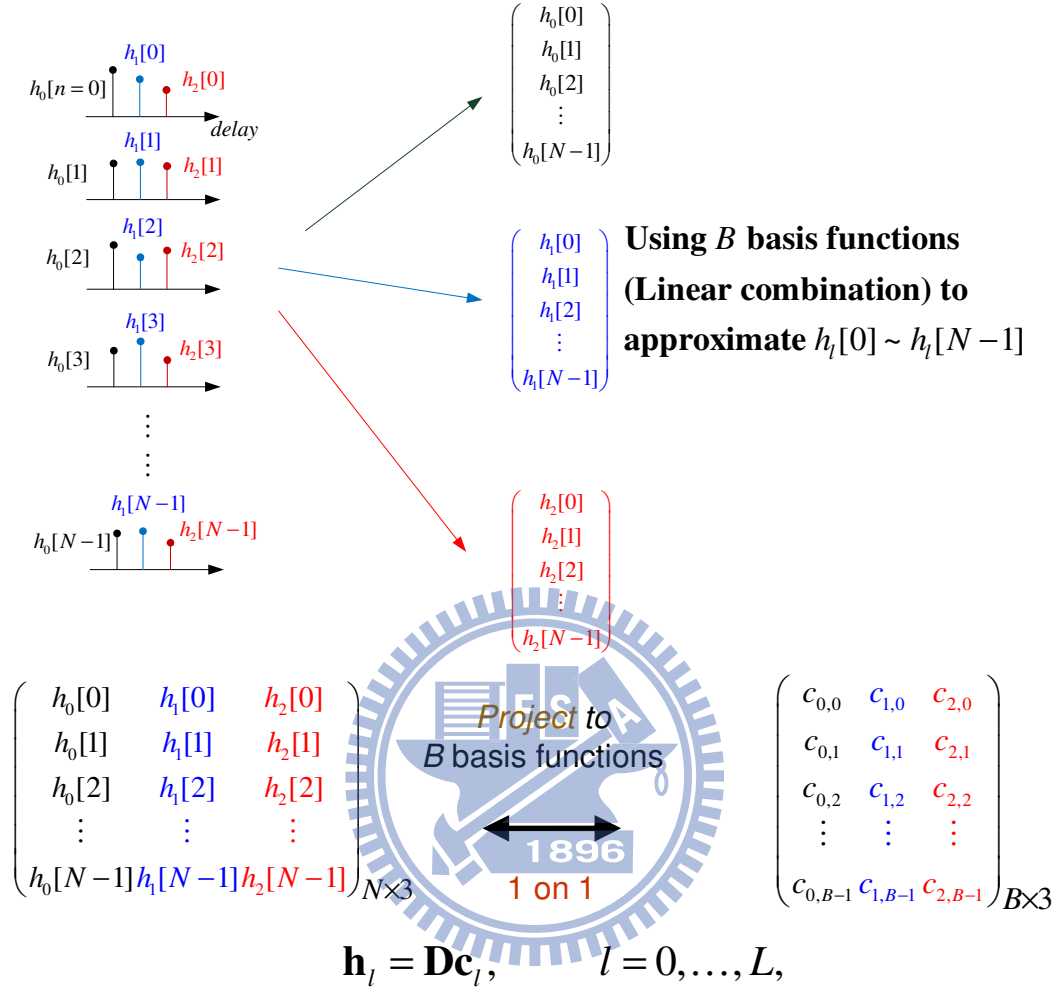


Figure 3.1 BEM for real time-varying channel

The time-varying channel vector \mathbf{h}_l ($N \times 1$) (note that N denotes the transmitting block length or the length of one basis function, and $L+1$ is the number of multipath channel impulse response) can be represented as BEM coefficients

$$\mathbf{c}_l = [c_{l,0}, c_{l,1}, \dots, c_{l,B-1}]^T_{(B \times 1)} \quad (3.1.1)$$

(note that B denotes the number of basis functions we used) by a known bases matrix:

$$\mathbf{D} = [\mathbf{d}_0, \mathbf{d}_1, \dots, \mathbf{d}_{B-1}]_{N \times B}$$

where $\mathbf{d}_1, \mathbf{d}_2, \dots, \mathbf{d}_B$ denote the basis functions in dimension $N \times 1$. And then we can

express \mathbf{h}_l as Eq.(3.1.1)

$$\mathbf{h}_l = c_{l,0}\mathbf{d}_0 + c_{l,1}\mathbf{d}_1 + \cdots + c_{l,B-1}\mathbf{d}_{B-1} \quad (3.1.2)$$

The parameters we interested will decrease ($N \gg B$), and moreover, we would like to have the good bases \mathbf{D} to model the real channel, and the following sections introduce some often seen bases.

Given some bases (CE, SVD, or Slepian), we can obtain the estimated BEM coefficients $\hat{\mathbf{c}}$ from the transmitting pilots and received signals by the least-squares method:

$$\begin{aligned} \mathbf{y} = \begin{bmatrix} y[0] \\ y[1] \\ \vdots \\ y[N-1] \end{bmatrix} &= \begin{bmatrix} h_0[0] & \mathbf{0} & h_L[0] & \cdots & \cdots & h_1[0] \\ h_1[1] & h_0[1] & \mathbf{0} & h_L[1] & \cdots & h_2[1] \\ \vdots & \vdots & \ddots & \vdots & \ddots & \vdots \\ \vdots & \vdots & \vdots & \vdots & \vdots & h_L[L-1] \\ h_L[L] & \vdots & \vdots & \vdots & \mathbf{0} & \vdots \\ \vdots & \vdots & \vdots & \vdots & \vdots & \vdots \\ \mathbf{0} & \vdots & h_L[N-1] & \cdots & h_0[N-1] & \vdots \end{bmatrix} \begin{bmatrix} s[0] \\ s[1] \\ \vdots \\ s[N-1] \end{bmatrix} + \mathbf{w} \\ &= \mathbf{H}\mathbf{s} + \mathbf{w} \\ &= \sum_{l=0}^L \mathbf{S}_l \mathbf{h}_l + \mathbf{w} \\ &= \sum_{l=0}^L \mathbf{S}_l \mathbf{D} \mathbf{c}_l + \mathbf{w} \\ &= \mathbf{S} [\mathbf{I}_{L+1} \otimes \mathbf{D}] \mathbf{c} + \mathbf{w} \end{aligned}$$

where \mathbf{S}_l is defined in Eq.(3.3.8), $\mathbf{S} = [\mathbf{S}_0, \cdots, \mathbf{S}_L]$ and $\mathbf{c} = [\mathbf{c}_0, \cdots, \mathbf{c}_L]^T$. The notation

\otimes indicates the Kronecker product.

The advantages for BEM are the fewer parameters need to estimate ($\mathbf{c} \in \mathbb{C}^B$), in contrast, the conventional ML method need to estimate more parameters ($\mathbf{h}_{ML} \in \mathbb{C}^N$), where $N \gg B$.

3.2 Complex exponential basis expansion model

The CE-BEM has been widely used to model time-varying communication channels [1-2]. It represents the channel as the sum of complex exponentials, which are uniform sampling in the frequency domain and symmetric about the zero frequency. For the case where the channel has $L+1$ taps, and the l th ($l = 0, 1, \dots, L-1$) tap, $h_l[n]$ will be modeled using $B+1$ basis coefficients $\bar{c}_{l,k}$ (for an even value of B):

$$h_l[n] = \sum_{k=-B/2}^{B/2} \bar{c}_{l,k} e^{j\omega_k n} \quad \text{where } \omega = \frac{2\pi f_d}{B/2} \quad (3.2.1)$$

It can be interpreted as Fourier series approximation. This means that there are $(B+1)(L+1)$ coefficients to estimate, note that there were $N(L+1)$ coefficients to estimate without BEM. For block transmission with packet length N , the received signal \mathbf{y} can be denoted as

$$\begin{aligned} \mathbf{y} &= \mathbf{H}\mathbf{s} + \mathbf{w} \\ &= \sum_{k=-B/2}^{B/2} \mathbf{D}_k \mathbf{S} \bar{\mathbf{c}}_k + \mathbf{w} \\ &= \mathbf{D} [\mathbf{I}_{B+1} \otimes \mathbf{S}] \bar{\mathbf{c}} + \mathbf{w} \end{aligned} \quad (3.2.2)$$

where $\mathbf{S} = N \times (L+1)$ is lower triangular Toeplitz matrix with its first column $[s[0], \dots, s[N-1]]^T$,

$$\mathbf{D}_k = \begin{bmatrix} 1 & & & 0 \\ & e^{j\omega_k} & & \\ & & \ddots & \\ 0 & & & e^{j\omega_k(N-1)} \end{bmatrix}, \quad k = -B/2, \dots, B/2$$

$$\mathbf{D} = [\mathbf{D}_{-B/2}, \dots, \mathbf{D}_{B/2}]$$

$$\bar{\mathbf{c}}_k = [\bar{c}_{0,k}, \dots, \bar{c}_{L,k}]^T, \quad k = -B/2, \dots, B/2$$

$$\bar{\mathbf{c}} = [\bar{\mathbf{c}}_{-B/2}^T, \dots, \bar{\mathbf{c}}_{B/2}^T]$$

The least-squares estimation of $\bar{\mathbf{c}}$ is:

$$\hat{\bar{\mathbf{c}}} = (\mathbf{D} [\mathbf{I}_{B+1} \otimes \mathbf{S}])^\dagger \mathbf{y} \quad (3.2.3)$$

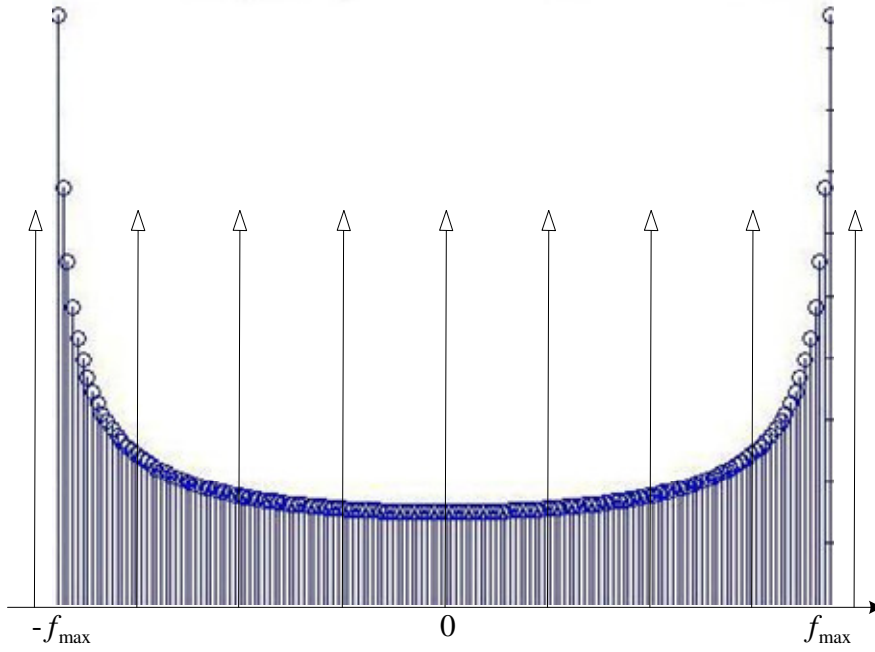


Figure 3.2 CE-BEM sampling in Jake's model PSD

3.2.1 Oversampling CE-BEM approach

Since the channel is limited in the Doppler range with non-uniform distribution, it might be beneficial to reduce the sidelobes by taking more samples within the range.

Therefore, we can rewrite Eq.(3.2.1) in

$$h_l^{(K)}[n] = \frac{1}{KN} \sum_{q=-B/2}^{B/2} \bar{c}_{l,q}^{(K)} e^{j\omega'qn} \quad (3.2.4)$$

where $\omega' = \frac{2\pi f_d}{KB/2}$, and $n = 0, 1, \dots, KN - 1$

Define

$$\mathbf{h}_l^{(K)} = [h_l^{(K)}[0], \dots, h_l^{(K)}[KN - 1]]^T,$$

and

$$\bar{\mathbf{c}}_l^{(K)} = [\bar{c}_{l,-B/2}^{(K)}, \dots, \bar{c}_{l,B/2}^{(K)}],$$

the least-squares fit for $\bar{\mathbf{c}}_l^{(K)}$ could be obtain by solving

$$\min_{\bar{\mathbf{c}}_l^{(K)}} \left\| \mathbf{h}_l^{(K)} - \frac{1}{KN} \mathbf{D}^{(K)} \bar{\mathbf{c}}_l^{(K)} \right\|, \quad (3.2.5)$$

where $\mathbf{D}^{(K)}$ is also the basis matrix that can be represented as

$$\mathbf{D}^{(K)} = \begin{bmatrix} 1 & \dots & 1 \\ e^{-j\pi B/KN} & & e^{j\pi B/KN} \\ \vdots & & \vdots \\ e^{-j\pi B(KN-1)/KN} & \dots & e^{j\pi B(KN-1)/KN} \end{bmatrix}$$

We can derive the least-squares solution in Eq.(3.2.5)

$$\bar{\mathbf{c}}_l^{(K)} = \mathbf{KND}^{(K)\dagger} \mathbf{h}_l^{(K)} \quad (3.2.6)$$

3.2.2 Non-uniform sampling approach CE-BEM

Because of the non-uniform distribution of the Doppler power spectral density, in Section 3.2 the uniform sampling of the PSD does not sample the most important frequency as the complex-exponential basis, it might be beneficial to sample more significant frequencies, which means the high frequency close to the maximum Doppler frequency in the Jake's model case.

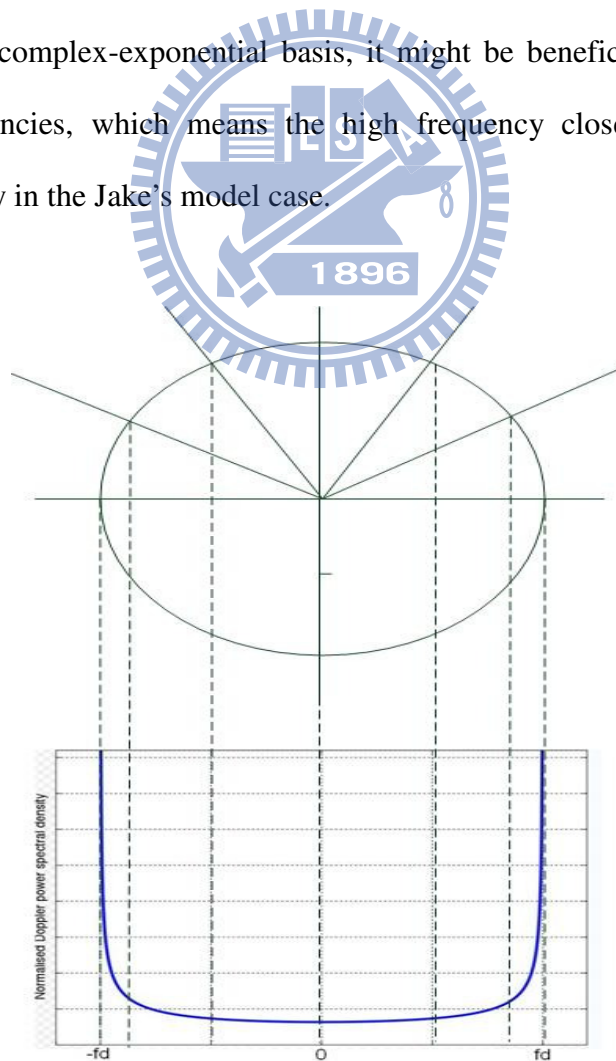


Figure 3.3 Non-uniform sampling under Doppler PSD

Assume the $B+1$ basis coefficients we use, from $-\tilde{f}_d$ to \tilde{f}_d the overall interval, the sampling frequencies we take could be represented as

$$\left\{ -\tilde{f}_d, \dots, \cos\left(\frac{(B+2)\pi}{2B}\right)\tilde{f}_d, 0, \cos\left(\frac{(B-2)\pi}{2B}\right)\tilde{f}_d, \cos\left(\frac{(B-4)\pi}{2B}\right)\tilde{f}_d, \dots, \cos\left(\frac{\pi}{B}\right)\tilde{f}_d, \tilde{f}_d \right\}$$

Each sector consists of two successive sampling frequencies has the same energy. Note that the density is higher in both ends and the lengths of the every sector are the Doppler shift. And then we can rewrite Eq.(3.2.1)

$$h_l[n] = \sum_{q=-B/2}^{B/2} \bar{c}_{l,k} e^{j\omega_q n} \quad (3.2.7)$$

where $\omega_q = \cos\left(\frac{(B-2q)\pi}{2B}\right)\tilde{f}_d$

$$\mathbf{D}_q = \begin{bmatrix} 1 & & & 0 \\ & e^{j\omega_q} & & \\ & & \ddots & \\ & & & e^{j\omega_q(N-1)} \\ 0 & & & & 0 \end{bmatrix}, q = -B/2, \dots, B/2$$

$$\mathbf{D} = [\mathbf{D}_{-B/2}, \dots, \mathbf{D}_{B/2}]$$

The least-squares estimation of $\bar{\mathbf{c}}$ is:

$$\hat{\bar{\mathbf{c}}} = (\mathbf{D}[\mathbf{I}_{B+1} \otimes \mathbf{S}])^\dagger \mathbf{y} \quad (3.2.8)$$

3.3 SVD Basis Expansion Model

We use the singular value decomposition to find the best basis from the Jake's model Rayleigh channel. In time-varying wireless channel, since only one block is considered, the n th received sample can be expressed as in [4]

$$y[n] = \sum_{l=0}^L h_l[n]x[n-l] + \omega[n] \quad (3.3.1)$$

And the matrix representation in (3.2.2)

$$\mathbf{y} = \begin{bmatrix} y[0] \\ y[1] \\ \vdots \\ y[N-1] \end{bmatrix} = \begin{bmatrix} h_0[0] & \mathbf{0} & h_L[0] & \cdots & \cdots & h_1[0] \\ h_1[1] & h_0[1] & \mathbf{0} & h_L[1] & \cdots & h_2[1] \\ \vdots & \ddots & \ddots & \ddots & \ddots & \vdots \\ \vdots & \vdots & \vdots & \ddots & \ddots & h_L[L-1] \\ h_L[L] & \vdots & \vdots & \ddots & \ddots & \mathbf{0} \\ \vdots & \mathbf{0} & h_L[N-1] & \cdots & h_0[N-1] & \vdots \end{bmatrix} \begin{bmatrix} x[0] \\ x[1] \\ \vdots \\ x[N-1] \end{bmatrix}$$

$$= \mathbf{H}\mathbf{x} \quad (3.3.2)$$

$$h_l[n] = \sum_{k=0}^B c_{l,k} f_{k,Basis}[n], \quad n=0, \dots, N-1 \quad (3.3.3)$$

where $f_{k,Basis}$ denotes the SVD basis come from the eigenvectors channel correlation matrix $\mathbf{R}_{h,l}$ following the Jake's model in chapter 2. And we can obtain the singular

$$\text{value decomposition of } \mathbf{R}_{h,l} = \mathbf{Q}_l \mathbf{\Lambda}_l \mathbf{Q}_l^H. \quad (3.3.4)$$

And Eq.(3.3.3) could also be represented using matrix notation

$$\mathbf{h}_l = \begin{bmatrix} h_l[0] \\ h_l[1] \\ \vdots \\ h_l[N] \end{bmatrix} = \mathbf{D} \begin{bmatrix} c_{l,0} \\ c_{l,1} \\ \vdots \\ c_{l,B} \end{bmatrix} = \mathbf{D}\mathbf{c}_l, \quad l=0, \dots, L, \quad (3.3.5)$$

where \mathbf{D} and \mathbf{c}_l are $N \times (B+1)$ dimensional bases matrix and the projected BEM coefficients respectively

According to the definition, Eq.(3.3.4) and (3.3.5), the channel correlation matrix

$$\mathbf{R}_{h,l} = E[\mathbf{h}_l \mathbf{h}_l^H] = \mathbf{D} E[\mathbf{c}_l \mathbf{c}_l^H] \mathbf{D}^H = \mathbf{Q}_l \mathbf{\Lambda}_l \mathbf{Q}_l^H, \quad l=0, \dots, L \quad (3.3.6)$$

We can conclude that $\mathbf{D} = \mathbf{Q}_l(:, 1:(B+1))$ from Eq.(3.3.6).

Based on Eq.(3.3.2) and (3.3.5), the BEM coefficients and estimated channel vector through LS is

$$\hat{\mathbf{c}}_l = (\mathbf{S}_l \mathbf{D})^H \mathbf{y} \quad \text{and} \quad \hat{\mathbf{h}}_l = \mathbf{D} (\mathbf{S}_l \mathbf{D})^H \mathbf{y} \quad (3.3.7)$$

where the transmitted signal matrix

$$\mathbf{S}_l = \frac{1}{\sigma_x^2} \text{diag}(\{x(N-l+n) \bmod N\}_{n=0}^{N-1}) \quad (3.3.8)$$

where $l=0, \dots, L$, σ_x^2 : the variance of \mathbf{x}

3.4 Slepian Basis Expansion Model

In [23], Zemen and Mecklenbräuer first applied the Slepian sequences to the BEM for channel estimation. The Slepian method exploits a set of orthogonal functions that optimize energy concentration both in time and frequency [22]. These basis functions are the discrete prolate spheroidal sequences. We assume the length of Slepian sequences $v[n]$ is N , which are band-limited to the $[-f_d T_s, f_d T_s]$ in frequency domain. These sequences are generated from the following eigenvalue equation.

$$\sum_{l=1}^N \frac{\sin(2\pi f_d T_s (l-n))}{\pi(l-n)} v_l[l] = \lambda_i(v_{\max}, N) v_i[n] \quad (3.4.1).$$

To solve the eigen-equation and acquire the eigenvector solutions, we can see it as the thing to get the eigenvectors from a square matrix \mathbf{A} :

$$\mathbf{A}_{N \times N} = \begin{bmatrix} 2f_d T_s & \frac{\sin(2\pi f_d T_s)}{\pi} & \dots & \frac{\sin(2(N-1)\pi f_d T_s)}{(N-1)\pi} \\ \frac{\sin(-2\pi f_d T_s)}{-\pi} & 2f_d T_s & & \frac{\sin(2(N-2)\pi f_d T_s)}{(N-2)\pi} \\ \vdots & \vdots & \ddots & \vdots \\ \frac{\sin(2(1-N)\pi f_d T_s)}{(1-N)\pi} & \frac{\sin(2(2-N)\pi f_d T_s)}{(2-N)\pi} & \dots & 2f_d T_s \end{bmatrix} \quad (3.4.2)$$

The eigenvectors are normalized so that:

$$\sum_{n=1}^N (v_i[n])^2 = 1 \quad (3.4.3)$$

where the matrix $\mathbf{A}_{N \times N}$ can be considered as the channel correlation matrix and

compared to the $\mathbf{R}_{h,l}$ in Eq. (3.3.6).

Therefore, \mathbf{h}_l can be approximated as a linear combination of the Slepian sequences $v_i[n]$ of length N , which are bandlimited to $[-f_d T_s, f_d T_s]$ as

$$h_l[n] \approx \sum_{i=1}^B v_i[n] c_i, \quad n = 1, \dots, N \quad (3.4.4)$$

where $B = \lceil 2f_d T_s N \rceil + 1$ is the number of principle eigenvectors we choose.

When the relative mobility between the transmitter and the receiver is small (i.e., when the Doppler frequency is small), this method requires very much long Slepian sequences to accurately model the channel. This is because we should take a long period time to observe the slow variation channel.

In the right part of Table 3.1 shows that for a given length sequences, as the maximum normalized Doppler frequency $f_d T_s$ increases, λ increases, which means the Slepian BEM requires longer sequences to accurately model the channel in low $f_d T_s$. And then, we can continue observe the left part, the length of the Slepian sequences should be increased for a given $f_d T_s$. This implies that we need to observe more samples to estimate the channel especially in low Doppler frequency, which high computational complexity for decoding. Therefore, in a low mobility environment, the time-domain Slepian basis expansion model cannot represent the channel effectively.

Table 3.1 λ for different length of sequence and Doppler frequency

$f_d T_s = 0.001$					$N=130$					
N	B	λ_1	λ_2	λ_3	$f_d T_s$	B	λ_1	λ_2	λ_3	λ_4
130	1	0.25	small	small	0.001	1	0.25	small	small	small
250	1	0.48	small	small	0.005	2	0.88	0.35	small	small
500	2	0.79	0.22	small	0.008	3	0.92	0.71	0.25	small
1000	3	0.99	0.78	0.27	0.01	4	0.99	0.9	0.52	0.11

3.5 Analysis of the basis expansion model

In this section, we analyze and discuss some issue for BEM. First of all, we derive the theoretical channel estimation MSE in Section 3.5.1. In order to enhance the channel estimation performance using BEM, we apply the Wiener filter to adjust the power spectral density of the estimated channel in Section 3.5.2 that aims to filter out the noise and achieve the best signal to noise ratio. In Section 3.5.3, we discuss and compare the UB basis schemes to SVD-BEM, the UB is a post bases projection method. Finally, we discuss the difference of the conventional estimation method without applying basis expansion model (called non-BEM) and BEM methods in Section 3.5.4.

3.5.1 Derivation of the theoretical MSE

The total mean square error (MSE) of the channel is defined by

$$\mathbf{J} = E \left\{ \sum_{l=0}^L \|\mathbf{h}_l - \hat{\mathbf{h}}_l\|^2 \right\} \quad (3.5.1)$$

where L is the number of multipath taps and \mathbf{h}_l is an N -dimensional channel vector.

The received signal in Eq.(3.3.2) can be rewritten as

$$y = \sigma_x^2 \sum_{l=0}^L \mathbf{S}_l \mathbf{h}_l + \mathbf{w} \quad (3.5.2)$$

where σ_x^2 is the transmitting signal power and \mathbf{S}_l is denoted in Eq.(3.3.8) with

$\sigma_x^2 \mathbf{S}_l^H \mathbf{S}_l = \mathbf{I}$, and then we note that the estimated channel vector

$$\hat{\mathbf{h}}_l = \mathbf{D} \hat{\mathbf{c}}_l = \mathbf{D} (\mathbf{S}_l \mathbf{D})^H \mathbf{y}, \quad (3.5.3)$$

from Eq.(3.5.2) and (3.5.3), the channel estimated error

$$\mathbf{h}_l - \hat{\mathbf{h}}_l = (\mathbf{I} - \mathbf{D} \mathbf{D}^H) \mathbf{h}_l - \mathbf{D} (\mathbf{S}_l \mathbf{D})^H \sum_{i=0, i \neq l}^L \mathbf{S}_i \mathbf{h}_i - \mathbf{D} (\mathbf{S}_l \mathbf{D})^H \mathbf{w} \quad (3.5.4)$$

If the transmitting signal $\{x[n]\}$, ($n = 0 \sim N-1$) is the PSK or QAM constellation,

then from the Central Limit Theorem, the second term in Eq.(3.5.4),

$\mathbf{D} (\mathbf{S}_l \mathbf{D})^H \sum_{i=0, i \neq l}^L \mathbf{S}_i \mathbf{h}_i$ is equal to zero, therefore.

$$\mathbf{h}_l - \hat{\mathbf{h}}_l \approx (\mathbf{I} - \mathbf{D} \mathbf{D}^H) \mathbf{h}_l - \mathbf{D} (\mathbf{S}_l \mathbf{D})^H \mathbf{w} \quad (3.5.5)$$

since \mathbf{h}_l and \mathbf{w} are uncorrelated, we note that the total MSE in Eq.(3.5.5) can be considered as two part: the channel modeling error and the channel identification error,

the modeling error can be rewritten from Eq. (3.5.5) as

$$\begin{aligned} & E \left\{ \sum_{l=0}^L \left\| (\mathbf{I} - \mathbf{D} \mathbf{D}^H) \mathbf{h}_l \right\|^2 \right\} \\ &= E \left\{ \sum_{l=0}^L \text{trace} \left((\mathbf{I} - \mathbf{D} \mathbf{D}^H) \mathbf{h}_l (\mathbf{I} - \mathbf{D} \mathbf{D}^H) \mathbf{h}_l^H \right) \right\} \\ &= E \left\{ \sum_{l=0}^L \text{trace} \left((\mathbf{I} - \mathbf{D} \mathbf{D}^H) \mathbf{h}_l \mathbf{h}_l^H (\mathbf{I} - \mathbf{D} \mathbf{D}^H) \right) \right\} \quad (\because \text{trace}(AB) = \text{trace}(BA)) \\ &= E \left\{ \sum_{l=0}^L \text{trace} \left((\mathbf{I} - \mathbf{D} \mathbf{D}^H)^H (\mathbf{I} - \mathbf{D} \mathbf{D}^H) \mathbf{h}_l \mathbf{h}_l^H \right) \right\} \quad (\because (\mathbf{I} - \mathbf{D} \mathbf{D}^H)^H = (\mathbf{I} - \mathbf{D} \mathbf{D}^H)) \\ &= \sum_{l=0}^L \text{trace} \left((\mathbf{I} - \mathbf{D} \mathbf{D}^H)^H (\mathbf{I} - \mathbf{D} \mathbf{D}^H) E[\mathbf{h}_l \mathbf{h}_l^H] \right) \\ &= \sum_{l=0}^L \text{trace} \left((\mathbf{I} - \mathbf{D} \mathbf{D}^H) (\mathbf{I} - \mathbf{D} \mathbf{D}^H) \mathbf{R}_l \right) \quad (\because (\mathbf{I} - \mathbf{D} \mathbf{D}^H)^2 = (\mathbf{I} - \mathbf{D} \mathbf{D}^H)) \end{aligned}$$

$$= (L+1)\text{trace}\left(\mathbf{I} - \mathbf{D}\mathbf{D}^H\right)\mathbf{R}_l \quad (3.5.6)$$

Similarly, the channel identification error that resulted from AWGN is

$$\begin{aligned} & E \left\{ \sum_{l=0}^L \left\| \mathbf{D}(\mathbf{S}_l \mathbf{D})^H \mathbf{w} \right\|_F^2 \right\} \\ &= E \left\{ \sum_{l=0}^L \text{trace} \left(\mathbf{D}(\mathbf{S}_l \mathbf{D})^H \mathbf{w} \cdot (\mathbf{D}(\mathbf{S}_l \mathbf{D})^H \mathbf{w})^H \right) \right\} \\ &= E \left\{ \sum_{l=0}^L \text{trace} \left(\mathbf{D}(\mathbf{S}_l \mathbf{D})^H \mathbf{w} \cdot \mathbf{w}^H (\mathbf{S}_l \mathbf{D}) \mathbf{D}^H \right) \right\} \\ &= E \left\{ \sum_{l=0}^L \text{trace} \left(\mathbf{w} \mathbf{w}^H \mathbf{S}_l \mathbf{D} \mathbf{D}^H \mathbf{D} \mathbf{D}^H \mathbf{S}_l^H \right) \right\} \\ &= E \left\{ \sum_{l=0}^L \text{trace} \left(\mathbf{w} \mathbf{w}^H \mathbf{S}_l \mathbf{D} \mathbf{D}^H \mathbf{S}_l^H \right) \right\} = (L+1) E[\mathbf{w}^H \mathbf{w}] \text{trace} \left(\mathbf{D}^H \mathbf{S}_l^H \mathbf{S}_l \mathbf{D} \right) \\ &= (L+1) \sigma_w^2 \frac{1}{\sigma_x^2} \text{trace} \left(\mathbf{D}^H \mathbf{D} \right) = (L+1) \sigma_w^2 \frac{1}{\sigma_x^2} \text{trace} \left(\mathbf{I}_{B+1} \right) \\ &= (L+1)(B+1) \frac{\sigma_w^2}{\sigma_x^2} \end{aligned} \quad (3.5.7)$$

where σ_w^2 and σ_x^2 denote the variances of the noise and the transmitted signal, respectively. Eventually, by summing up Eq.(3.5.6) and (3.5.7), the total mean square error of channel vector estimation in Eq.(3.5.1) is

$$E \left\{ \sum_{l=0}^L \left\| \mathbf{h}_l - \hat{\mathbf{h}}_l \right\|^2 \right\} = (L+1) \left(\text{trace}(\mathbf{R}_l - \mathbf{D}\mathbf{D}^H \mathbf{R}_l) + (B+1) \frac{\sigma_w^2}{\sigma_x^2} \right) \quad (3.5.8)$$

Obviously, to minimize the channel estimation MSE in Eq.(3.5.8), we need to minimize both the channel modeling error and the channel identification error. For a fixed B , L , as well as SNR, we just need to minimize the modeling error which corresponds to the channel modeling MSE:

$$\begin{aligned}
& \min_{\mathbf{D}} \text{trace}(\mathbf{I} - \mathbf{D}\mathbf{D}^H)\mathbf{R}_l \\
& = \max_{\mathbf{D}} \text{trace}(\mathbf{D}\mathbf{D}^H\mathbf{R}_l) \\
& = \max_{\mathbf{D}} \text{trace}(\mathbf{D}^H\mathbf{R}_l\mathbf{D}) \leq \sum_{i=0}^{B-1} \lambda_i \tag{3.5.9}
\end{aligned}$$

where λ_i denotes the eigenvalues from the real channel correlation matrix \mathbf{R}_l , which comes from Jake's model in this thesis.

The equality holds true if and only if the basis matrix \mathbf{D} is taken from the first B columns of \mathbf{Q}_l in Eq.(3.3.6) which correspond to the B significant eigenvalues. Thus, the SVD-BEM will offer the minimum mean squared channel estimation error.

3.5.2 Wiener filter

We would like to enhance the channel estimation that can achieve the maximum SNR and conform to the theoretical power spectral density by utilizing the Wiener filter [14]. Consider the block diagram of Fig.3.4 built around a linear discrete-time Wiener filter. The filter input consists of a time series $\hat{h}[0], \hat{h}[1], \dots$, and the filter is itself characterized by the impulse response w_0, w_1, w_2, \dots . At some discrete time n , the filter produces an output $\hat{h}_w[n]$. The output is used to provide an estimate of a desired response designated by $h[n]$ (real channel: \mathbf{d}). Where the power spectrum density of \mathbf{d} was defined in Eq.(2.4.3),

$$\mathbf{P}_d(f) = \frac{P_0}{\sqrt{1 - (f/f_d)^2}}, \tag{3.5.10}$$

With the filter input and the desired response representing single realizations of respective stochastic processes, the estimation is ordinarily accompanied by an error with statistical characteristics of its own. In particular, the estimation error, denoted by $e[n]$, is defined as the difference between the desired response and the filter output.

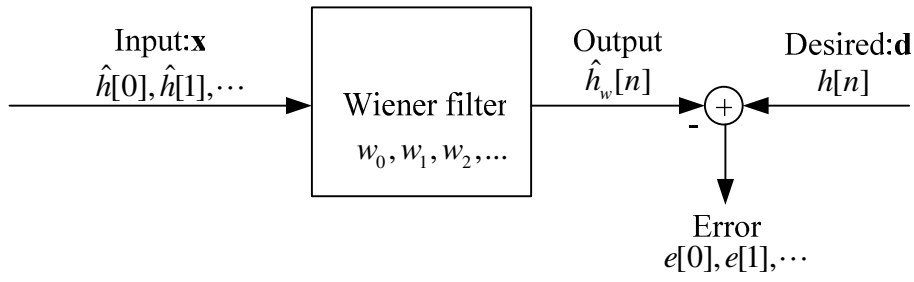


Figure 3.4 Block diagram representation of the statistical filtering problem

The optimum linear filter in Fig.3.4 is shown in Eq.(3.5.11), where the input (estimated channel vector) can be seen as the desired signal (real channel vector) plus the noise vector \mathbf{w} , which can be expressed as $\mathbf{w}=\mathbf{x}-\mathbf{d}$, and the variance of noise vector \mathbf{w} is σ_w^2 . Assuming that $\mathbf{P}_x(f) \neq 0$ for all f , we find the following transfer function of the non-causal Wiener filter:

$$\mathbf{G}(f) = \frac{\mathbf{P}_{xd}(f)}{\mathbf{P}_x(f)} = \frac{\mathbf{P}_d(f)}{\mathbf{P}_d(f) + \mathbf{P}_w(f)} = \frac{\frac{P_0}{\sqrt{1-(f/f_d)^2}}}{\frac{P_0}{\sqrt{1-(f/f_d)^2}} + \sigma_w^2} \quad (3.5.11)$$

If the weights (importance) of each basis do not conform to the Jake's PSD as in Fig. 2.9 (like Fig.5.17 in $f_d=10$), the Wiener filter may not be valid.

3.5.3 Comparison of UB-BEM

UB-BEM is a post-processing method to project the estimated channel onto a set of orthogonal functions known as the Universal Basis (UB) that were defined in [26].

The PDP (power delay profile) of the multipath channel is defined as $F(\tau)$. The channel autocorrelation matrix \mathbf{R} can be expressed as

$$\mathbf{R} = \sum_{i=1}^M \sigma_i^2 \mathbf{g}_i \mathbf{g}_i^T, \quad (3.5.12)$$

where \mathbf{g} is defined in [24], denoted the combined impulse response of the band-limiting filters.

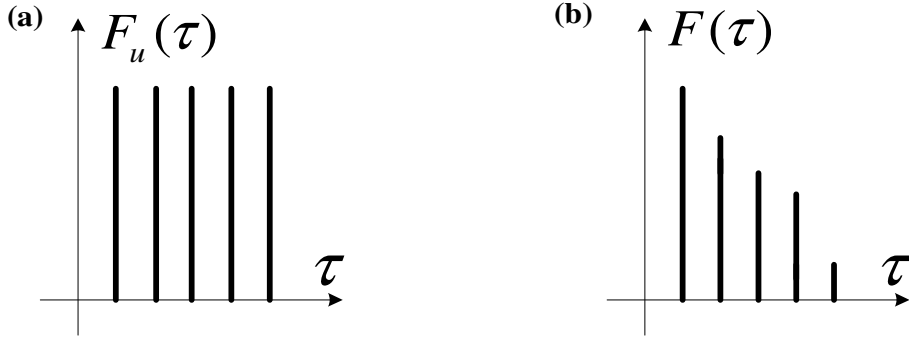


Figure 3.5 (a) Universal power delay profile. (b) Particular power delay profile.

The UB (universal basis) is formed by the significant eigenvectors of a specific universal channel autocorrelation matrix \mathbf{R}_u , which is obtained as $\mathbf{R}_u = \sum_{i=1}^Q \mathbf{g}_i \mathbf{g}_i^T$.

One possible universal PDP $F_u(\tau)$ associated to the matrix \mathbf{R}_u is given by

$$F_u(\tau) = \begin{cases} 1, & \tau \leq N \\ 0, & \text{otherwise} \end{cases} \quad (3.5.13)$$

Once the receiver does not have the knowledge of the channel PDP, this method offers good bases for channel approximation. Given a estimated channel vector $\hat{\mathbf{h}}$ in conventional method such as [25], (Fig. 3.6) we can project $\hat{\mathbf{h}}$ onto the UB subspace in order to constrain the estimator to the admissible subspace of channel realizations.

$$\hat{\mathbf{h}}_u = \Delta \Delta^H \hat{\mathbf{h}} \quad (3.5.14)$$

where the matrix Δ contains the eigenvectors from \mathbf{R}_u .

The projection improved channel estimation when compared to raw superimposed training (ST) based channel estimation schemes. The performance depends on the raw ST method effective or not. If the method works with much error, the post projection would not remove the distortion entirely. Compare to Section 3.3 (SVD-BEM), we directly exploit the same bases as UB (post BEM) to estimate channel but with the

same or better performance.



Fig.3.6 The UB flowchart

3.5.4 Complexity comparison with the conventional method

Without exploiting the BEM methods for time-varying channel estimation, [18] used a traditional MMSE estimate of channel based on the cost function from the Maximum a posteriori (MAP) method.

$$\begin{aligned}
 \hat{\mathbf{h}} &= \arg \max_{\mathbf{h}} p(\mathbf{y} | \mathbf{h}) p(\mathbf{h}) \\
 &= \arg \max_{\mathbf{h}} \frac{1}{\sigma^2} \|\mathbf{y} - \mathbf{S}\mathbf{h}\|^2 + \mathbf{h}^H \mathbf{R}_h^{-1} \mathbf{h} \\
 &= (\mathbf{S}^H \mathbf{S} + \sigma^2 \mathbf{R}_h^{-1})^{-1} \mathbf{S}^H \mathbf{y}
 \end{aligned} \tag{3.5.15}$$

where \mathbf{S} is the stacked \mathbf{S}_l matrices, $\mathbf{S} = [\mathbf{S}_0, \mathbf{S}_1, \dots, \mathbf{S}_{L-1}]$, \mathbf{S}_l are the same in Eq. (3.3.8), and \mathbf{h} is also the stacked \mathbf{h}_l matrices, $\mathbf{h} = [\mathbf{h}_0, \mathbf{h}_1, \dots, \mathbf{h}_{L-1}]$

$$\mathbf{R}_h = \begin{bmatrix} \mathbf{R}_{h,0} & & & \mathbf{0} \\ & \mathbf{R}_{h,1} & & \\ & & \ddots & \\ \mathbf{0} & & & \mathbf{R}_{h,L-1} \end{bmatrix} \tag{3.5.16}$$

Comparison of two channel estimation by exploiting between BEM and non-BEM respectively, in the equation for estimated channel Eq.(3.3.7) and (3.5.15), we can discover that there is a matrix inverse which should be calculated in the receiver, on the other hand, the traditional method needs much more computations than BEM

system, and more parameters to calculate. We can also compare the performance under criterion of the accuracy of estimated channel in MSE in Chapter 5.

3.6 Consideration of CFO and PHN

Due to the mismatch of oscillator and receiver, the phase noise and the carrier frequency offset effects are key problems that can lead to severe system performance degradation (Fig.3.7). To solve these problems, we use the mixed channel of PHN and TVCIR (Time-Varying Channel Impulse Response) based on the SVD-BEM method in Section 3.3 to reduce the PHN effect in Section 3.6.1. And apply the modified Moose CFO estimator under PHN existing condition in Section 3.6.2.

3.6.1 Mixed channel in the presence of PHN

The receive signal could be rewrote from Eq. (3.6.1) in consideration of PHN $\varphi(n)$

$$y[n] = \sum_{l=0}^L h_l[n]x[n-l]e^{j\varphi(n)} + \omega[n] \quad (3.6.1)$$

The PHN $\varphi(n)$ is generally modeled as a Wiener process [3]. The phase noise discrete time equation is denoted as

$$\varphi[n] = \varphi[n-1] + \xi[n-1] \quad (3.6.2)$$

where $\xi(n)$ is a random variable following the Gaussian distribution,

$$\xi(n) \sim N(0, \sigma_\xi^2)$$

with $\sigma_\xi^2 = 4\pi f_{3dB} T_s$

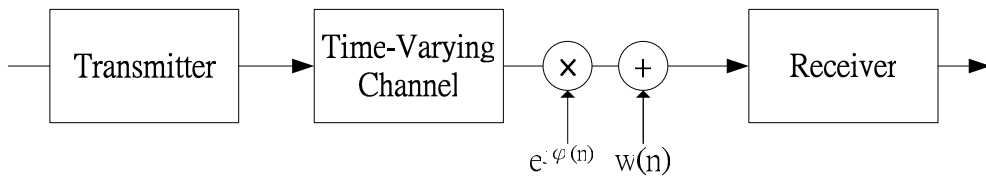


Fig.3.7 OFDM system in the presence of phase noise

We define the mixed channel $g_l(n)$ is equal to $h_l(n)e^{j\varphi(n)}$, as the same as before

$$g_l[n] = \sum_{k=0}^B c_{l,k} f_{k,Basis}[n] \quad (3.6.3)$$

The expression Eq. (3.2.4) could be modified still using matrix notation

$$\mathbf{g}_l = \begin{bmatrix} g_l[0] \\ g_l[1] \\ \vdots \\ g_l[N] \end{bmatrix} = \mathbf{D}'_l \begin{bmatrix} c_{l,0} \\ c_{l,1} \\ \vdots \\ c_{l,B} \end{bmatrix} = \mathbf{D}'_l \mathbf{c}_l, \quad (3.6.4)$$

The mixed channel correlation matrix of l th tap :

$$\mathbf{R}_{g,l} = E[\mathbf{g}_l \mathbf{g}_l^H] = E[\mathbf{D}'_l \mathbf{c}_l \mathbf{c}_l^H \mathbf{D}'_l{}^H] = \mathbf{D}'_l E[\mathbf{c}_l \mathbf{c}_l^H] \mathbf{D}'_l{}^H \quad (3.6.5)$$

and the SVD of $\mathbf{R}_{g,l} = \mathbf{Q}'_l \mathbf{\Lambda}'_l \mathbf{Q}'_l{}^H$ (3.6.6)

Observing the above two equation, we could find that

$$\mathbf{D}'_l = \mathbf{Q}'_l(:, 1:(B+1)) \quad (3.6.7)$$

Based on the Eq.(3.6.4) and (3.6.5), the (m,n) th elements of $\mathbf{R}_{g,l}$ denotes

$$E[g_l[m]g_l^H[n]] = E[h_l[m]h_l^*[m]]E[e^{j(\varphi(m)-\varphi(n))}], \text{ where } \varphi(m)-\varphi(n) \text{ is also a}$$

Gaussian random variable $\varphi(m)-\varphi(n) \sim N(0, |m-n| \sigma_\xi^2)$, so $E[e^{j(\varphi(m)-\varphi(n))}]$

conforms to the characteristic function $\Phi_{mn}(1) = e^{-|m-n| \frac{\sigma_\xi^2}{2}}$. Note the first part

$E[h_l[m]h_l^*[m]]$ is the same as Section 3.3. Finally, the \mathbf{D}'_l in Eq.(3.6.7) can be

obtained, so the LS channel estimate

$$\hat{\mathbf{h}}_l = \mathbf{D}'_l (\mathbf{S}_l \mathbf{D}'_l)^H \mathbf{y} \quad (3.6.8)$$

3.6.2 The CFO estimation scheme

It is beneficial to obtain a closed-form for CFO ε where the receiver has very limited computational power. In [5], the Moose's CFO estimator has the extraordinary

performance only when no PHN is present. First, pilot signal we transmit is easily generated [6] by transmitting the same $N/2$ training symbols on the even subcarriers and zero on the odd. The received signal $\mathbf{r}=[\mathbf{r}_1^T \ \mathbf{r}_2^T]^T$, the dimension of \mathbf{r}_1 and \mathbf{r}_2 are the equal to $N/2$, and the estimated Moose's CFO

$$\hat{\varepsilon} = \frac{1}{\pi} \angle \mathbf{r}_1^H \mathbf{r}_2 \quad (3.6.9)$$

In the presence of PHN, the Eq.(3.6.9) fails. The closed-form that optimally accounts for PHN can be derived [7], which is a similar form to Eq.(3.6.9) except for the weighting matrix that account for the distortion caused by PHN.

$$\hat{\varepsilon} = \frac{1}{\pi} \angle \mathbf{r}_1^H (\text{diag}(\mathbf{r}_1) \mathbf{\Phi}_\Delta \text{diag}(\mathbf{r}_1)^H + 4\sigma^2 \mathbf{I})^{-1} \mathbf{r}_2 \quad (3.6.10)$$

where $\mathbf{\Phi}_\Delta = 2\mathbf{\Phi}_{N/2} - \mathbf{\Upsilon} - \mathbf{\Upsilon}^T$ and the PHN correlation matrix $\mathbf{\Phi} = \begin{bmatrix} \mathbf{\Phi}_{N/2} & \mathbf{\Upsilon} \\ \mathbf{\Upsilon}^T & \mathbf{\Phi}_{N/2} \end{bmatrix}$.

To summarize this chapter, the often seen BEM methods for channel estimation in doubly-selective channel have been introduced. We proposed the post Wiener filter to enhance the accuracy after using BEM, and we derived the theoretical MSE for BEMs. The CFO and PHN problems were also considered. But for reduce computational complexity, we will propose the adaptive BEM methods to track channel, and the asymptotic bases when Doppler frequency changes.

Chapter 4

Adaptive BEM Estimation

In Chapter 3, we introduced the several BEMs method for channel estimation. It works fine in time variant channel with Doppler effect. In this chapter, the problems which are the Doppler frequency changes and the projected coefficients updating will be discussed.

This chapter is organized as follows. A brief introduction of the BEM coefficients adaptive using LMS and EW-RLS method based on the past receiving information is given in Section 4.1.1. And the theoretical MSE analysis for LMS is derived in Section 4.1.2. The modified method which takes the significance of the basis into account applying the results of Section 4.1.2 is proposed in Section 4.1.3.

Furthermore, when the Doppler frequency changes in different blocks due to the mobility problem, the eigenvalues and eigenvectors adaptive schemes for the new bases methods (can reduce the complexity) are derived in Section 4.2.1 and 4.2.2.

4.1 BEM parameters tracking

Since the time-varying nature of the channel is well captured in Section 3 by the known bases, the time variation of the (unknown) BEM coefficients is likely much slower than that of the channel. We would like to track the coefficients variation (fewer parameters for consideration) rather than the real channel using adaptive algorithms (the LMS and RLS algorithms in Section 4.1.1 and 4.1.3 respectively).

4.1.1 Adaptive algorithm

1. Exponential Weighted RLS

This method for tracking BEM coefficients is the subblockwise tracking [16] with recursive least-squares (RLS) algorithm. Stack the BEM coefficients in Eq. (3.1.1) of p -th block into vectors

$$\mathbf{c}_l(p) := [\bar{c}_{l,-B/2} \cdots \bar{c}_{l,B/2}]^T$$

$$\mathbf{c}(p) := [\mathbf{c}_0 \ \mathbf{c}_1 \ \cdots \ \mathbf{c}_L]^T$$

of size $B \times 1$ and $B(L+1)$ respectively. We emphasize that the p -th block and the $(p+1)$ -st block differ by m_s symbols. Based on Eq. (3.2.2), the received signal at time n can be written as

$$y[n] = \mathbf{S}^T(n) [\mathbf{I}_{L+1} \otimes \mathbf{D}(n)] \bar{\mathbf{c}}(p) + \mathbf{w}[n]$$

where $\mathbf{D}(n) := [e^{-j\omega_{-B/2}} \cdots e^{-j\omega_{B/2}}]^T$ and $\mathbf{S}(n) := [s(n) \ s(n-1) \ \cdots \ s(n-L)]^T$,

Further defining

$$\mathbf{G}_i(p) := \mathbf{S}^T(pm_s) [\mathbf{I}_{L+1} \otimes \mathbf{D}(pm_s + i)]^H, \quad \mathbf{G}(p) := [\mathbf{G}_0^T(p) \ \mathbf{G}_1^T(p) \ \cdots \ \mathbf{G}_{m_s-1}^T(p)]^T,$$

we have

$$\mathbf{y}_{ms}(p) = \begin{bmatrix} y_{ms}(pm_s) \\ y_{ms}(pm_s + 1) \\ \vdots \\ y_{ms}(pm_s + m_s - 1) \end{bmatrix} = \mathbf{G}(p)\mathbf{c}(p) + \mathbf{w}_{ms}(p) \quad (4.1.1)$$

Based on Eq. (4.1.1), our objective is apply exponentially-weighted RLS (EW-RLS) algorithm [14] to track an unknown $\mathbf{c}(p)$. Choose \mathbf{c} to minimize the cost function

$$\beta \|\mathbf{c}\|^2 + \sum_{i=0}^p \lambda^{p-i} \|\mathbf{y}_{ms}(i) - \mathbf{G}(i)\mathbf{c}(p)\|^2 \quad (4.1.2)$$

where $\beta > 0$ denotes a regularization parameter, and

$0 < \lambda < 1$ denotes the forgetting factor.

EW-RLS tracking comprised the following steps:

1. Initialization: $\hat{\mathbf{c}}(-1) = \mathbf{0}_{M \times 1}$ and $\mathbf{P}(-1) = \beta^{-1} \mathbf{I}_M$

2. For $p = 0, 1, \dots$

$$\mathbf{\Gamma}(p) = \lambda \mathbf{I}_{m_s} + \mathbf{G}(p)\mathbf{P}(p-1)\mathbf{G}^H(p), \quad (4.1.3)$$

$$\mathbf{K}(p) = \mathbf{P}(p-1)\mathbf{G}^H(p)\mathbf{\Gamma}^{-1}(p), \quad (4.1.4)$$

$$\mathbf{P}(p) = \lambda^{-1}[\mathbf{I}_M - \mathbf{K}(p)\mathbf{G}(p)]\mathbf{P}(p-1), \quad (4.1.5)$$

$$\hat{\mathbf{c}}(p) = \hat{\mathbf{c}}(p-1) + \mathbf{K}(p)[\mathbf{y}_{ms}(p) - \mathbf{G}(p)\hat{\mathbf{c}}(p-1)], \quad (4.1.6)$$

2. Least mean squares (LMS)

$$\hat{\mathbf{c}}(p) = \hat{\mathbf{c}}(p-1) + \mu(\mathbf{y}_c(p) - \hat{\mathbf{c}}(p-1)), \quad (4.1.7)$$

Similar as Eq. (4.1.6), $\hat{\mathbf{c}}(p)$ can also be updated using least mean squares algorithm in Eq. (4.1.7). The μ denotes the time-invariant stepsize for every coefficients updating.

After RLS and LMS recursion for every p , we can generate the estimated channel coefficients by CE-BEM or SVD-BEM in chapter 3. To predict the channel $\hat{h}_l[n]$, the BEM coefficient estimates in our receiver are given by multiplying the basis matrix :

$$\mathbf{D}_l \hat{\mathbf{c}}_l(p)$$

4.1.2 Derivation of the theoretical MSE and the optimum time-variant stepsize matrix

The estimated channel $\hat{\mathbf{h}}(p)$ is a linear combination of basis functions where is a matrix whose columns are the B basis functions, $\hat{\mathbf{h}}(p) = \mathbf{D}\hat{\mathbf{c}}(p)$

As before in Eq.(3.5.1), the channel MSE can be represented as $J(p)$,

$$\begin{aligned} J(p) &= E \left[(\mathbf{h}(p) - \mathbf{D}\hat{\mathbf{c}}(p))^T (\mathbf{h}(p) - \mathbf{D}\hat{\mathbf{c}}(p)) \right] \\ &= E \left[\mathbf{e}_o(p)^T \mathbf{e}_o(p) \right] + E \left[\mathbf{v}(p)^T \mathbf{v}(p) \right] - 2E \left[\mathbf{v}(p)^T \mathbf{D}^T \mathbf{e}_o(p) \right] \end{aligned} \quad (4.1.8)$$

Eq.(4.1.8) can be rewritten as the following with $\hat{\mathbf{c}}(p) = \mathbf{c}_o + \mathbf{v}(p)$ and $\mathbf{e}_o(p) = \mathbf{h}(p) - \mathbf{D}\mathbf{c}_o$, where \mathbf{c}_o denotes the true BEM coefficients, we set

$$J^o(p) = E \left[\mathbf{e}_o(p)^T \mathbf{e}_o(p) \right], \text{ and } J^{ex}(p) = E \left[\mathbf{v}(p)^T \mathbf{v}(p) \right] - 2E \left[\mathbf{v}(p)^T \mathbf{D}^T \mathbf{e}_o(p) \right],$$

where $\mathbf{D}^T \mathbf{e}_o(p) = \mathbf{D}^T (I - \mathbf{D}\mathbf{D}^T) \mathbf{h}_o + \mathbf{D}^T \mathbf{n}(p) = \mathbf{D}^T \mathbf{n}(p)$, thus

$$J^{ex}(p) = E \left[\mathbf{v}(p)^T \mathbf{v}(p) \right] - 2E \left[\mathbf{v}(p)^T \mathbf{D}^T \mathbf{n}(p) \right]$$

$J^o(p)$ is the same as derivation in Section 3.5.1.

we can obtain the LMS expression by the $\mathbf{c}(p+1) = \mathbf{c}(p) - \frac{\mu}{2} \left(\frac{\partial J}{\partial \mathbf{c}} \right)$, where

$$\frac{\partial J}{\partial \mathbf{c}} = 2\mathbf{D}^T \mathbf{D}\mathbf{c} - 2\mathbf{D}^T \mathbf{h}, \text{ thus,}$$

$$\hat{\mathbf{c}}(p+1) = \hat{\mathbf{c}}(p) - \mu \mathbf{D}^T (\mathbf{D}\hat{\mathbf{c}}(p) - \mathbf{h}(p)) \quad (4.1.9)$$

The scalar stepsize in this equation is replaced by a stepsize matrix A ,

where $A = \begin{pmatrix} a_1 & \mathbf{0} \\ \ddots & \ddots \\ \mathbf{0} & a_B \end{pmatrix}$ denotes the stepsize matrix and we assume $\mathbf{D}^T \mathbf{D} = I$, then

we can obtain

$$\hat{\mathbf{c}}(p+1) = (I - A)\hat{\mathbf{c}}(p) + A\mathbf{D}^T(p)\mathbf{h}(p) \quad (4.1.10)$$

The weight error vector at p -th occurrence $\mathbf{v}(p) = \mathbf{c}(p) - \mathbf{c}_0$ can be written as

$$\begin{aligned} \mathbf{v}(p+1) &= (I - A)\mathbf{v}(p) + A\mathbf{G}^T \mathbf{n}(p) \\ &= (I - A)^p \mathbf{v}_0 + A \sum_{j=0}^{p-1} (I - A)^{p-1-j} \mathbf{G}^T \mathbf{n}(j) \end{aligned} \quad (4.1.11)$$

Therefore the $J^{ex}(p) = E[\mathbf{v}(p)^T \mathbf{v}(p)] - 2E[\mathbf{v}(p)^T \mathbf{D}^T \mathbf{n}(p)]$ can be calculated as

$$\begin{aligned} (1) E[\mathbf{v}(p)^T \mathbf{v}(p)] &= \text{trace} \left((I - A)^{2p} E[\mathbf{v}_0 \mathbf{v}_0^T] \right) \\ &+ E \left[\mathbf{v}_0^T (I - A)^p A \sum_{j=0}^{p-1} (I - A)^{p-1-j} \mathbf{G}^T \mathbf{n}(j) \right] \\ &+ E \left[\sum_{j=0}^{p-1} \mathbf{n}(j)^T \mathbf{G} (I - A)^{p-1-j} \mathbf{v}_0 \right] \\ &+ \text{trace} \left[A^2 \left(\sum_{j=0}^{p-1} (I - A)^{2(p-1-j)} \right) \mathbf{G}^T \mathbf{R}_N \mathbf{G} \right] \end{aligned}$$

Where \mathbf{R}_N denotes the noise correlation matrix

Note if $\mathbf{D}^T \mathbf{D} \neq I$ like CE-BEM,

$$E[\mathbf{v}(p+1)^T \mathbf{v}(p+1)] = E[\text{trace}((I - A\mathbf{D}^T \mathbf{D})^{p+1} (I - A\mathbf{D}^T \mathbf{D})^{T p+1} \mathbf{v}(0)\mathbf{v}(0)^T)] + E[\sum \text{trace}(\dots)]$$

is hard to simplify. Thus we consider only the orthogonal bases.

$$\begin{aligned} (2) E[\mathbf{v}(p)^T \mathbf{D}^T \mathbf{n}(p)] &= (I - 2A)^p E[\mathbf{v}_0^T \mathbf{D}^T \mathbf{n}(p)] + \sum_{j=0}^{p-1} (I - 2A)^{p-1-j} E[\mathbf{n}(j) \mathbf{D} \mathbf{D}^T \mathbf{n}(p)] \\ &= (I - 2A)^p E[\mathbf{v}_0^T \mathbf{D}^T \mathbf{n}(p)] \end{aligned}$$

So the $J^{ex}(p)$ is equal to (1)+(2), and the total MSE = $J^o(p) + J^{ex}(p)$,

For the converging steady state ($p \rightarrow \infty$), the total MSE can be simplified as

$$\begin{aligned}
J_\infty &= J^o(\infty) + \text{trace} \left[A^2 \left(\sum_{j=0}^{p-1} (I-A)^{2(p-1-j)} \right) \mathbf{D}^T \mathbf{R}_N \mathbf{D} \right] \\
&= J^o(\infty) + \text{trace} \left[A^2 (2A - A^2)^{-1} \mathbf{D}^T \mathbf{R}_N \mathbf{D} \right]
\end{aligned} \tag{4.1.12}$$

In case of white noise, Eq. (4.1.11) can be written as

$$\begin{aligned}
J_\infty &= J^o(\infty) + \text{trace} \left[A^2 (2A - A^2)^{-1} \sigma_w^2 \mathbf{D}^T \mathbf{D} \right] \\
&= J^o(\infty) + \text{trace} \left[A (2I_B - A)^{-1} \right] \sigma_w^2
\end{aligned} \tag{4.1.13}$$

The total MSE are correlated with the bases type, stepsize matrix and the noise. Moreover, we would like to find the optimum time-variant stepsizes for each BEM coefficient which could minimize the coefficient MSE $E[\mathbf{v}(p+1)^T \mathbf{v}(p+1)]$, where $\mathbf{v}(p+1)$ can be represented as Eq. (4.1.11), we use the column matrix property: $\mathbf{v}^T \mathbf{v} = \text{trace}(\mathbf{v} \mathbf{v}^T)$, thus

$$\begin{aligned}
E[\mathbf{v}(p+1)^T \mathbf{v}(p+1)] &= E[\text{trace}((I-A)^2 \mathbf{v}(p)^T \mathbf{v}(p))] \\
&\quad + E[\text{trace}(\mathbf{A} \mathbf{D}^T \mathbf{n}(p)^T \mathbf{v}(p)^T (I-A))] \\
&\quad + E[\text{trace}((I-A) \mathbf{v}(p) \mathbf{n}(p)^T \mathbf{D} \mathbf{A})] \\
&\quad + E[\text{trace}(\mathbf{A} \mathbf{D}^T \mathbf{n}(p) \mathbf{n}(p)^T \mathbf{D} \mathbf{A})]
\end{aligned}$$

then

$$\begin{aligned}
E[\mathbf{v}(p+1)^T \mathbf{v}(p+1)] &= \text{trace} \left((I-A)^2 E[\mathbf{v}(p)^T \mathbf{v}(p)] \right) \\
&\quad + \text{trace} \left((I-A) \mathbf{A} \mathbf{D}^T E[\mathbf{n}(p) \mathbf{v}(p)^T] \right) \\
&\quad + \text{trace} \left(\mathbf{D} \mathbf{A} (I-A) E[\mathbf{v}(p) \mathbf{n}(p)^T] \right) \\
&\quad + \text{trace} \left(\mathbf{D} \mathbf{A}^2 \mathbf{D}^T E[\mathbf{n}(p) \mathbf{n}(p)^T] \right)
\end{aligned} \tag{4.1.14}$$

And we assume $\mathbf{n}(p)$ and $\mathbf{v}(p)$ are zero mean and mutually statistically independent stationary signal, thus we can simplify Eq. (4.1.14) as

$$\begin{aligned}
E[\mathbf{v}(p+1)^T \mathbf{v}(p+1)] &= \sum_{i=1}^B (1-a_i) b_i^2(p) + 4\sigma^2 \text{trace} \left(\sum_{i=1}^B a_i^2 \mathbf{d}_i \mathbf{d}_i^T \right) \quad (b_i^2(p) = E[v_i(p)^2]) \\
&= \sum_{i=1}^B \left((1-a_i) b_i^2(p) + 4\sigma^2 a_i^2 \right)
\end{aligned}$$

And then we can derive the optimum stepsize a_i as discussed in [48],

$$\frac{\partial E[\mathbf{v}(p+1)^T \mathbf{v}(p+1)]}{\partial a_i} = 0$$

$$\text{The result is } a_i = \frac{b_i^2(p)}{\sum_B b_i^2(p) + 4\sigma^2} \propto b_i^2(p), \quad (4.1.15)$$

where $b_i^2(p)$ denotes the each coefficient MSE ($E[(c_i(p) - c_{o,i})^T (c_i(p) - c_{o,i})]$)

At initial state ($p=0$), $\mathbf{c}_o = \mathbf{0}$, then

$$a_i = \frac{b_i^2(0)}{\text{const}} = \frac{E[\mathbf{c}_o \mathbf{c}_o^T]}{\text{const}} = \frac{E[\mathbf{D}^T \mathbf{h}_o \mathbf{h}_o^T \mathbf{D}]}{\text{const}} = \frac{\mathbf{D}^T E[\mathbf{h}_o \mathbf{h}_o^T] \mathbf{D}}{\text{const}} = \frac{\mathbf{D}^T \mathbf{R}_l \mathbf{D}}{\text{const}} \quad (4.1.16)$$

Note the $\mathbf{D}^T \mathbf{R}_l \mathbf{D}$ denotes the diagonal matrix whose diagonal elements contains the eigenvalues of the real channel correlation matrix \mathbf{R}_l .

In practice $b_i^2(p)$ is unknown and a_i should be adjusted for each step p since

$[b_1^2(p), \dots, b_B^2(p)]$ changes as the algorithm converges. As discussed in [48], when

a_i are set proportional to $b_i(0)$, the optimum time-invariant stepsizes can be obtained.

4.1.3 Eigen weighted for adaptive algorithms

Knowledge of the significance of Jake's bases is rarely used in conventional algorithms. An adaptive algorithm taking into account the importance weights of the basis is expected to improve convergence.

From the derivation of Section 4.1.2, the proposed eigen-weighted EW-RLS algorithm uses a different stepsizes for each principle basis. These stepsizes are

time-invariant and weighted proportional to the importance of the eigenvectors. The algorithm is based on the fact that the importance of the eigenvectors becomes progressively smaller along diagonal elements of the matrix Λ_l in Eq.(3.3.4) as the importance decay. As a result, the algorithm adjusts coefficients with more important basis in large steps, and coefficients with less important basis in small steps. The proposed algorithm requires only the same amount of computation as the conventional LMS and RLS.

Incorporating this knowledge of the significance of the bases into the conventional EW-RLS, we propose to adjust coefficients with more importance in more adaptive information and coefficients with less importance in less adaptive information. For this purpose, a stepsize matrix \mathbf{S} with diagonal form is introduced:

$$A = \begin{pmatrix} a_0 & & 0 \\ & \ddots & \\ 0 & & a_{B-1} \end{pmatrix} \quad (4.1.17)$$

As discussed in last section, $a_i \propto b_i(0) \propto \sqrt{\lambda_i}$

where $a_i = \frac{\lambda_i}{\sum_{i=0}^{B-1} \lambda_i} \times B$ ($i = 0, \dots, B-1$) and B is the number of principle bases we

exploited, elements u_i are time-invariant and decreasing from u_0 . The modified adaptive algorithm compared to Eq.(4.1.3)-(4.1.6), called the eigen-weighted EW-RLS algorithm from [48] is expressed as

$$\begin{aligned} \mathbf{U}(p) &= \mathbf{A}\mathbf{C}^H(p)(\lambda\mathbf{I}_{ms} + \mathbf{C}(p)\mathbf{I}\mathbf{C}^H(p))^{-1} \\ \hat{\mathbf{c}}(p) &= \hat{\mathbf{c}}(p-1) + \mathbf{U}(p)[\mathbf{y}_{ms}(p) - \mathbf{G}(p)\hat{\mathbf{c}}(p-1)], \end{aligned} \quad (4.1.18)$$

The scalar stepsize in EW-RLS is replaced by a stepsize matrix \mathbf{S} , and the eigen weighted LMS can be also expressed by replacing μ in Eq.(4.1.7) as time-invariant stepsize matrix \mathbf{S} .

4.2 BEM bases tracking

In both Slepian and SVD BEM methods, we obtain the bases by means of the channel correlation matrix \mathbf{R}_l which can be decomposed by the eigen-decomposition, then we acquired the eigenvalues and eigenvectors. The eigenvectors denote the bases we exploited to approximate the channel, and the eigenvalues corresponding to the eigenvectors denote the weight of eigenvectors importance. When f_d changing, we need to a Doppler frequency estimator like [52-53], then we have to calculate the new bases, this task has much more difficulty than CE-BEM.

The channel correlation matrix \mathbf{R}_l could be composed through the Jake's model or the Slepian model with two parameters: the symbol rate $\frac{1}{T_s}$ and the Doppler frequency f_d . The symbol rate are almost fixed in communication procedure, therefore, we focus on the influence when Doppler frequency changes.

In Section 3.4, we face a problem that in a low mobility (low Doppler frequency) environment, the time-domain Slepian basis expansion model cannot represent the channel effectively. As the result, we would like to track the BEM bases when Doppler frequency changes within the low frequency range.

Thus, we will propose the numerical method to track the variation of the principle eigenvalues and eigenvectors in Section 4.2.1 and 4.2.2 respectively.

4.2.1 Principle eigenvalues adaptive

Figure 4.1 and 4.2 shows the eigenvalues variation under Doppler frequency changes. We can observe that in low Doppler frequency (about 10 to 30 for Slepian bases and 10 to 40 for Jake's bases) the number of principle eigenvalues might be two to four, which conclude most importance in corresponding principle eigenvectors.

Focus on Jake's bases, we like to track the eigenvalues when Doppler frequency does not fixed. After Doppler frequency shifts, the basis also changes due to the channel correlation changes, hence if we can track the new eigenvalue, the new basis can be obtained easily than before.

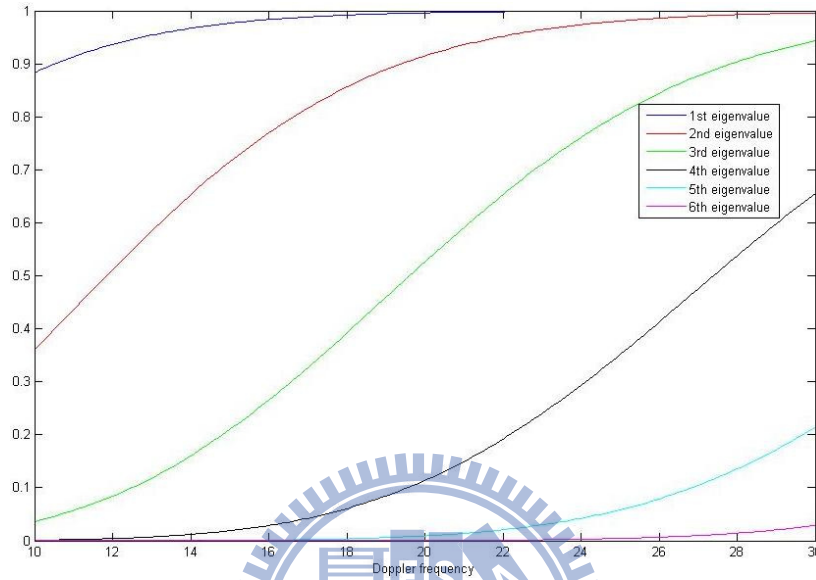


Figure 4.1 Eigenvalues variation under f_d changes in Slepian bases

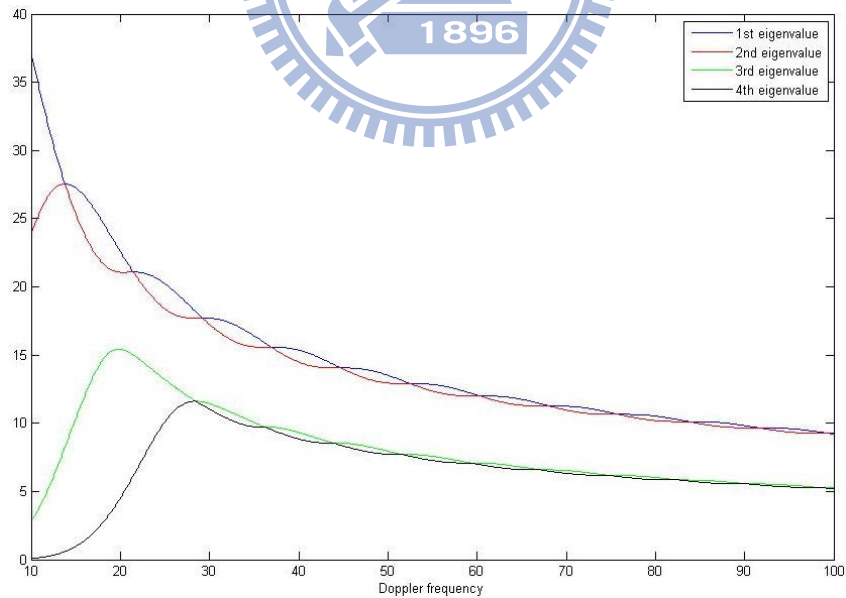


Figure 4.2 Eigenvalues variation under f_d changes in Jake's bases

- Linear fitting

In order to find the relationship of the eigenvalues and Doppler frequency below forty hertz, we first use two straight lines to fit the curve in Fig. 4.2.

Assume the eigenvalue locus can be approximated in a linear form

$$\lambda_K = p_{1,K} f_d + p_{2,K} \quad (4.2.1)$$

Where K denotes the K -th principle eigenvalues (here we consider $K=1,2$), and $p_{1,K}$ and $p_{2,K}$ are parameters must to obtained.

The solutions for $\begin{bmatrix} p_{1,K} \\ p_{2,K} \end{bmatrix}$ can be derived using least-square numerical method,

$$\begin{bmatrix} p_{1,1} \\ p_{2,1} \end{bmatrix} = (A^H A)^{-1} A^H b_1 = \begin{bmatrix} -0.60 \\ 36.75 \end{bmatrix} \quad (4.2.2)$$

$$\begin{bmatrix} p_{1,2} \\ p_{2,2} \end{bmatrix} = (A^H A)^{-1} A^H b_2 = \begin{bmatrix} -0.42 \\ 30.22 \end{bmatrix} \quad (4.2.3)$$

Where $A = \begin{bmatrix} 10 & 1 \\ 11 & 1 \\ \vdots & \vdots \\ 40 & 1 \end{bmatrix}$ and $b_K = \begin{bmatrix} \lambda_{K,fd=10} \\ \lambda_{K,fd=11} \\ \vdots \\ \lambda_{K,fd=40} \end{bmatrix}$.

Thus we can obtain Eq. (4.2.1) in

$$\begin{cases} \lambda_1 = -0.60 f_d + 36.75 \\ \lambda_2 = -0.42 f_d + 30.22 \end{cases} \quad (4.2.4)$$

- Quadratic fitting

Assume the eigenvalue locus can be approximated in a quadratic form

$$\lambda_K = p_{1,K} f_d^2 + p_{2,K} f_d + p_{3,K} \quad (4.2.5)$$

The solutions for $\begin{bmatrix} p_{1,K} \\ p_{2,K} \\ p_{3,K} \end{bmatrix}$ can be derived using least-square numerical method,

$$\begin{bmatrix} p_{1,1} \\ p_{2,1} \\ p_{3,1} \end{bmatrix} = (A^H A)^{-1} A^H b_1 = \begin{bmatrix} 0.025 \\ -1.86 \\ 50.42 \end{bmatrix} \quad (4.2.6)$$

$$\begin{bmatrix} p_{1,2} \\ p_{2,2} \\ p_{3,2} \end{bmatrix} = (A^H A)^{-1} A^H b_2 = \begin{bmatrix} 0.008 \\ -0.84 \\ 34.75 \end{bmatrix} \quad (4.2.7)$$

Where $A = \begin{bmatrix} 10^2 & 10 & 1 \\ 11^2 & 11 & 1 \\ \vdots & \vdots & \vdots \\ 40^2 & 40 & 1 \end{bmatrix}$ and $b_K = \begin{bmatrix} \lambda_{K,fd=10} \\ \lambda_{K,fd=11} \\ \vdots \\ \lambda_{K,fd=40} \end{bmatrix}$.

Thus we can obtain Eq. (4.2. 5) in

$$\begin{cases} \lambda_1 = 0.025 f_d^2 - 1.86 f_d + 50.42 \\ \lambda_2 = 0.008 f_d - 0.84 f_d + 34.75 \end{cases} \quad (4.2.8)$$

- Exponential fitting

Assume the eigenvalue locus can be approximated in a exponential decayed form

$$\lambda_K = p_{1,K} \times e^{p_{2,K} f_d} + p_{3,K} \quad (4.2.9)$$

The solutions for $\begin{bmatrix} p_{1,K} \\ p_{2,K} \\ p_{3,K} \end{bmatrix}$ can be derived using least-square numerical method,

Just a little difference from above procedure, we first omit the constant $p_{3,K}$, and then

$$\lambda_K = p_{1,K} \times e^{p_{2,K} f_d} \rightarrow \ln(\lambda_K) = \ln(p_{1,K}) + p_{2,K} f_d$$

$$\begin{bmatrix} \ln(p_{1,K}) \\ p_{2,K} \end{bmatrix} = (A^H A)^{-1} A^H b_K \quad K = 1, 2 \quad (4.2.10)$$

where $A = \begin{bmatrix} 10 & 1 \\ 11 & 1 \\ \vdots & \vdots \\ 40 & 1 \end{bmatrix}$ and $b_K = \begin{bmatrix} \ln(\lambda_{K,fd=10}) \\ \ln(\lambda_{K,fd=11}) \\ \vdots \\ \ln(\lambda_{K,fd=40}) \end{bmatrix}$.

Then we would obtain $\begin{bmatrix} \ln(p_{1,K}) \\ p_{2,K} \end{bmatrix}$ then to easily obtain $\begin{bmatrix} p_{1,K} \\ p_{2,K} \end{bmatrix}$.

Do not forget there is a constant $p_{3,K}$ must to calculate. Run a loop for the constant

changes, we can quickly choose $p_{3,K}$ is equal to 14 and 10 for the best $\begin{bmatrix} p_{1,K} \\ p_{2,K} \\ p_{3,K} \end{bmatrix}$

($K=1,2$) in Eq. (4.2.9) that can approximate the true line with minimum square error.

Thus we already obtain Eq. (4.2.9) in

$$\begin{cases} \lambda_1 = 53.69 \times e^{-0.09 f_d + 14} \\ \lambda_2 = 27.18 \times e^{-0.044 f_d + 10} \end{cases} \quad (4.2.11)$$

With the eigenvalues, we can obtain the corresponding eigenvectors (bases) through the power method algorithm in Table 4.1:

Table 4.1 The power method algorithm

Power method algorithm
0) Goals: given $\hat{\lambda}$ to find \hat{v}
1) Initialization: $v_0 = [1 \ 1 \ \dots \ \dots \ 1]^T$
2) for $i = 1$ to m
$v_{i+1} = (R_L - \hat{\lambda} I_N)^{-1} v_i;$
$v_{i+1} = v_{i+1} / \ v_{i+1}\ _2;$
<i>end</i>

4.2.2 Principle eigenvectors adaptive

After Doppler frequency shifts, the bases also change due to the channel correlation changes. More directly than Section 4.2.1, we like to track the principle eigenvectors when Doppler frequency does not fixed.

At first, we observe the principle basis waveform in several Doppler frequency in Fig. 4.4. Then we suppose these basis waveforms could be approximated through the sine function instead of the exponential or polynomial function in Section 4.2.1.

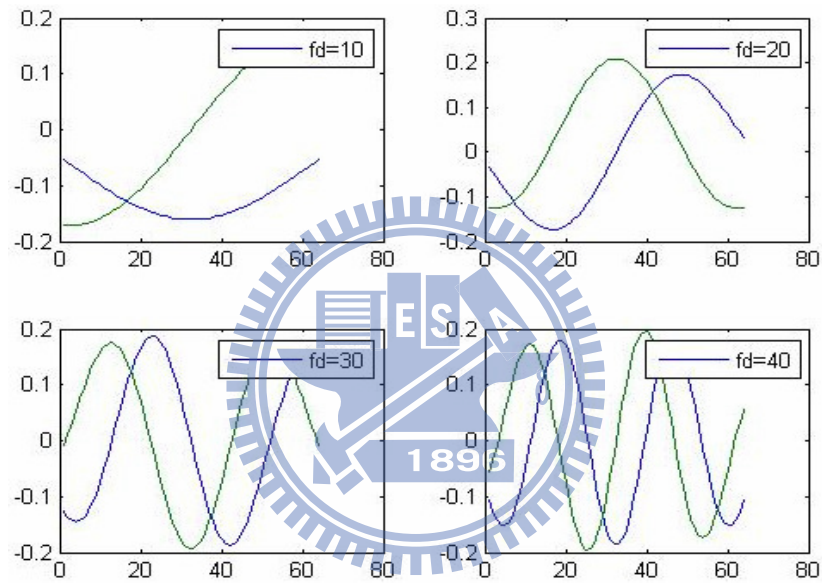


Figure 4.4 The principle bases waveform in different Doppler frequency. (N=64)

We assume the eigenvector shape can be approximated in a sinusoidal wave form in a fixed Doppler frequency f_d :

$$v_b[n] = p_{1,b} \times \sin(p_{2,b}n + p_{3,b}), \quad n = 0 \sim N-1 \quad (4.3.12)$$

where b denotes the b -th principle eigenvector (here we consider $b=1,2$), and $p_{1,b}$, $p_{2,b}$ and $p_{3,b}$ are parameters must to be obtained, which all are the function of f_d .

The similar procedure as 4.2.1, we would obtain three parameters $\begin{bmatrix} p_{1,b} \\ p_{2,b} \\ p_{3,b} \end{bmatrix}$ ($b=1,2$) for

each Doppler frequency ($f_d = 10 \sim 40$), and then the next step we would like to find the relationship between parameters and the f_d .

1. $p_{1,b}$ versus f_d :

We do not care $p_{1,K}$, the scalar of eigenvectors, we can simply set $p_{1,K}$ a constant.

2. $p_{2,b}$ versus f_d :

For several $p_{2,b}$ (frequency component of the sine wave) under f_d , we plot the Fig. 4.5(a) for observation. Then we suppose we can use a straight line with positive slope to fit. Repeat the procedure from Eq. (4.2.1) to (4.2.3), the linear fitting curve would be calculated as:

$$\begin{cases} p_{2,1} = 0.0059 f_d - 0.025 \\ p_{2,2} = 0.0061 f_d - 0.023 \end{cases} \quad (4.3.13)$$

For simplicity, we even see $p_{2,2}$ as $p_{2,1}$ because of the root mean square error (RMSE) for these two different lines are 0.00845 and 0.008464, which are both almost identical and small enough.

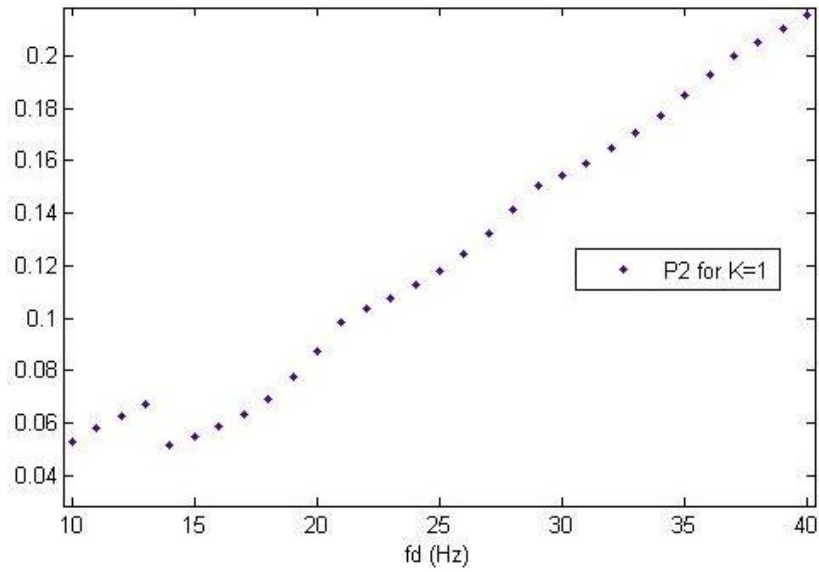


Figure 4.5 (a) $p_{2,1}$ versus Doppler frequency

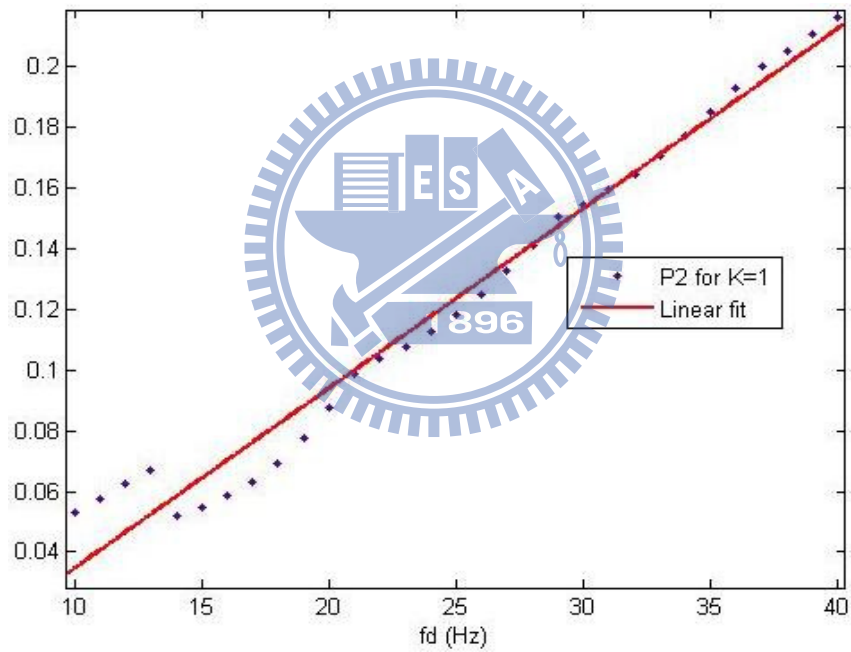


Figure 4.5 (b) Linear fitting for $p_{2,1}$

3. $p_{3,b}$ versus f_d :

For several $p_{3,b}$ under f_d , we plot the Fig. 4.6 for observation. We normalized the $p_{3,K}$ (phase component of the sine wave) in the range $[0, \pi]$. Then we suppose we

can use the piecewise-linear function to fit like before or directly establish a dictionary for $p_{3,b}$.

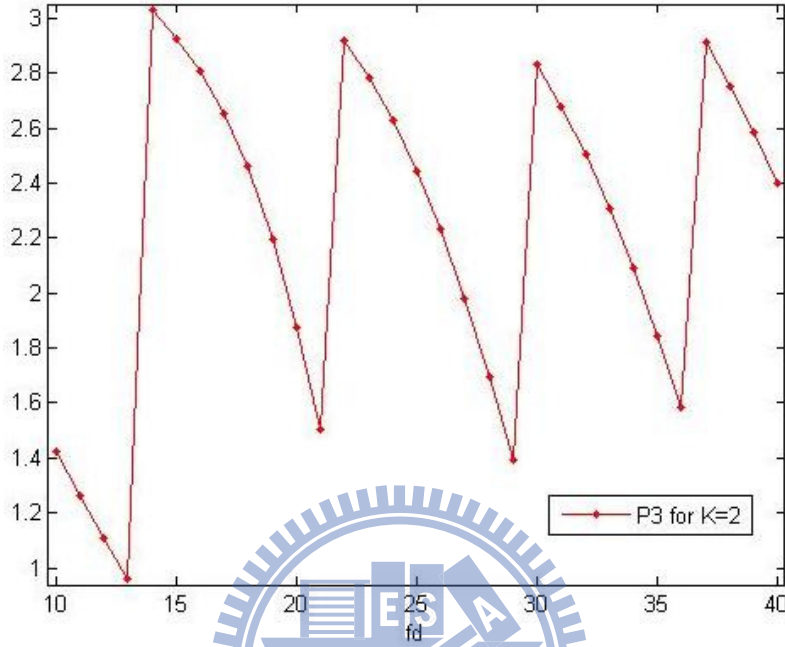


Figure 4.6 $p_{3,2}$ versus Doppler frequency

Finally, we could easily know the new three parameters $\begin{bmatrix} p_{1,b} \\ p_{2,b} \\ p_{3,b} \end{bmatrix}$ based on the relationship, and then quickly obtain the new approximated principle basis in Eq. (4.3.11).

To summarize, when Doppler frequency changes, there are four possible ways to derive the new bases, which can be roughly depicted in figure 4.7, where the methods 1 and 2 are the conventional schemes, and they waste either computational complexity or memory. And the proposed methods 3 and 4 are discussed in Section 4.2, the Table 4.2 depicts all the complexity and memory needed for them. Where N denotes the length of bases, d denotes the range of Doppler frequency, here we

choose 10~40 in our simulation, b is the number of the principle bases, here we choose 2~4 that ensure contain about 80% energy, and K represents the times of power method iterations ($K > 4$, $RMSE < 10^{-3}$).

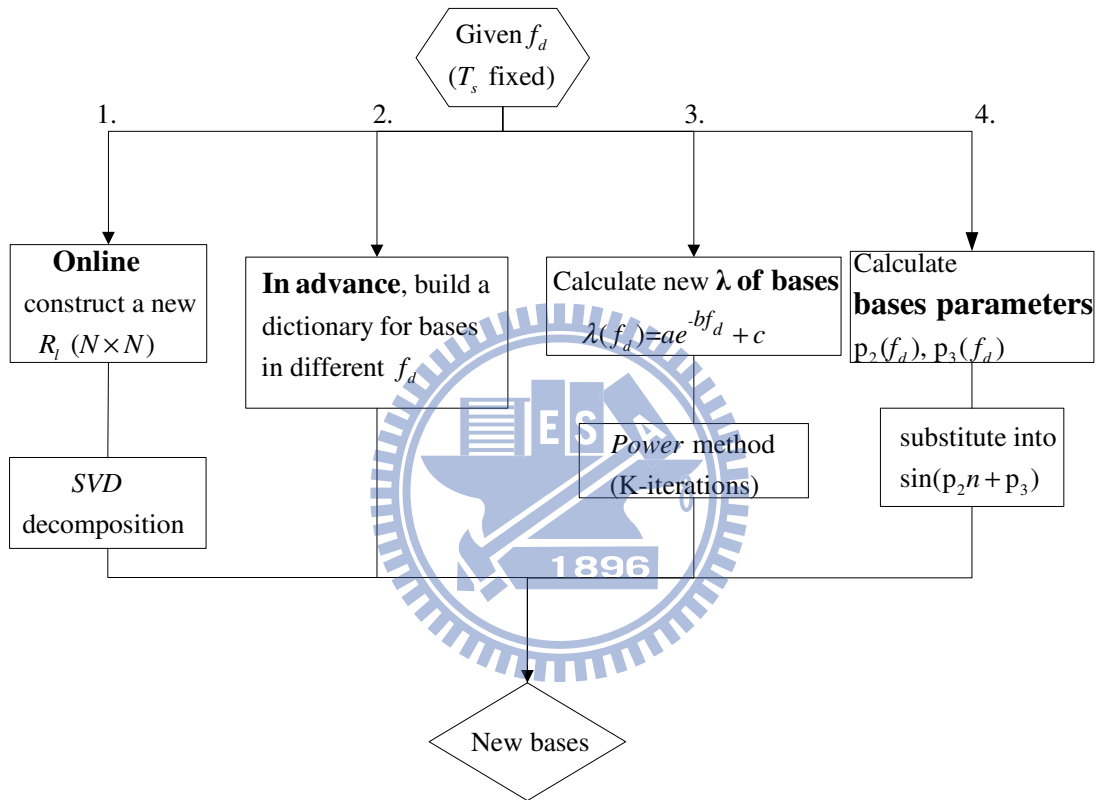


Figure 4.7 Four methods to obtain the new bases after f_d changes.

Table 4.2 Complexity and memory needed for four methods.

Way	1	2	3	4
Memory store	0	Nd	$3b$	$d + 2$
Complexity	$12N^3 + N$	0	$K(N^3 + N^2) + 4$	$b + 1$

To summarize this chapter, the eigen weighted adaptive algorithms (RLS and LMS) has been proposed. Since the BEM coefficients have different importance, we can derive the optimum stepsizes for each coefficient as discussed in [48]. Moreover, we can acquire the new bases when Doppler frequency changes with less complexity and memories.



Chapter 5

Computer Simulations

In this chapter, computer simulations are used to verify the algorithms and methods discussed in Chapter 2 to Chapter 4. At first we define some parameters of OFDM system we used in the whole thesis in Section 5.1, and in Section 5.2, we compare the conventional time and frequency-domain channel estimation and interpolation methods, then observe the constellation for BER-SNR curve, which has much relevance for channel MSE-SNR curve. The performance of the CE-BEM, SVD-BEM and their modified methods will be shown in Section 5.3 and 5.4 respectively. The issue of carrier frequency offset and phase noise will also be discussed in Section 5.5.

Adaptive method is a practical problem for BEM. In Section 5.6, we will update the BEM coefficients by exploiting EW-RLS algorithm, and then propose a method to enhance the convergence rate in fixed Doppler frequency. Moreover, when Doppler frequency unfixed environment, we compare two proposed methods to track the new basis under the new Doppler frequency in Section 5.7.

5.1 Simulation parameters

OFDM system parameters similar to those used in IEEE 802.11a are adopted here: the number of subcarriers is $N = 64$, and the system sampling rate is $f_s = 1$ KHz leading to a subcarrier spacing can be calculated as $\Delta f = f_s / N$, number of OFDM signals per packet $N_s = 10$ and the QPSK modulation is selected.

We assume to have perfect synchronization since the aim is to observe channel estimation performance. Moreover, we have chosen the guard interval to be greater than the maximum delay spread L in order to avoid inter-symbol interference.

In these simulations the signal to noise ratio (SNR) was varied from 0 to 40 dB. For each SNR value 300 Monte Carlo independent trials were conducted and the mean-square-error (MSE) and root-mean-square-error (RMSE) defined below was employed as a performance measure of the channel estimates:

$$MSE = \frac{1}{N_t} \sum_{i=1}^{N_t} \|\hat{\mathbf{h}}_i - \mathbf{h}\|^2 \quad RMSE = \sqrt{\frac{1}{N_t} \sum_{i=1}^{N_t} \|\hat{\mathbf{h}}_i - \mathbf{h}\|^2}$$

where N_t is the number of Monte Carlo trials, \mathbf{h} is the vector comprising the true channel coefficients, and $\hat{\mathbf{h}}_i$ is the estimate of the channel coefficients in the i -th trial.

5.2 Time-invariant channel estimation

The multi-path fading channel is Rayleigh fading has a power delay profile (PDP) of $1.2257 \times e^{-0.8l}$ ($0 \leq l < 10$) in Fig.5.1, which is normalized to unit energy.

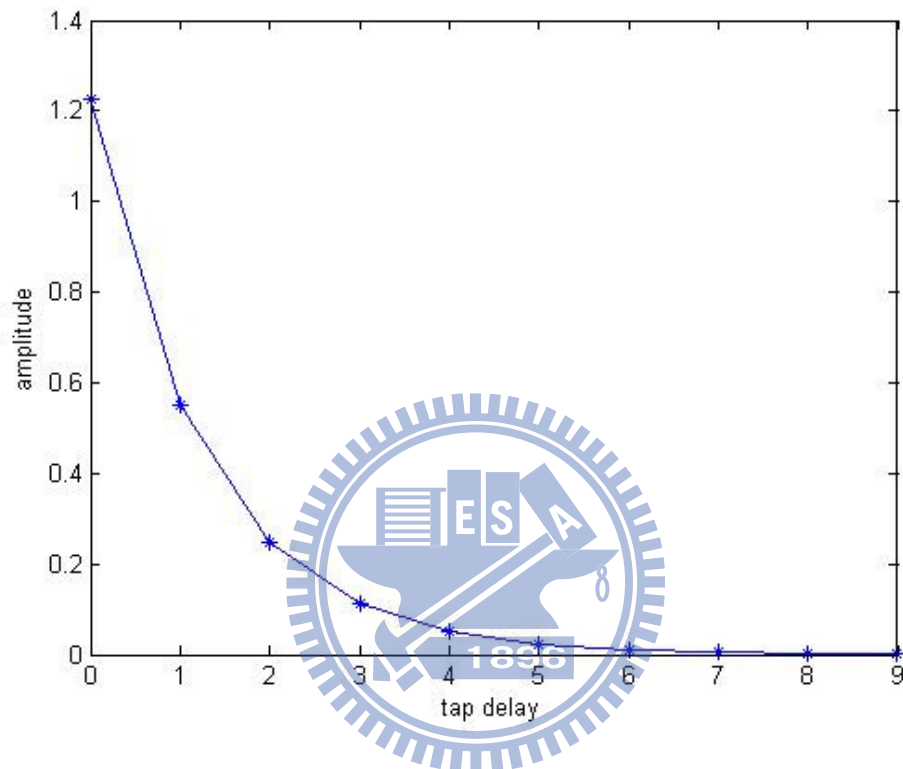


Figure 5.1 The power delay profile of the multi-path channel.

The conventional time and frequency-domain time-invariant channel estimation method are introduced in Section 2.3.

Figure 5.2 illustrates the performances of these schemes, we can find out that they have the almost the same performance, but there are some advantages and drawbacks for them, based on the purpose to choose from them.

Figure 5.3 and figure 5.5 both compare the different interpolation methods of comb type by using different criterion. And the received constellation can be shown in figure 5.4, it illustrates if there is not channel estimation before detection, the bit error

rate will be very terrible.

Figure 5.6 shows the performance comparison in different pilot ratio in block type, the result tells the more pilots we use, the lower MSE we have.

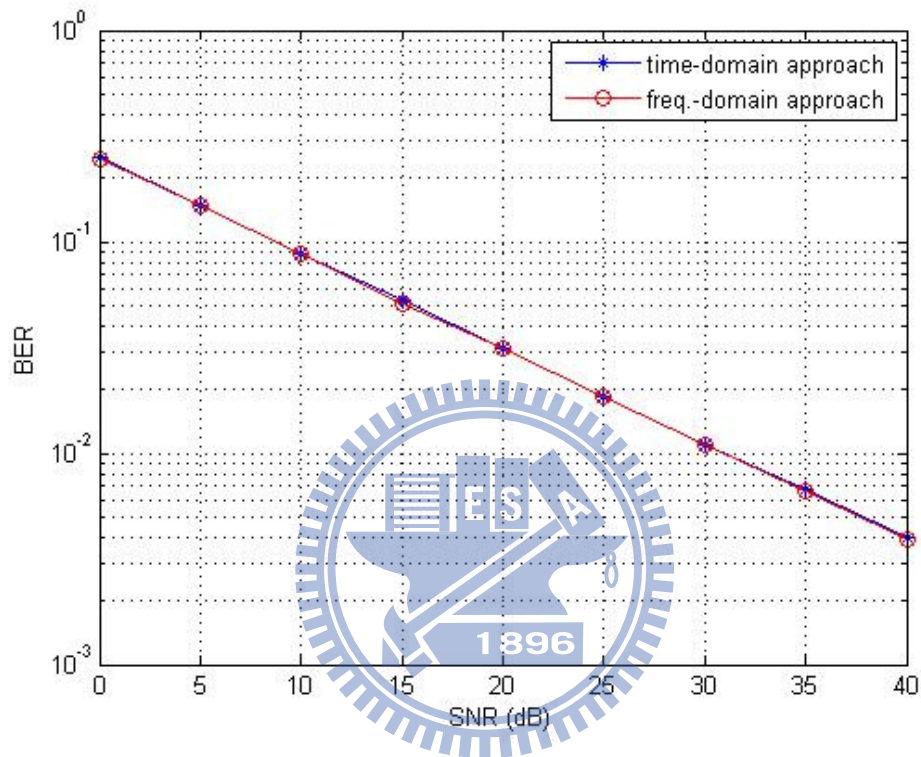


Figure 5.2 Comparison of time and frequency domain channel estimation

- Block type pilot arrangement

Each block consists of a fixed number of symbols, which is 30 in the simulation. Pilots are sent in all the sub-carriers of the first symbol of each block and channel estimation is performed by using LS estimation.

- Comb type pilot arrangement

All of the possible interpolation techniques (linear interpolation, second order interpolation, low-pass interpolation, spline cubic interpolation, and time domain

interpolation) are applied to LS estimation with pilot ratio 0.125.

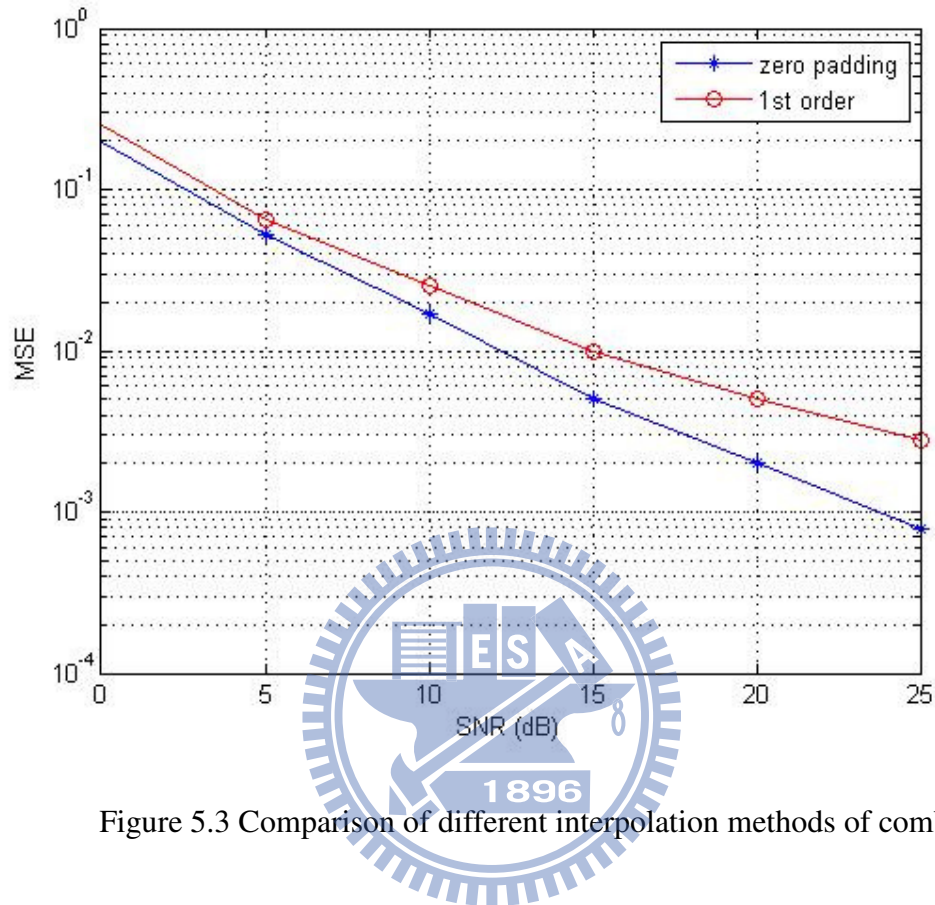


Figure 5.3 Comparison of different interpolation methods of comb type

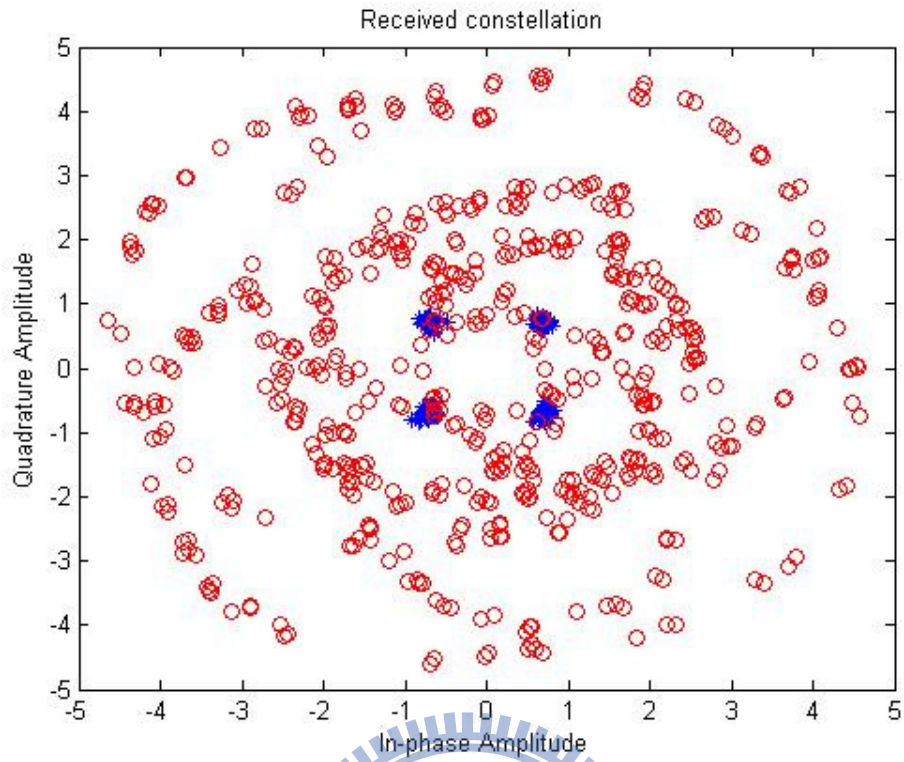


Figure 5.4 Received constellation with (*) and without (o) channel estimation (ZP)

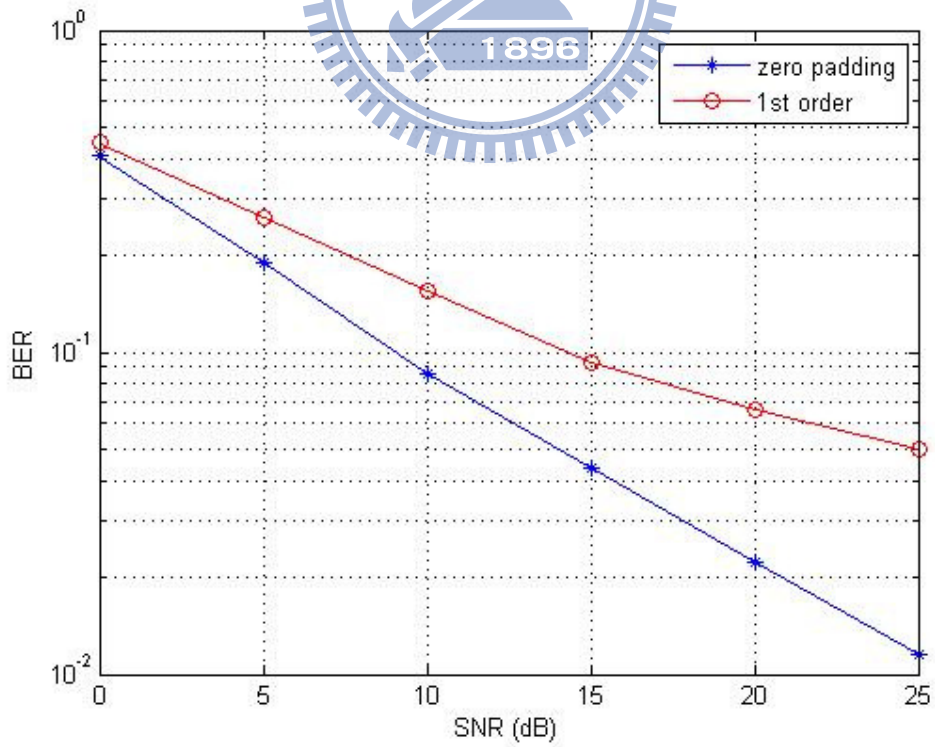


Figure 5.5 Comparison of different interpolation methods of comb type

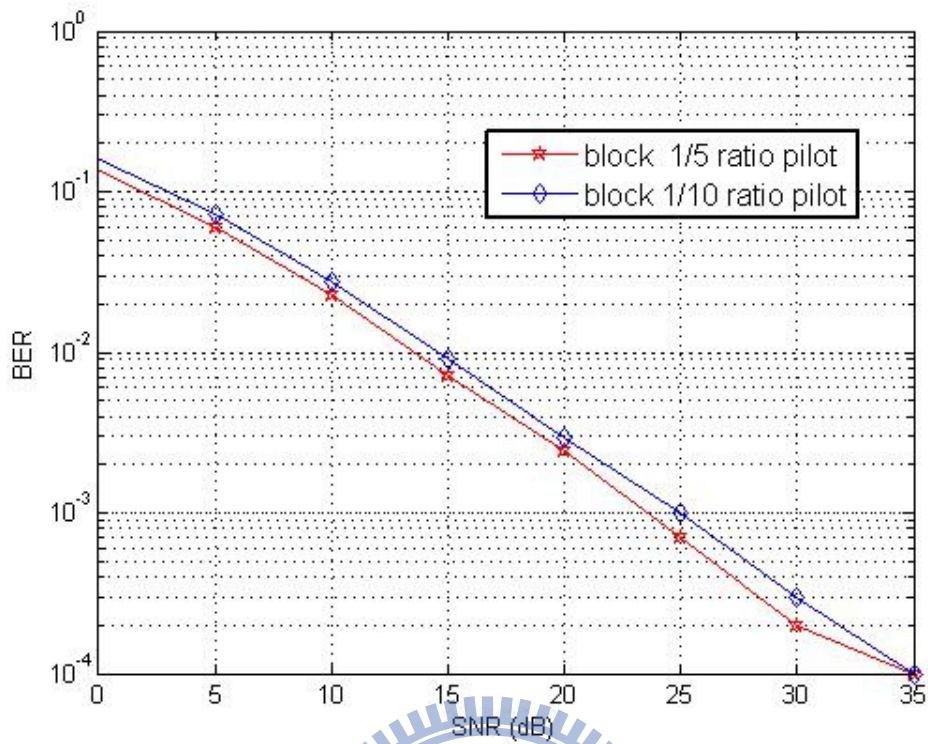


Figure 5.6 Comparison of different pilot ratio in block type

In figure 5.3 to 5.5, we conclude the estimated channel MSE and the BER for detector have the much highly relationship. We can depend on the MSE-SNR curve to estimate the tendency of BER-SNR curve.

5.3 CE-BEM

The complex-exponential basis expansion model is discussed in Section 3.1.1. And the modified methods (oversampling and non-uniform sampling) for CE-BEM are in Section 3.1.2 and 3.1.3.

Figure 5.7 illustrates the performances of these schemes, we can find out that the over-sampling ($K=2$) method and the non-uniform sampling method both also can enhance the CE-BEM.

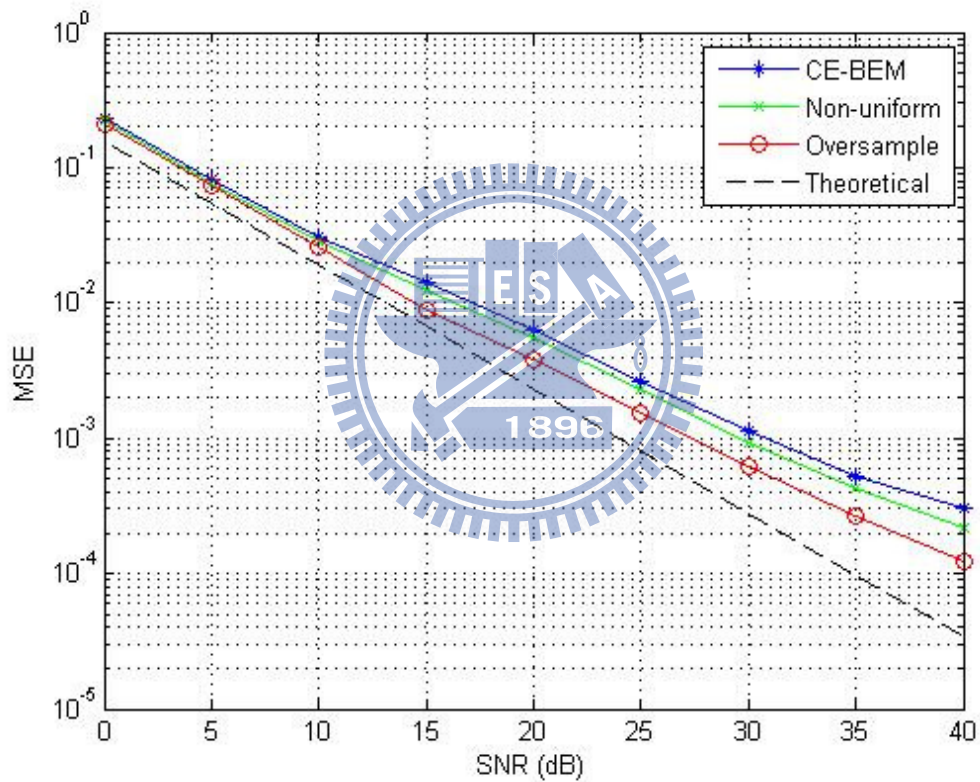


Figure 5.7 Comparison of different CE-based methods.

5.4 SVD-BEM

There are some basis expansion model discussed in Section 3.2, which are SVD-BEM, Wiener SVD-BEM, Slepian-BEM and UB-BEM. We will compare their performance in MSE criterion through computer simulation in this section.

Figure 5.8 distinguish the two main kind of basis, Jake's basis are derived from the zero-order Bessel function of first kind and the Slepian basis are generated from the Slepian sequence in (3.200). The ACF in figure 5.8 denotes the auto-correlation function and $f_d = 50$, $T_s = 0.001$. Moreover, figure 5.9 illustrates the principle basis for Jake's and Slepian model in $f_d = 18$ and $T_s = 0.001$.

Figure 5.10 illustrates the enhancement for SVD-BEM in different number of basis by adding the Wiener filter to increase the SNR. And for the purpose to compare their performance, Figure 5.11 plot their estimated channel MSE to the SNR curves, we could conclude that the SVD-BEM and UB-BEM have the almost same performance, but if the pre-estimator does not good (like CE in Jake's model), the UB would not as good as SVD-BEM.

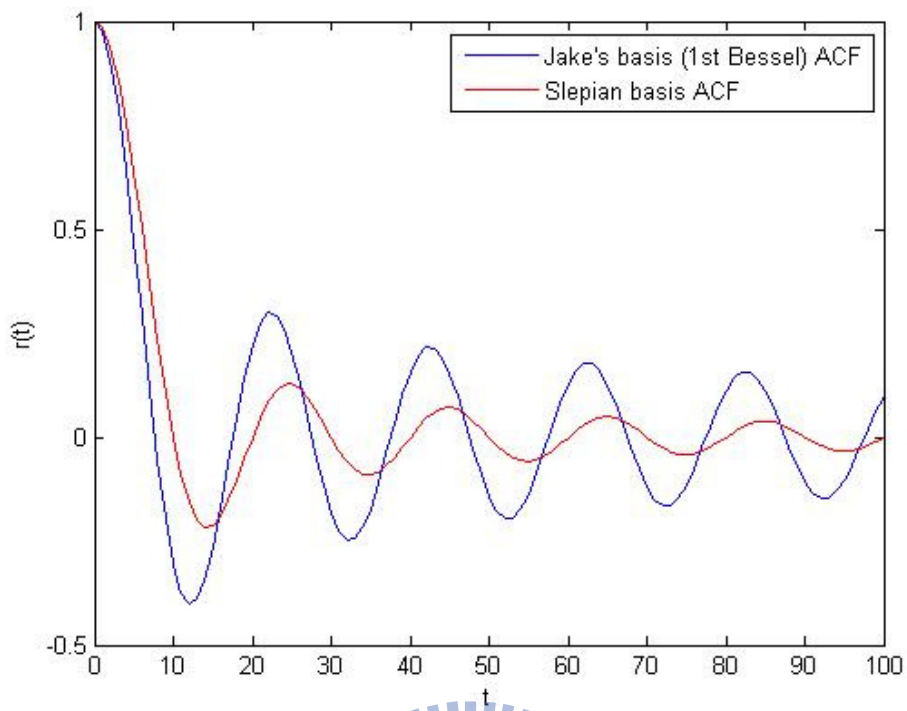


Figure 5.8 ACF of Jake's and Slepian basis ($f_d = 50$, $T_s = 0.001$)

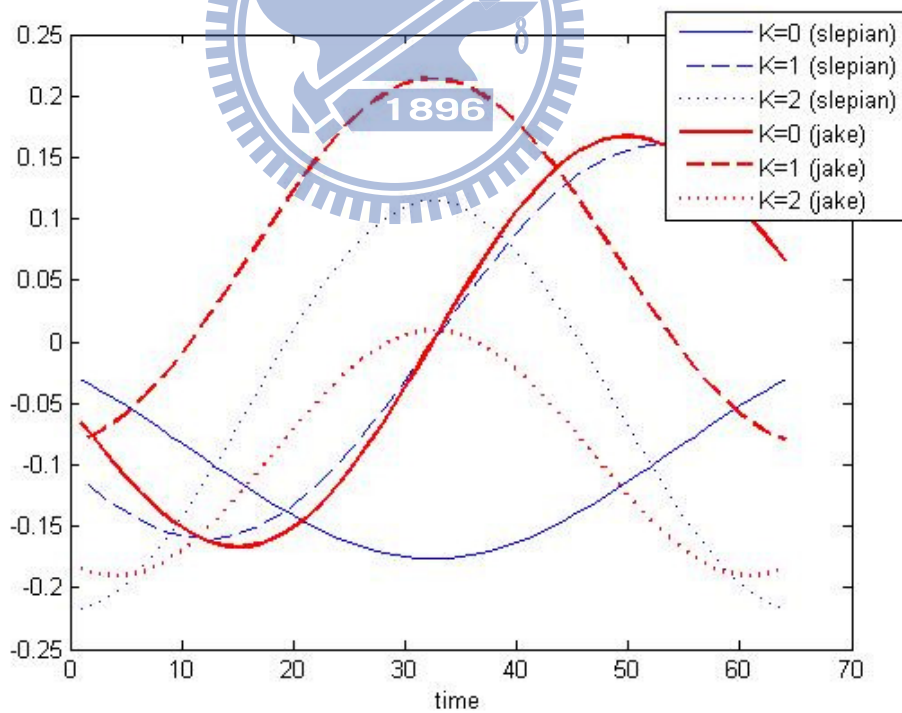


Figure 5.9 Principle basis for Slepian and Jake's model ($f_d = 18$, $T_s = 0.001$)

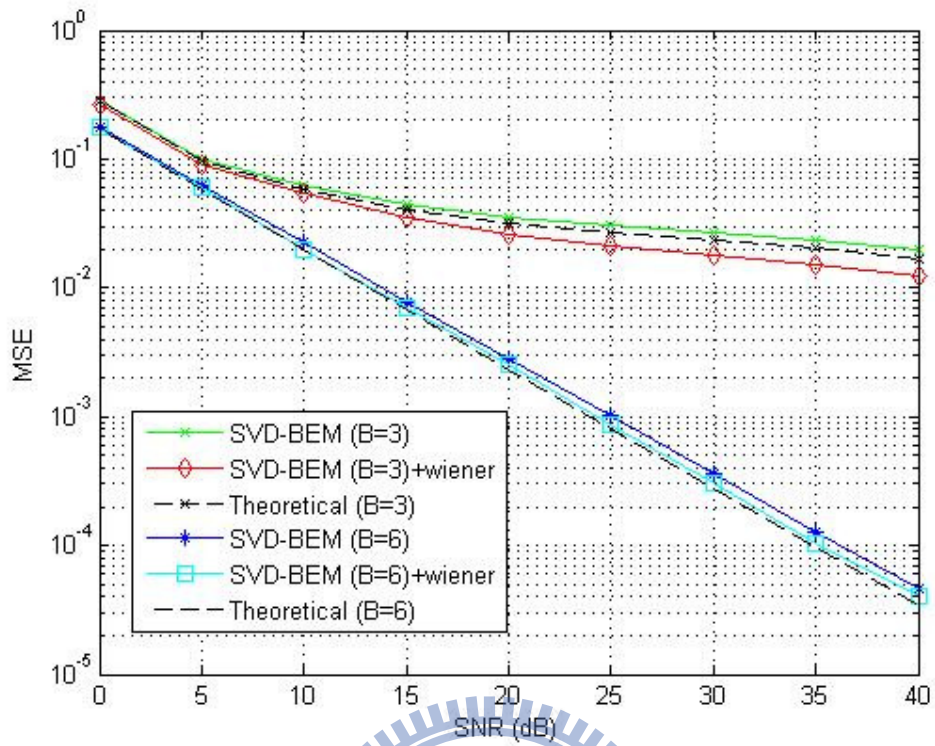


Figure 5.10 Comparison of SVD-BEM and Wiener filter applied

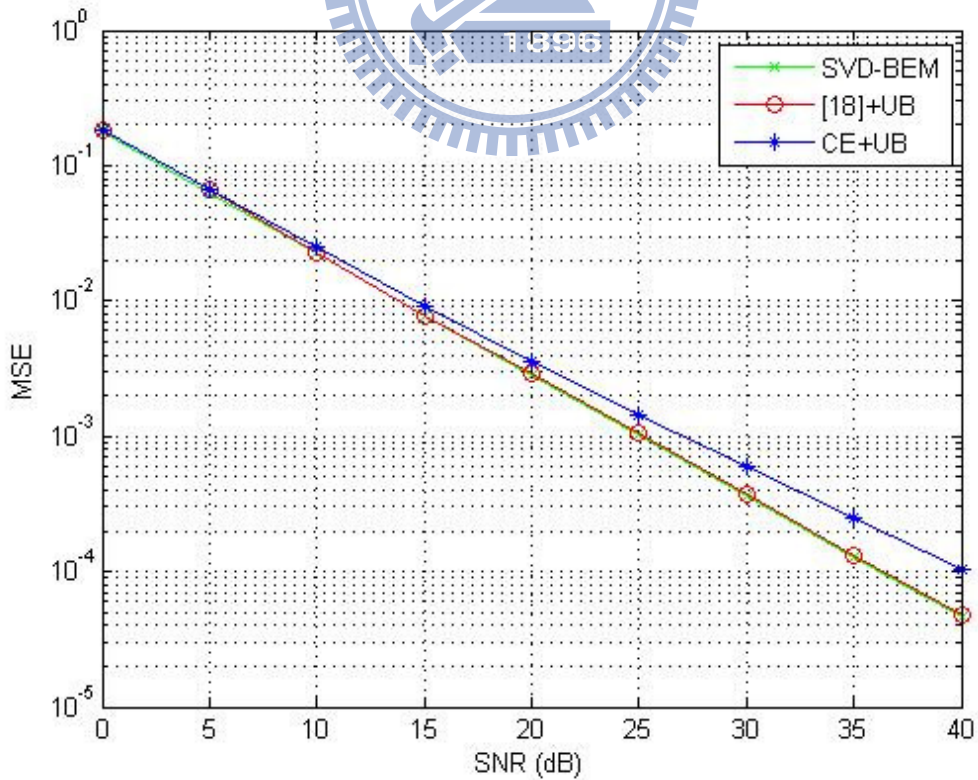


Figure 5.11 Comparison of SVD and UB.

5.5 Consideration of CFO and PHN

There is a practical issue that the effect of CFO and PHN discussed in Section 2.2, and we propose a method in Section 3.3 to deal with this problem.

Figure 5.12 illustrate the performance of mixed channel method in Section 3.3.1 when PHN occurs and them apply it. The phase noise is generated by the Wiener process with $f_{3dB} = 100Hz$. If without any mechanism for PHN effect, the channel estimator will fail.

In figure 5.13, we investigate the accuracy of CFO estimation. This figure plots the residual CFO at different SNRs. For each SNR, 300 independent CFO estimation are performed at the presence of phase noise, (Phase noise is simulated by passing a white Gaussian process through a one-pole Butterworth low pass filter with 3dB bandwidth

$f_o = 100KHz$. The covariance matrix of phase noise $(\mathbf{R}_\phi)_{m,n} = \left(\frac{\pi\phi_{rms}}{180}\right)^2 \exp\left(-\frac{2\pi f_o |m-n|}{f_s}\right)$,

and the CFO ε is generated as a uniform distribution over $[-1,1]$.). From this figure, it is obvious that the residual CFO is consistently close to zero.

Table 5.1 emphasizes it again, in different SNR, the CFO MSE are shown. Through the CFO estimator, the CFO effect can be removed clearly.

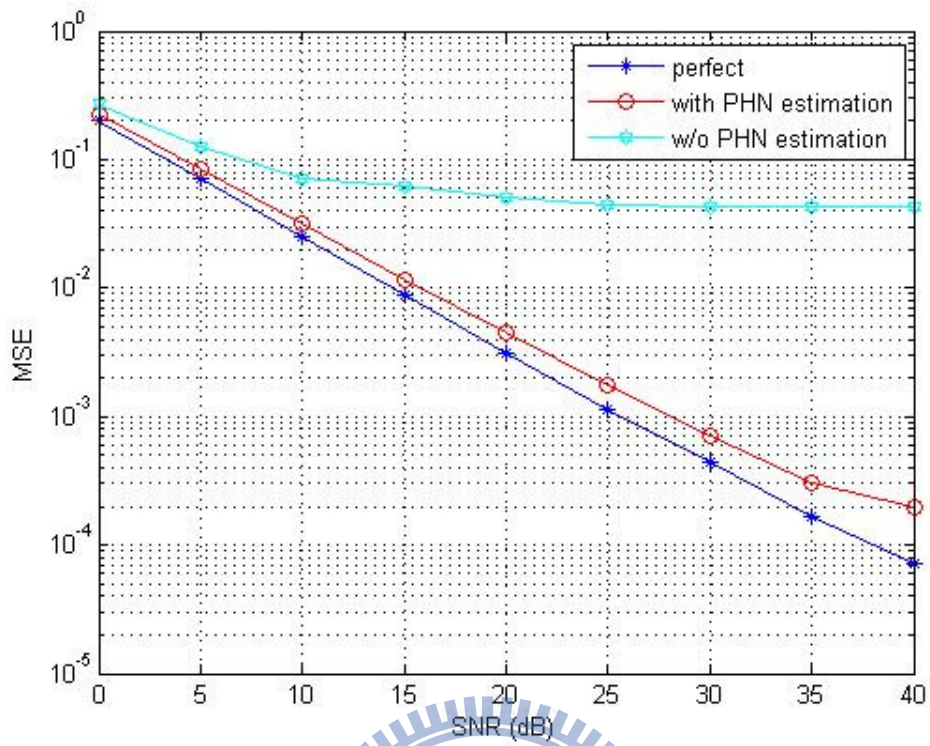


Figure 5.12 The mixed PHN channel estimation performance

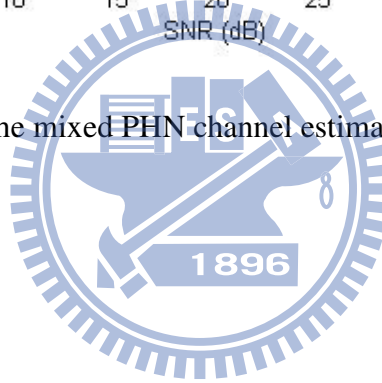


Table 5.1 CFO estimation MSE in different SNR

SNR (dB)	10	15	20
CFO MSE	7.18×10^{-4}	2.19×10^{-4}	7.23×10^{-5}

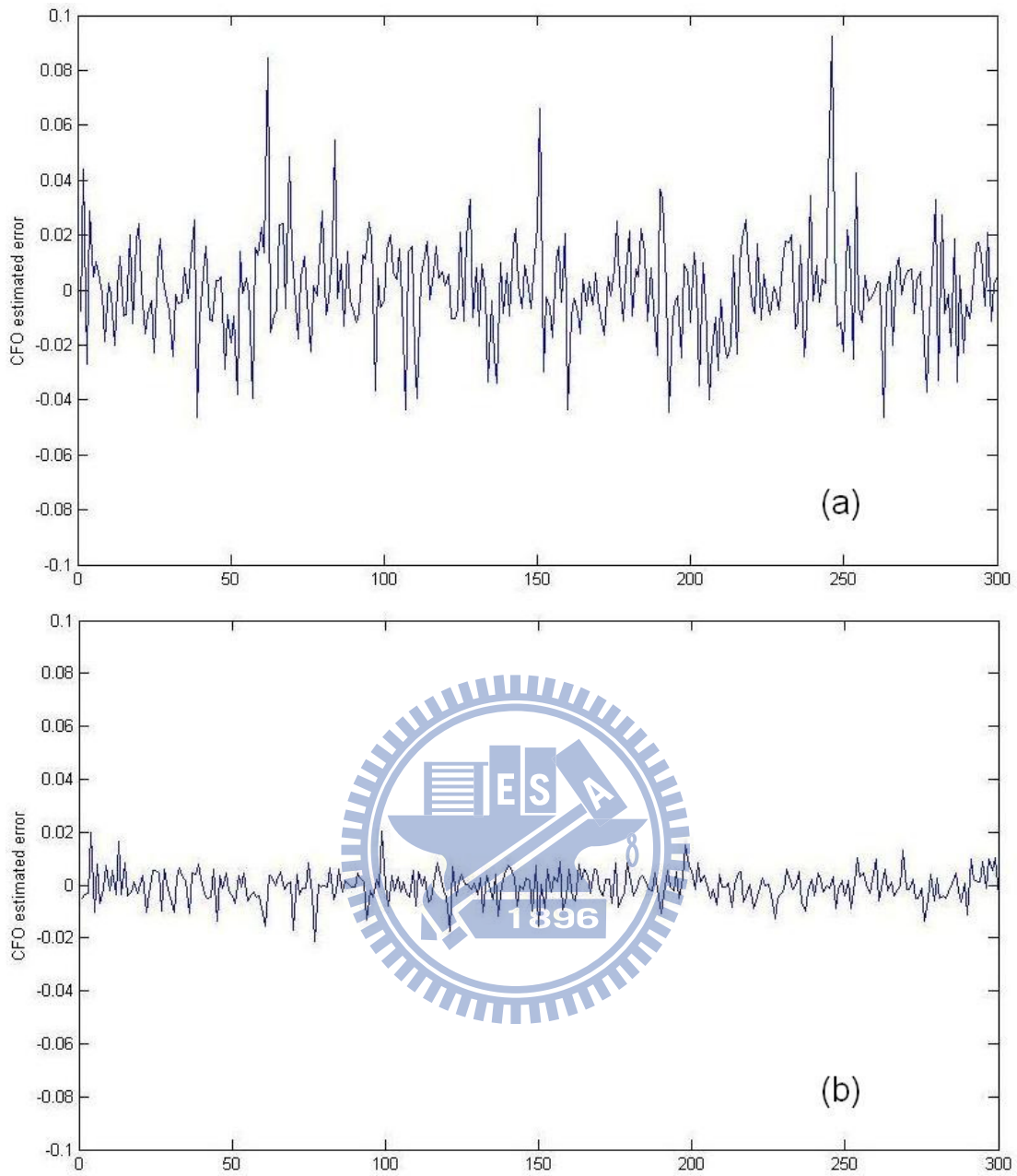


Figure 5.13 CFO estimation error in different SNR (a) SNR=10 (b) SNR=20 (dB)

5.6 EW-RLS with eigen weighting

We have discussed the EW-RLS BEM coefficients updating algorithm in fixed Doppler frequency environment in Section 4.2.1 and its modified method by exploiting the significance of each basis in Section 4.2.2.

Figure 5.14(a-b) illustrate the practical CE and SVD-BEM coefficients state change in five iterations (p), due to the slight difference in each iteration, we would like to track the BEM coefficients instead of the real channel.

Figure 5.15(a-i) illustrate the coefficients tracking under increasing iteration. We use nine basis ($B + 1=9$) in CE-BEM. After several iterations, the tracking line would lock the real value, despite the coefficients still varies due to time-invariant channel, the algorithm can always follow the variation. And Fig.5.16(a-c) are the similar but following the SVD-BEM, moreover, there is one more eigen weighted tracking line.

Figure 5.17 illustrates the learning curve of CE-BEM coefficients tracking in f_d changes at the 200-th iteration. And figure 5.18 also illustrates the learning curves of SVD-BEM coefficients tracking in f_d changes at the 200-th iteration, these two curves tell us the faster convergence rate the eigen-weighted EW-RLS method has.

Finally, figure 5.19 illustrate MSE versus SNR curve by using different ms (number of points consideration each iterations) after the algorithm converges.

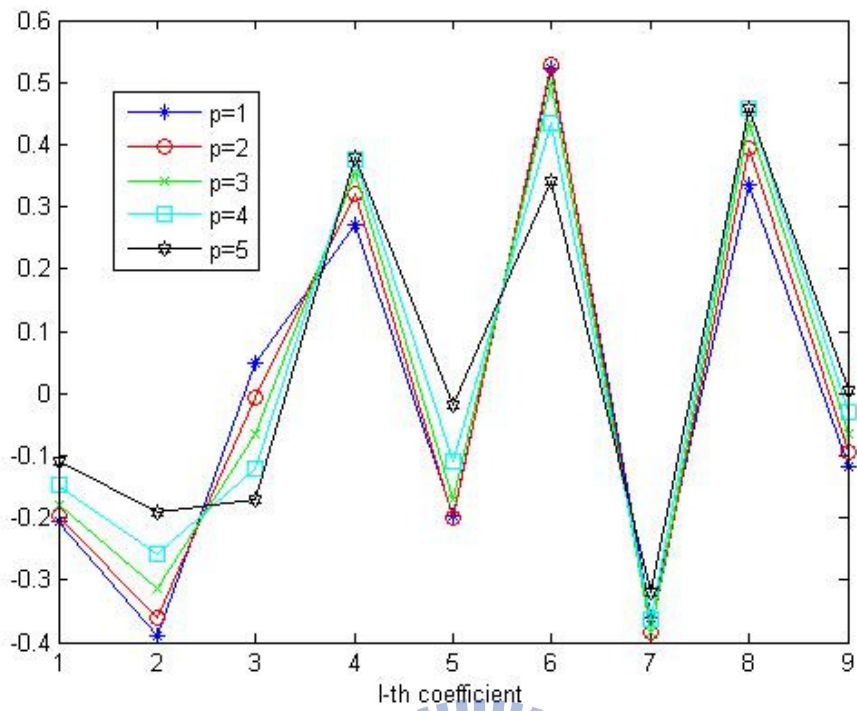


Figure 5.14(a) CE-BEM coefficients changes in successive iteration

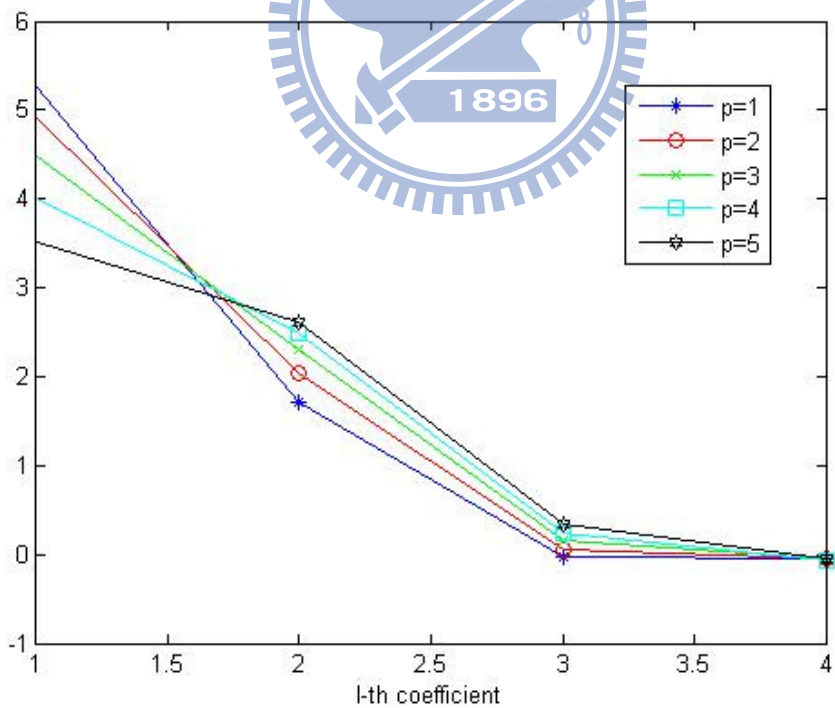


Figure 5.14 (b) SVD-BEM coefficients changes in successive iteration

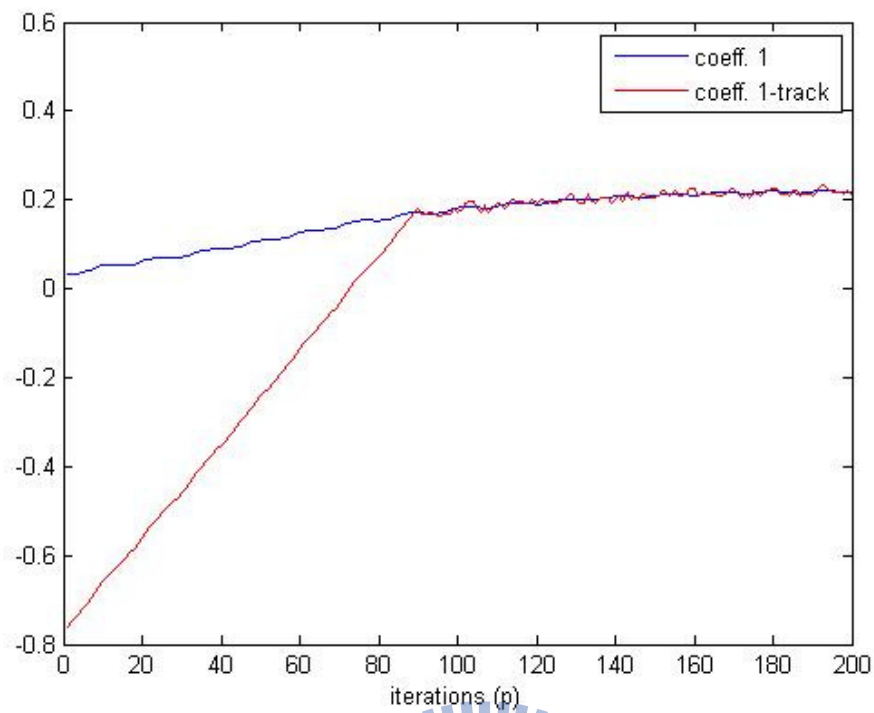


Figure 5.15(a) CE-BEM 1st-coefficient tracking

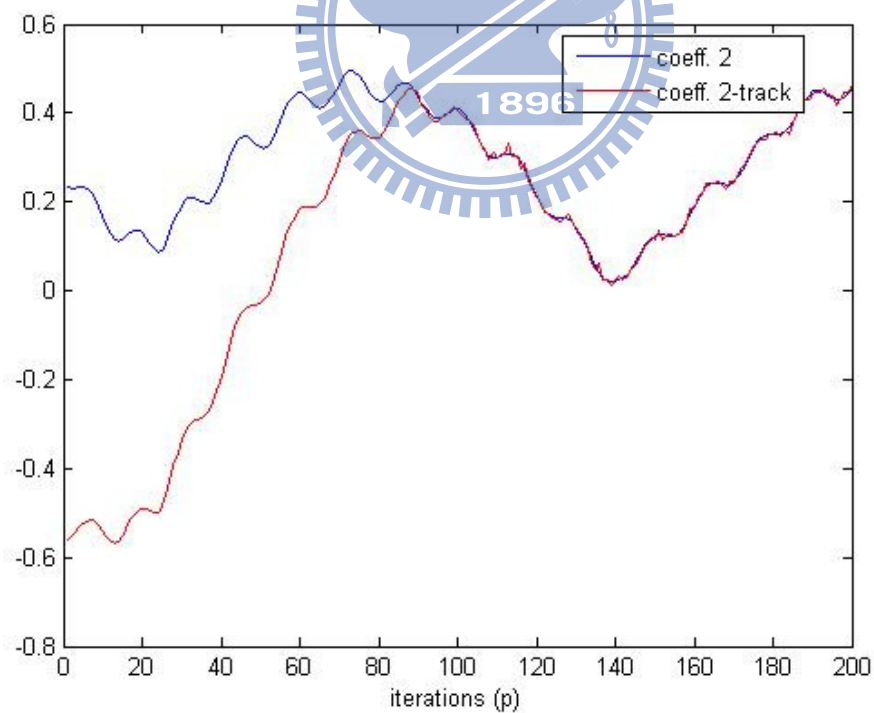


Figure 5.15 (b) CE-BEM 2nd-coefficient tracking

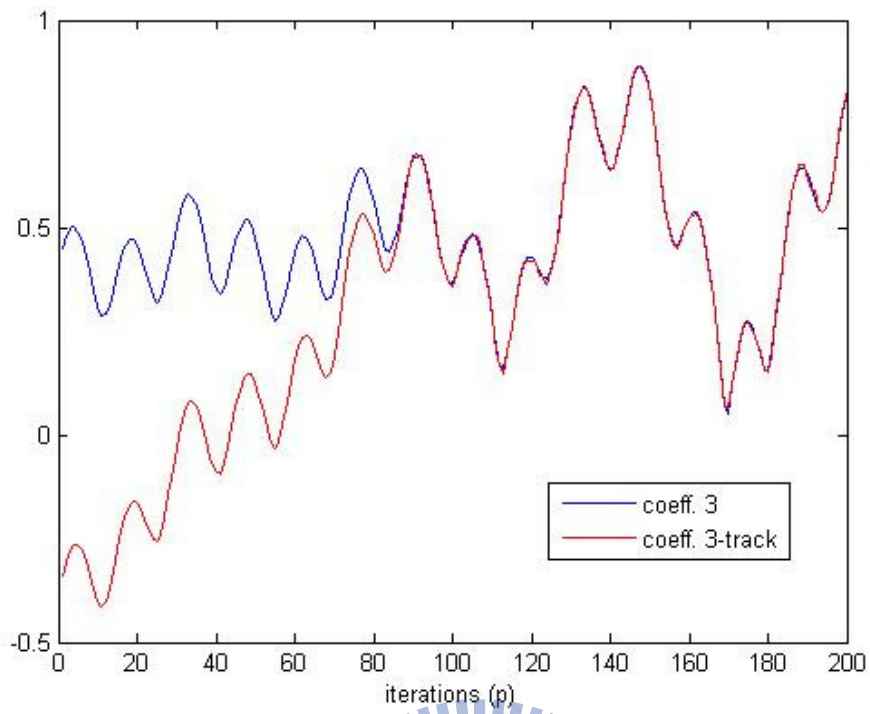


Figure 5.15 (c) CE-BEM 3rd-coefficient tracking

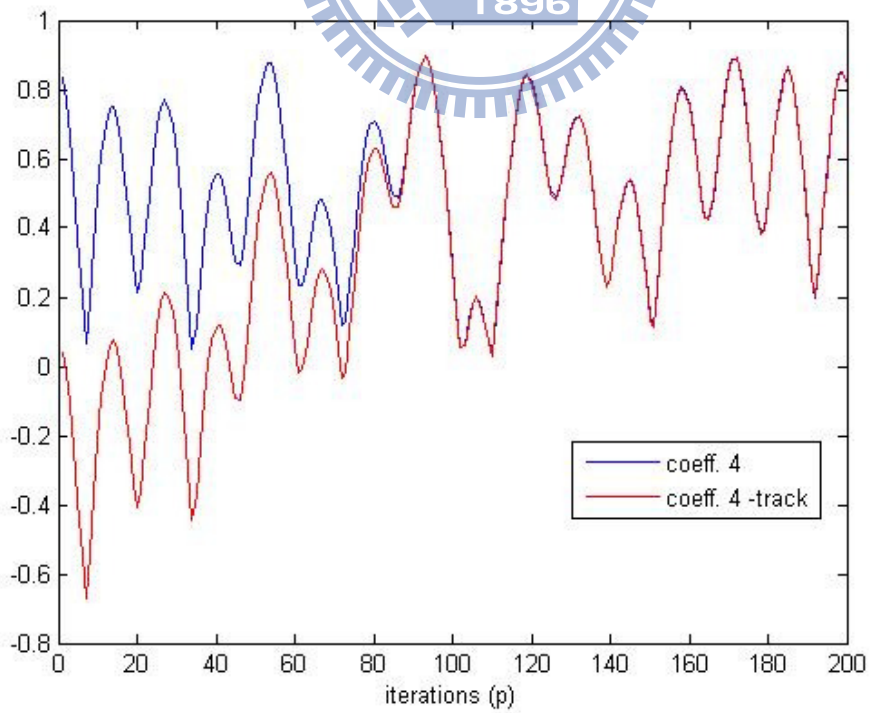


Figure 5.15 (d) CE-BEM 4th-coefficient tracking

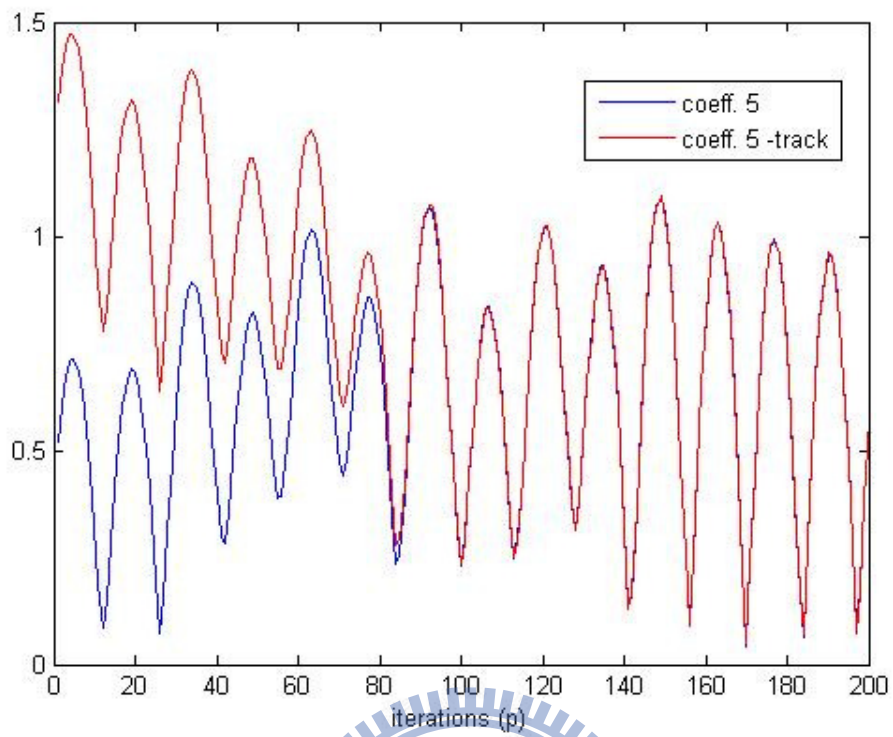


Figure 5.15 (e) CE-BEM 5th-coefficient tracking

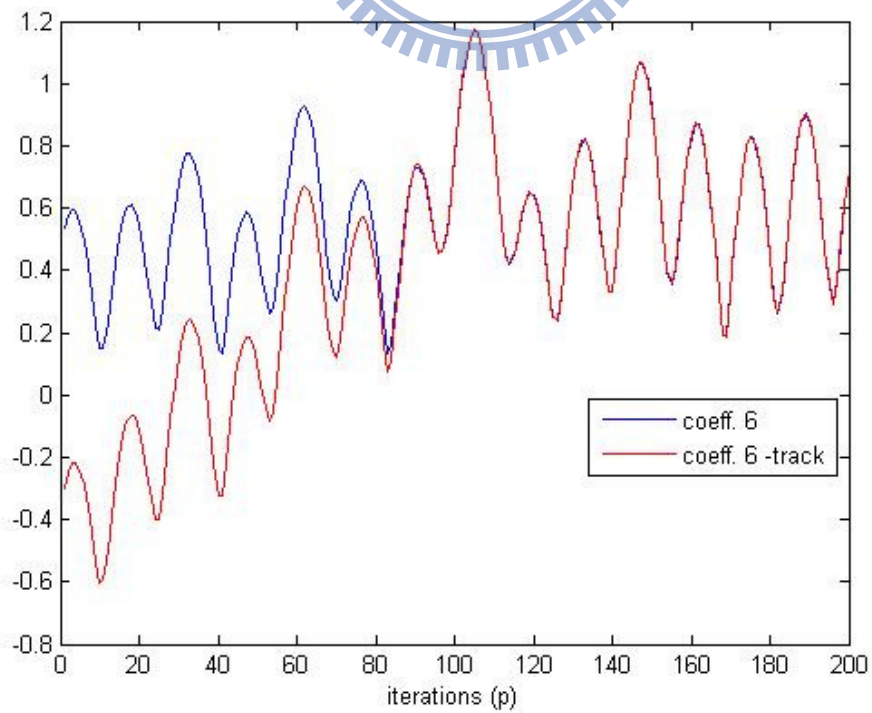


Figure 5.15 (f) CE-BEM 6th-coefficient tracking

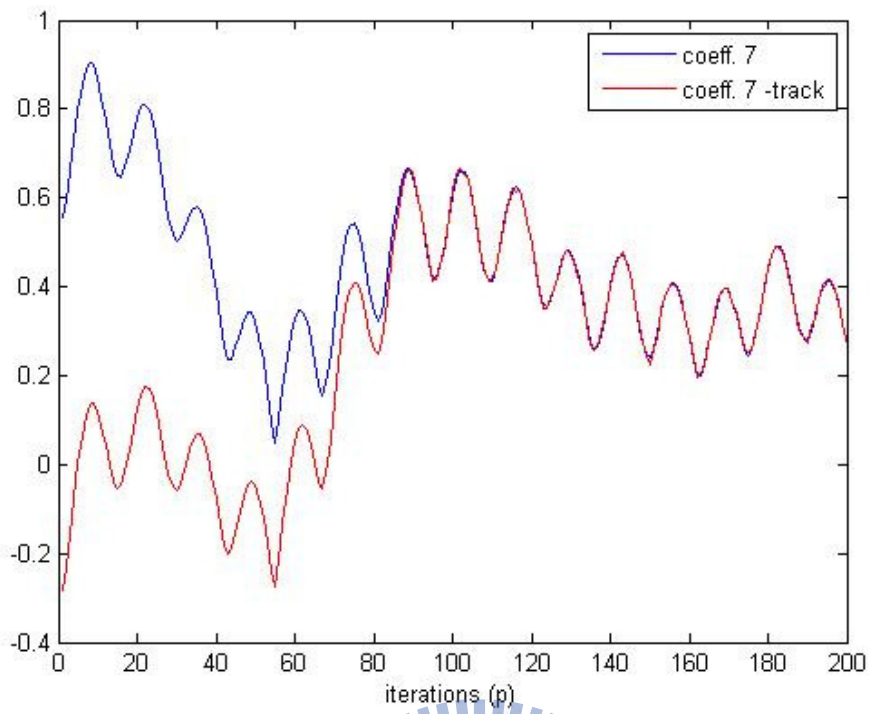


Figure 5.15 (g) CE-BEM 7th-coefficient tracking

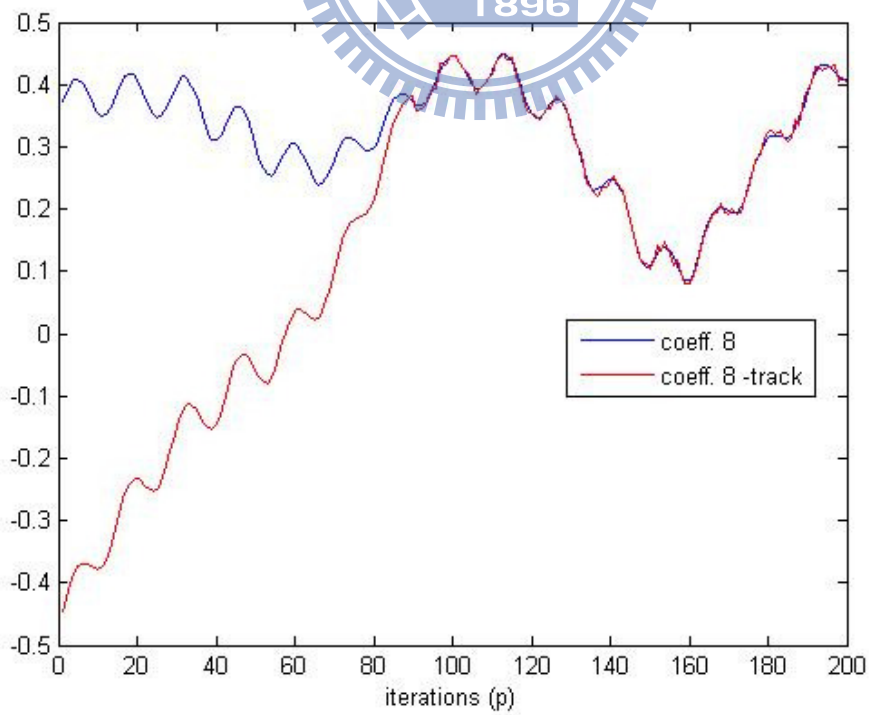


Figure 5.15 (h) CE-BEM 8th-coefficient tracking

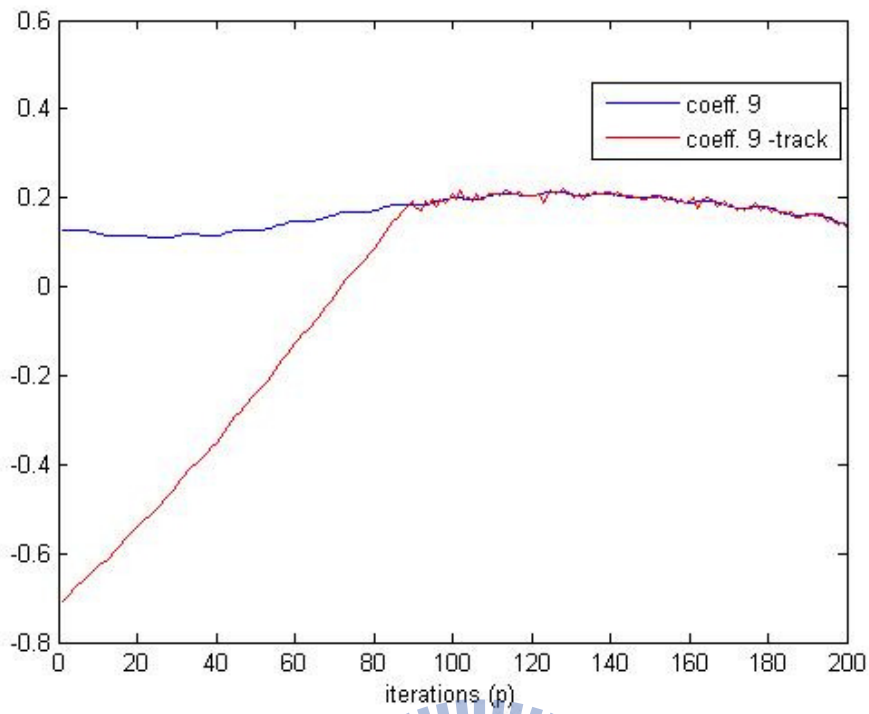


Figure 5.15 (i) CE-BEM 9th-coefficient tracking

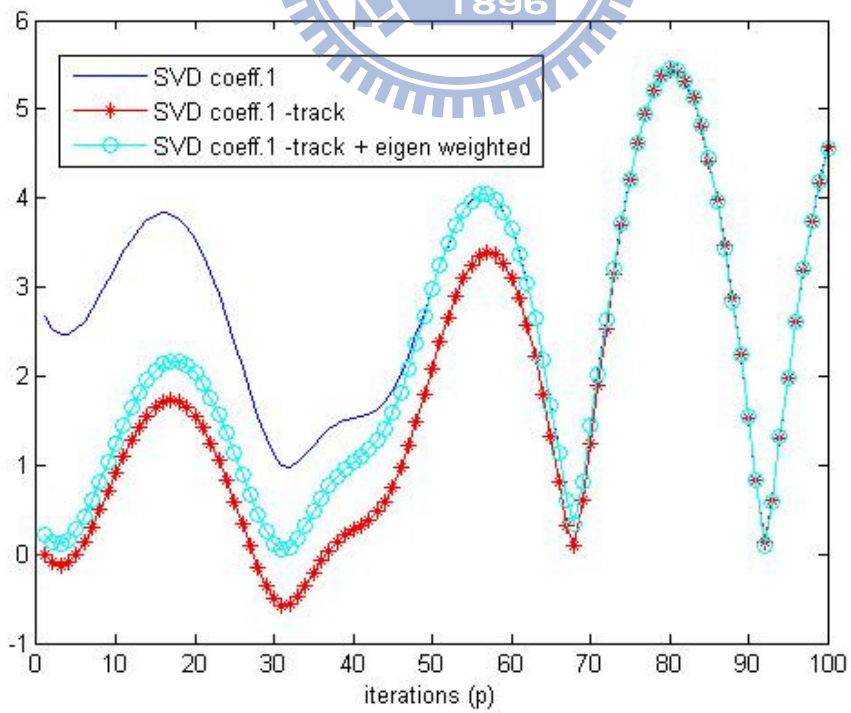


Figure 5.16(a) SVD-BEM 1st-coefficient tracking

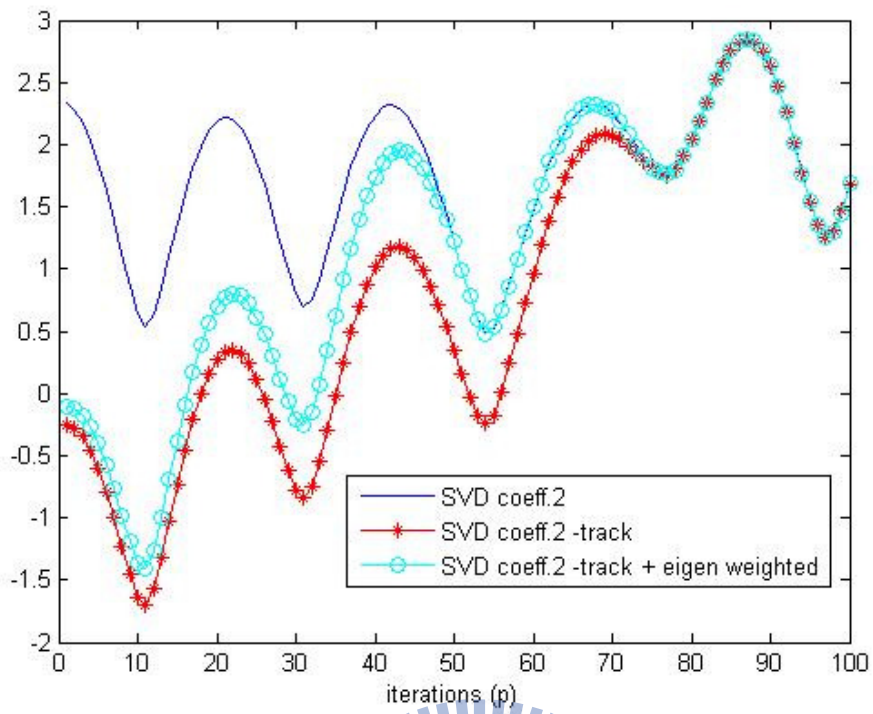


Figure 5.16(b) SVD-BEM 2nd-coefficient tracking

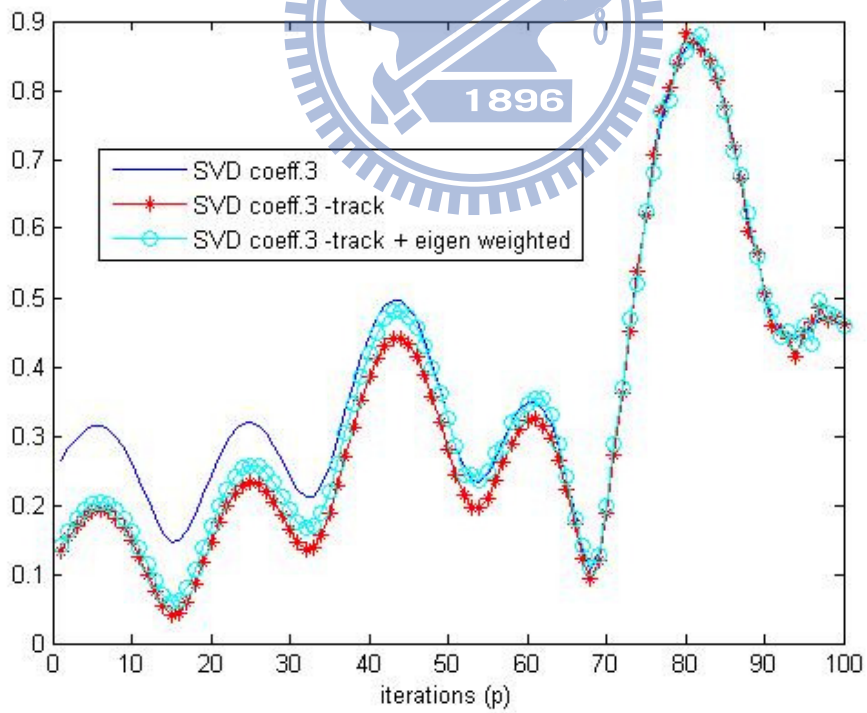


Figure 5.16(c) SVD-BEM 3rd-coefficient tracking

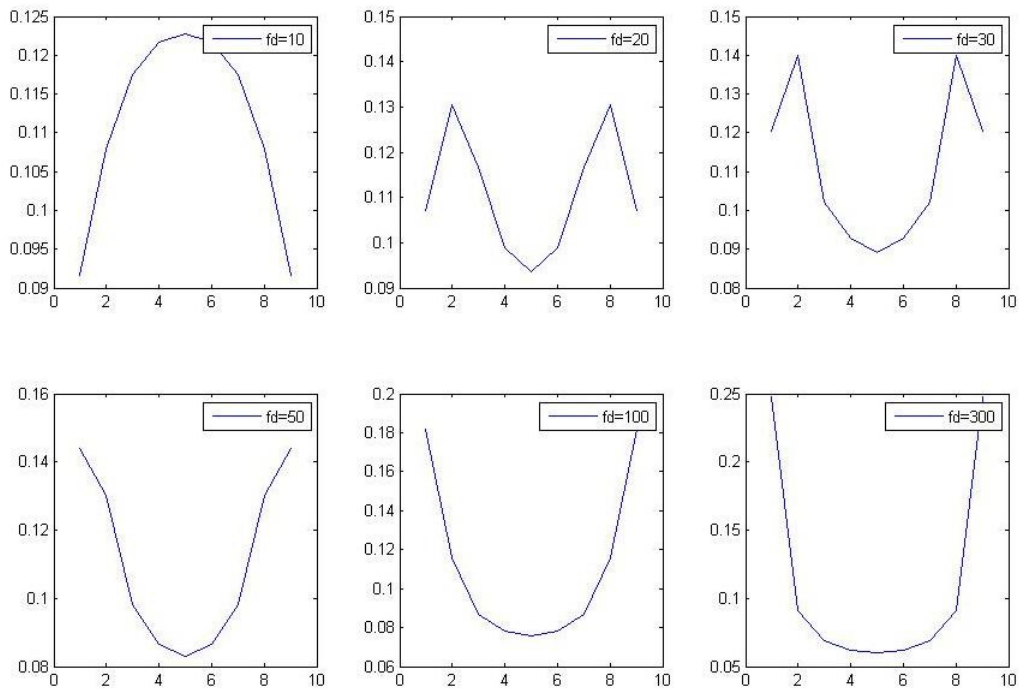


Figure 5.17 The weights of each basis in CE-BEM. ($B=9$)

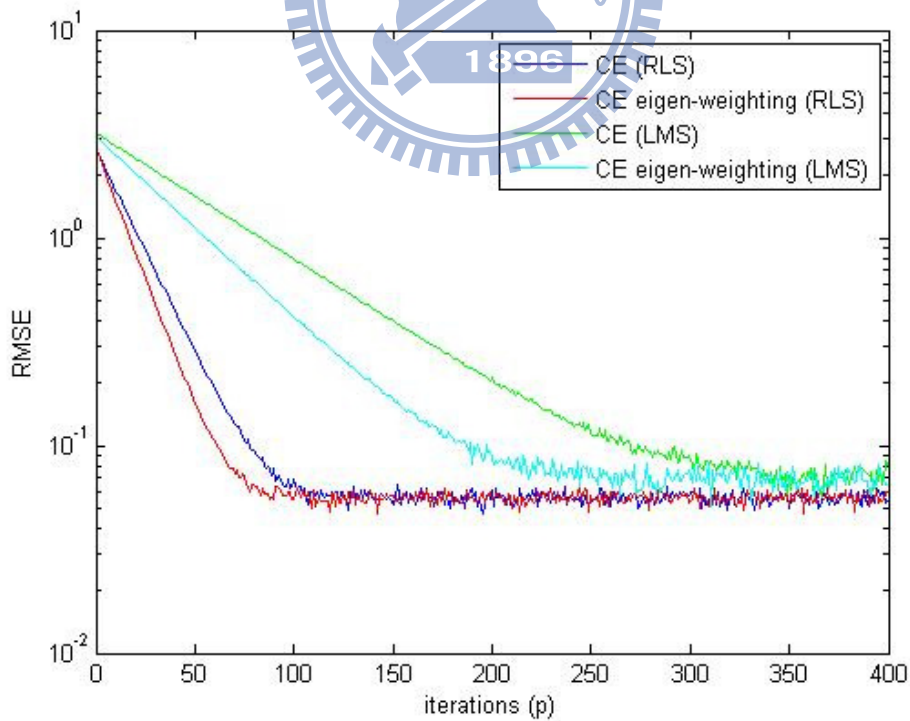


Figure 5.18(a) Learning curve of CE-BEM coefficients tracking

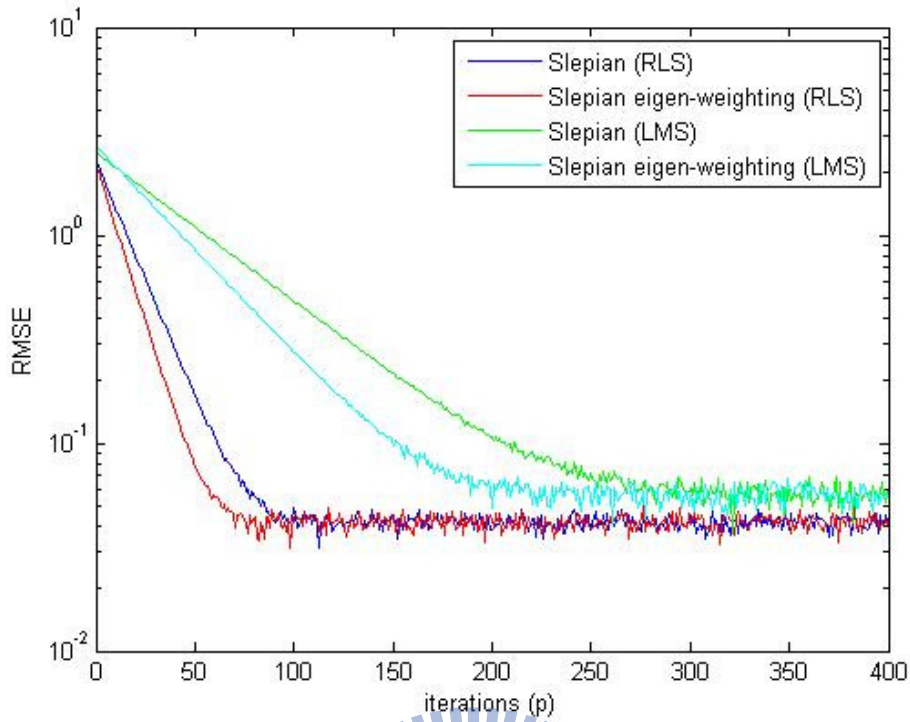


Figure 5.18(b) Learning curve of Slepian-BEM coefficients tracking

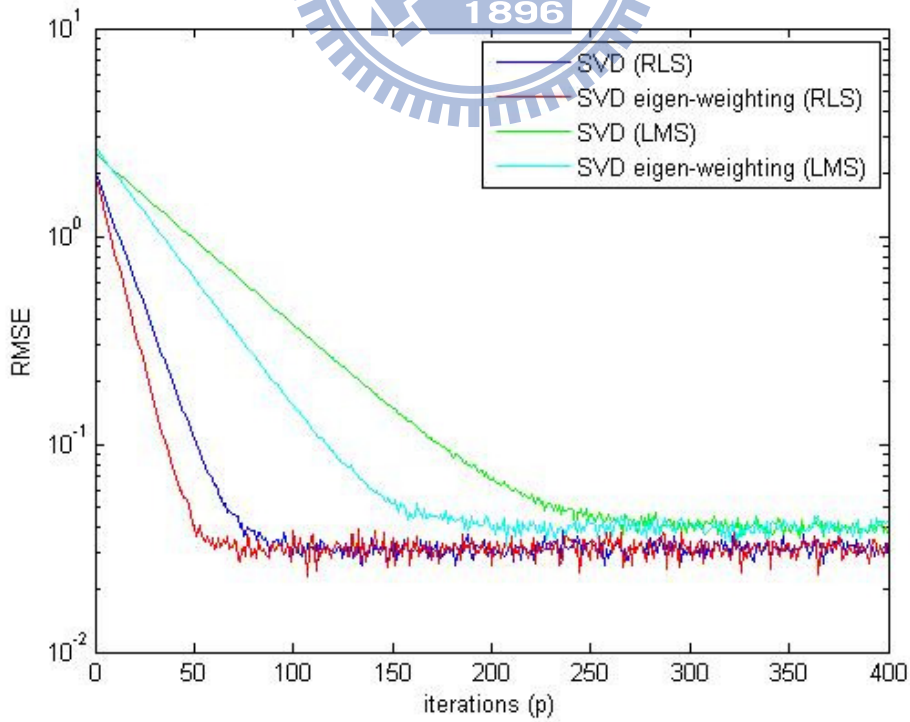


Figure 5.18(c) Learning curve of SVD-BEM coefficients tracking

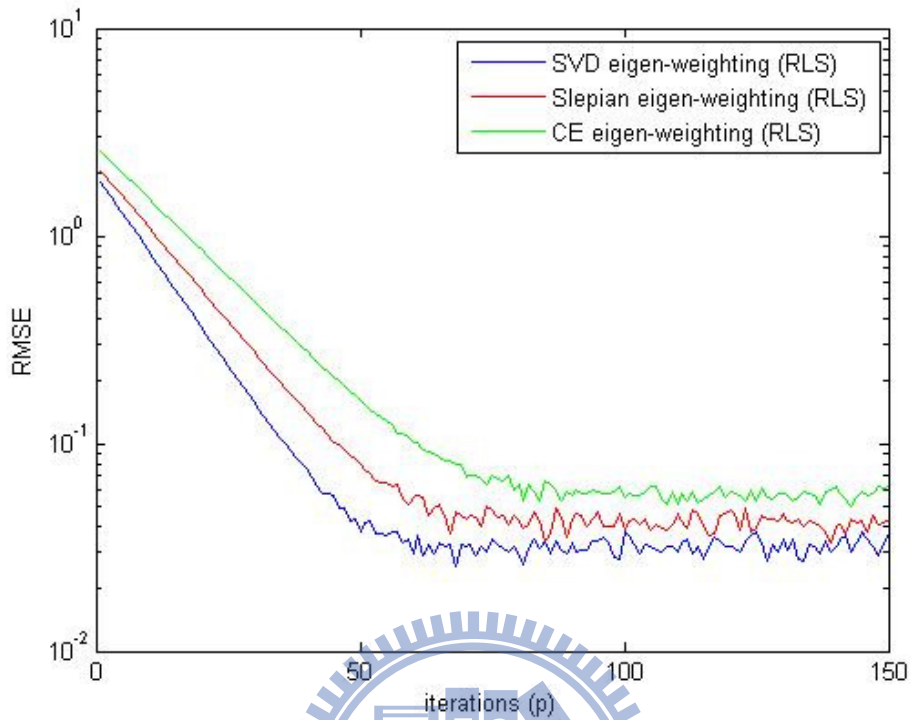


Figure 5.18(d) Comparison of three BEMs with eigen weighting

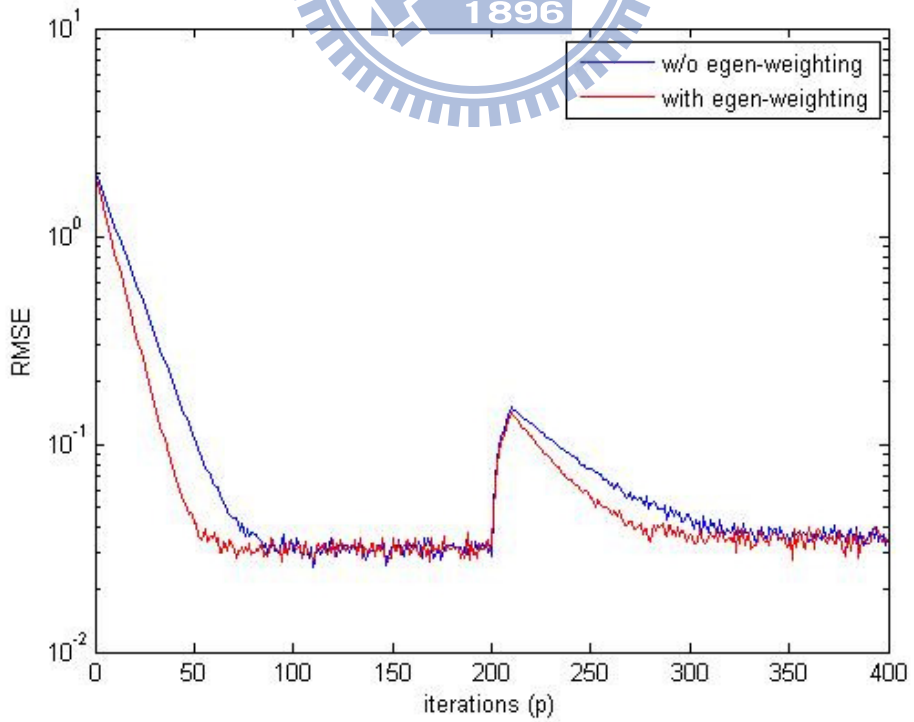


Figure 5.19(a) SVD-BEM coefficients tracking in f_d changes with new bases

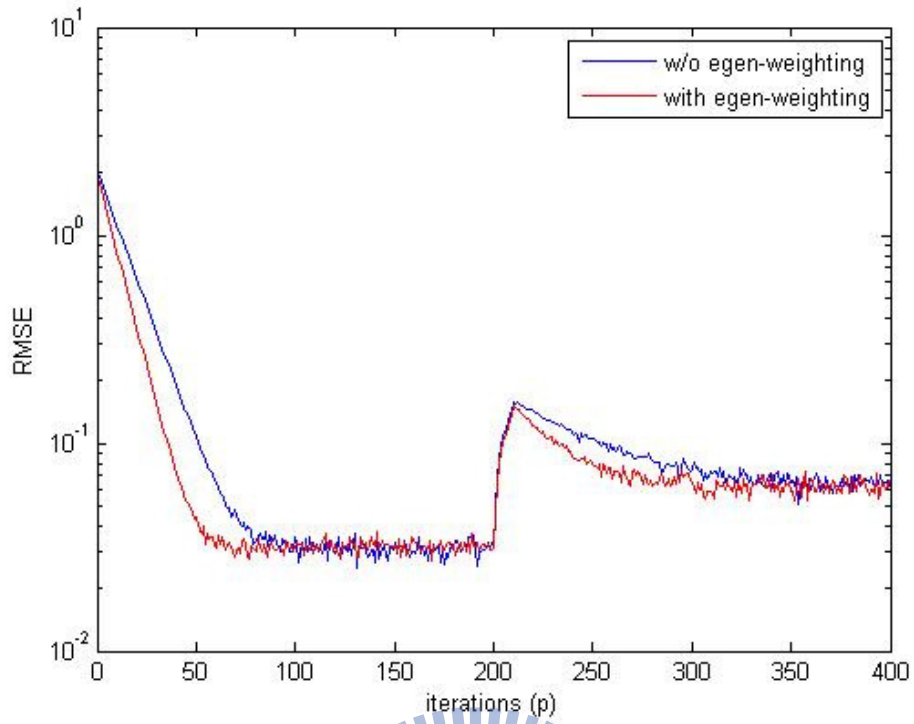


Figure 5.19(b) SVD-BEM coefficients tracking in f_d changes without new bases



5.7 BEM basis tracking

We have discussed the two basis tracking methods in unfixed Doppler frequency environment in Section 4.2.1 and 4.2.2.

Figure 5.20 illustrates the practical 1st-eigenvalue-to- f_d curve marked as (*) and three asymptotic line (linear, quadratic and exponential fitting) in SNR=40 dB and $T_s=0.001$. And we can realize that the mean square error of estimated and real principle eigenvalue in different fitting schemes.

Figure 5.21 and 5.22 illustrate the examples of two kind of basis tracking discussed in Section 4.2.1 and 4.2.2 respectively, which both have the ability of tracking the new basis (when f_d changes). And the comparison of these two methods under the channel MSE criterion is shown in figure 5.23.

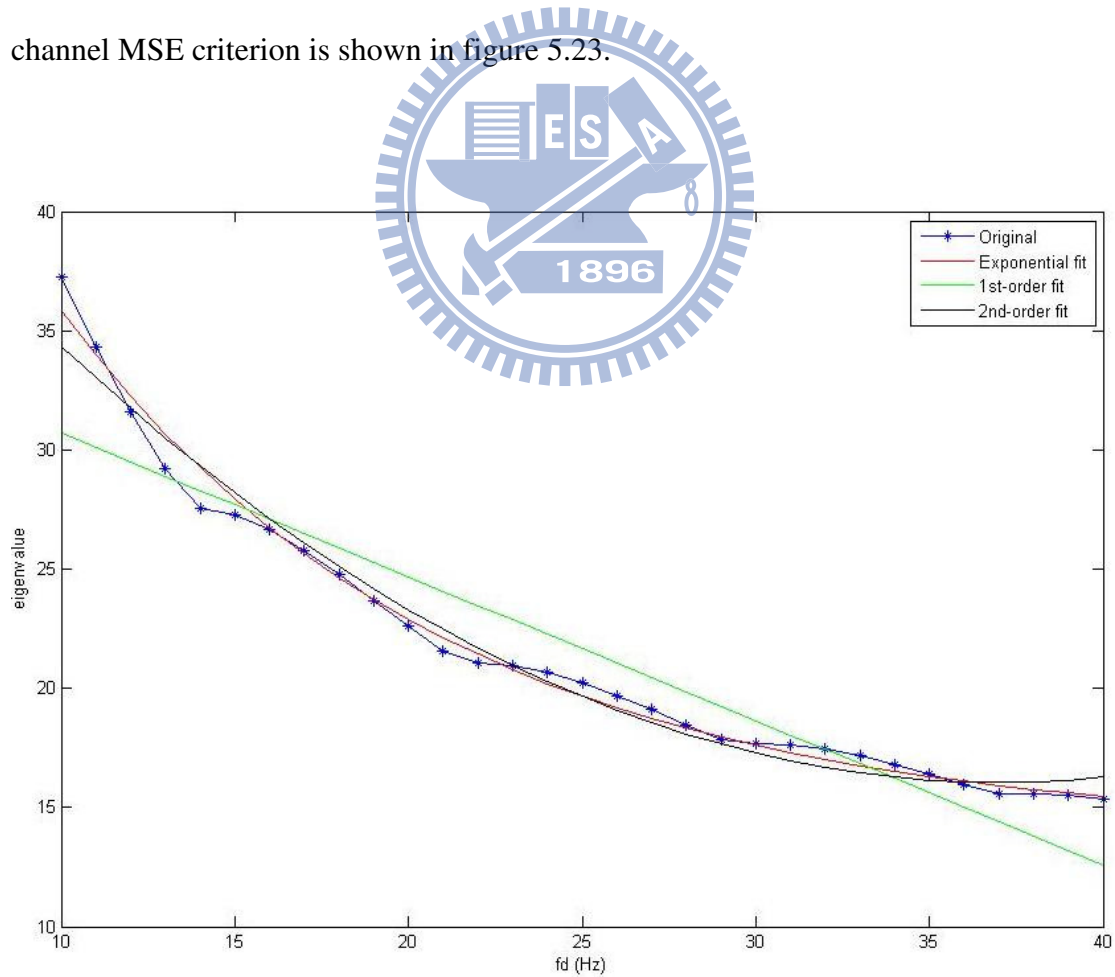


Figure 5.20 Three fitting methods for 1st-eigenvalue variation in f_d changes

Table 5.2 Three fitting methods for principle eigenvalues variation

	Linear	Quadratic	Exponential
1 st -eigenvalue MSE	3.968	0.758	0.334
2 nd -eigenvalue MSE	1.269	0.530	0.532

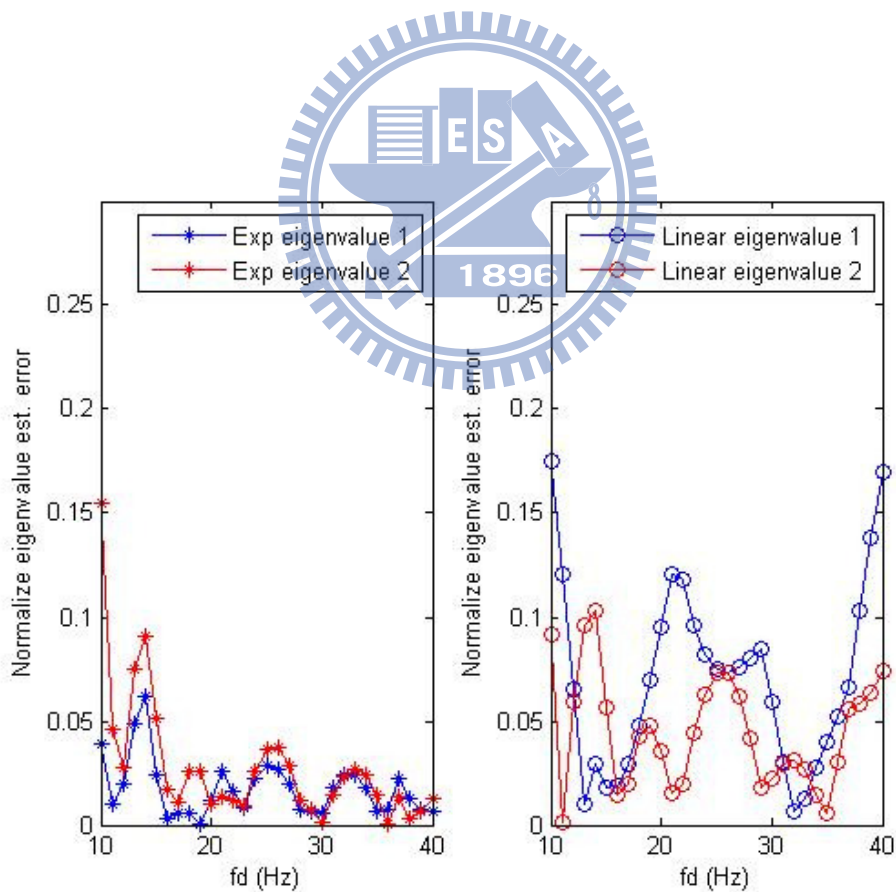


Figure 5.21 Eigenvalue estimated error between Exponential and Linear methods.

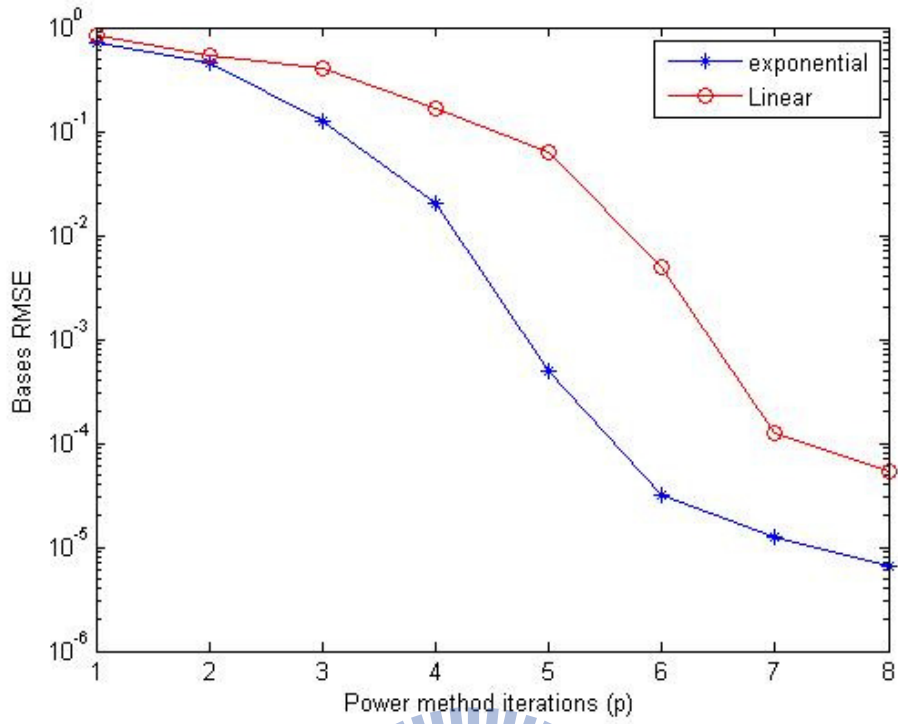


Figure 5.22 Bases estimated RMSE Under different Power method iteration times

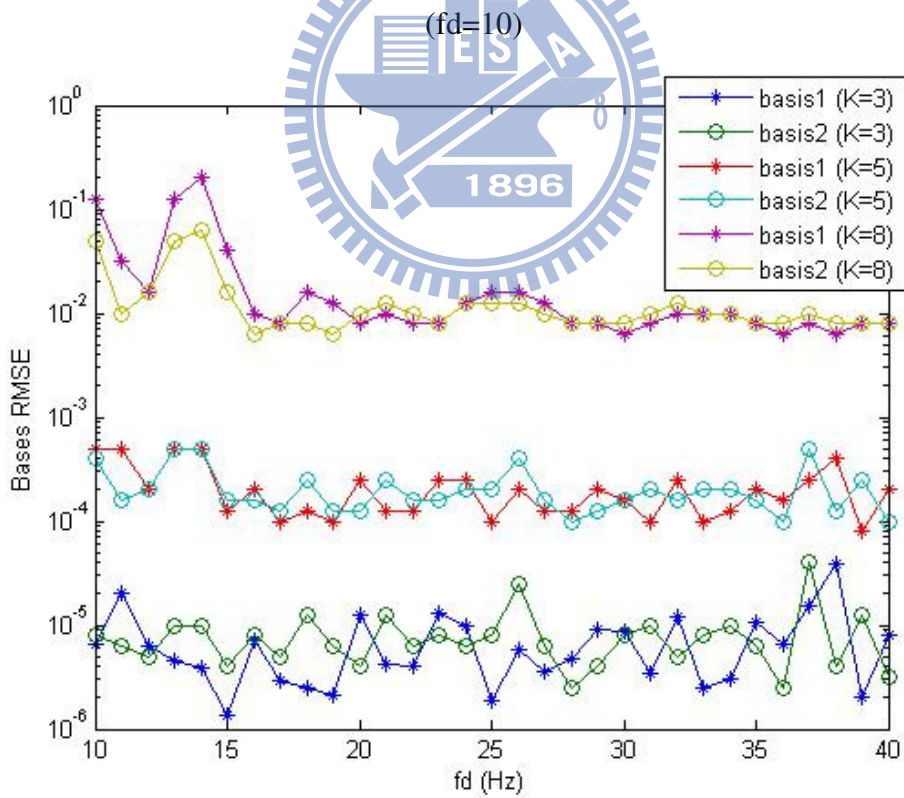


Figure 5.23 Bases estimated RMSE by way 3

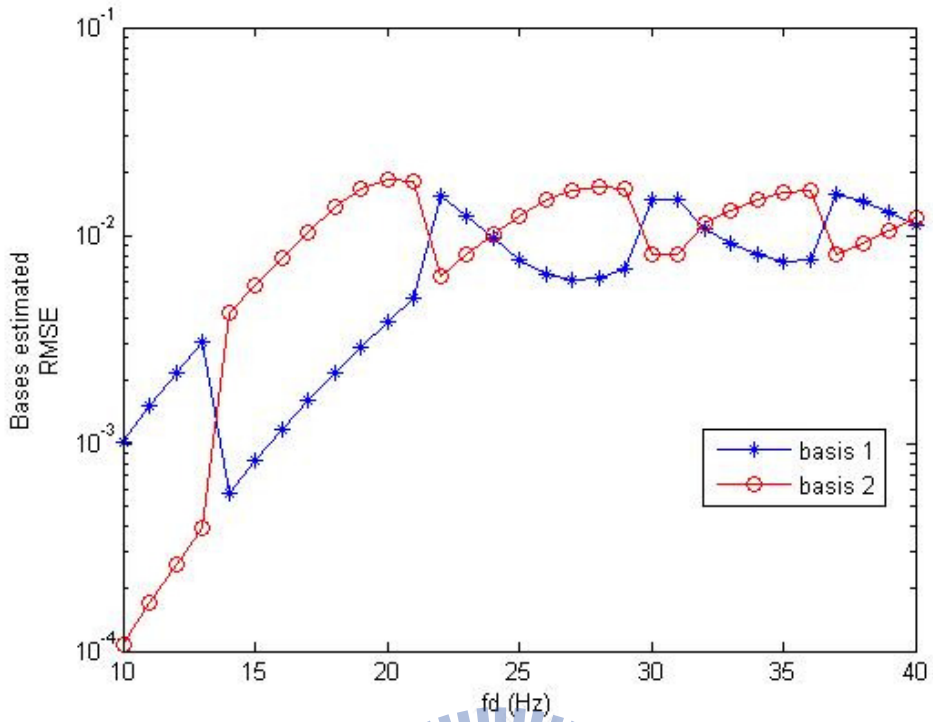


Figure 5.24 Bases estimated RMSE by way 4

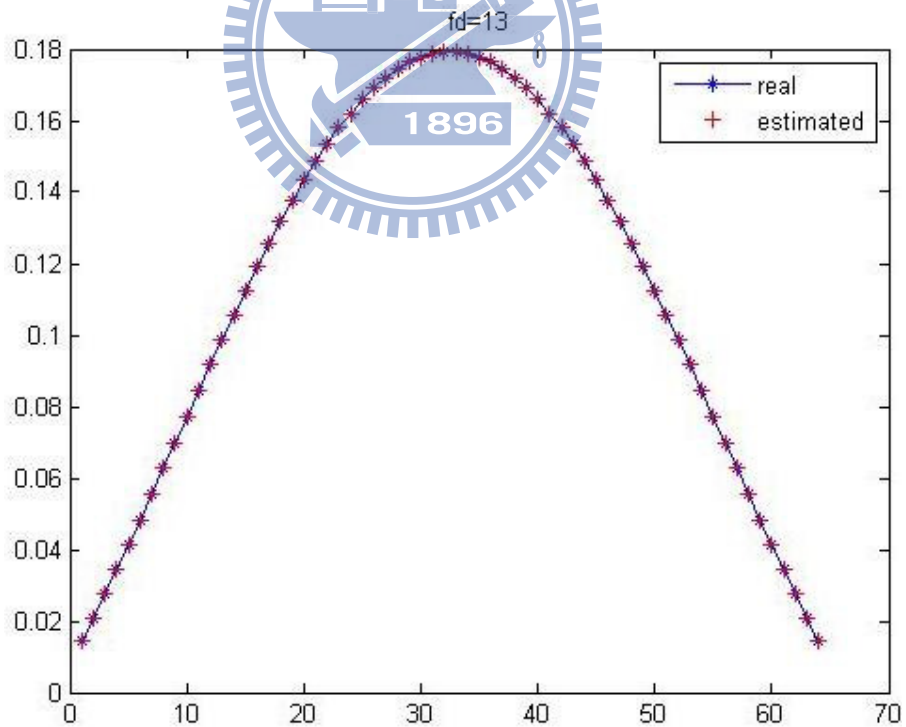


Figure 5.25 Example of basis estimation by the power method. (K=6

$$\lambda_{1st} = 29.2 \quad f_d = 13)$$

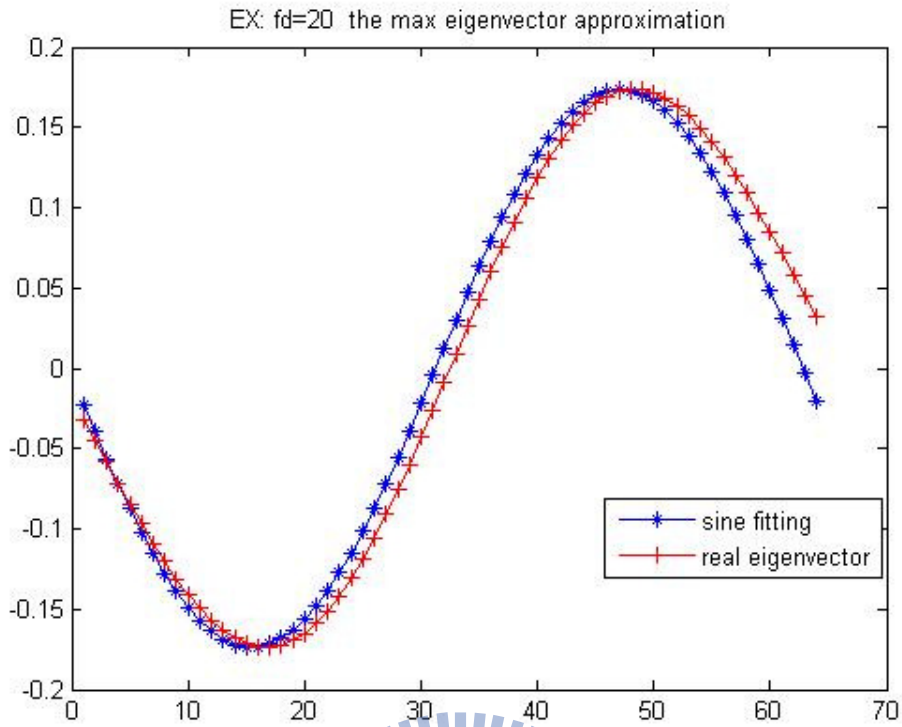


Figure 5.26 Example of basis estimation by directly eigenvector fitting. ($f_d=20$)

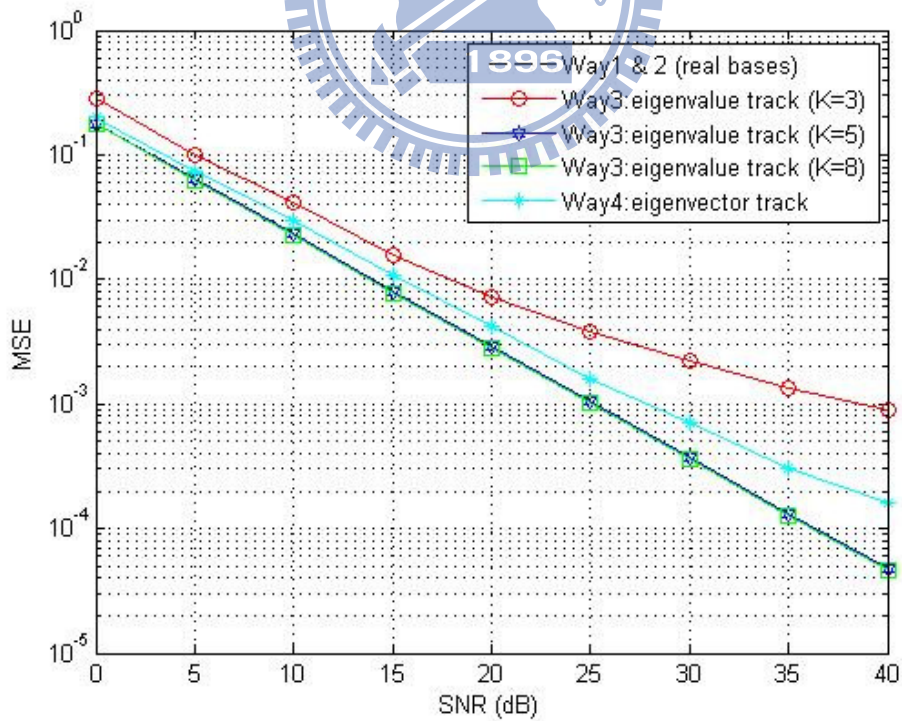


Figure 5.27 Comparison of principle eigenvalues and eigenvectors tracking

Chapter 6

Conclusions

In this thesis, we employ the basis expansion model to deal with the time varying channel estimation in OFDM system.

For the sake of lower data error rate at receiver, we have to estimate the wireless channel before detection. In Chapter 2, we introduce the OFDM structure and the practical channel model, and take CFO, PHN and Doppler frequency into account.

In Chapter 3, we compared several BEM schemes, and propose a post Wiener filtering scheme to achieve better MSE under the Jake's model environment. Besides, we also improve the CE-BEM with changing the sampling manner in Section 3.2 and resist the disturbance of CFO and PHN in Section 3.6.

For the purpose to reduce complexity, we updated the BEM coefficients and considered the importance of each basis. We derive the theoretical MSE and obtain the optimum time-invariant stepsizes for each BEM coefficients. Moreover, we approximated the bases curves with very few parameters, which could reduce the complexity effectively. The computer simulations such as theoretical analysis validation, Un-weighting, and weighted adaptive algorithm for BEM coefficients tracking are shown in Chapter 5, which could justify our analysis and show the

improved performance such as the proposed eigen-weighting scheme can accelerate convergence rate, the Wiener filter can enhance the channel estimation accuracy, the bases tracking can save the complexity for getting the new bases. These proposed models demonstrate a significantly better performance than the conventional methods when they are applied in OFDM system.



Bibliography

- [1] Y. Liang and V. V. Veeravalli, “Capacity of noncoherent time-selective Rayleigh fading channels,” *IEEE Trans. on Information Theory*, vol. 50, pp. 3095–3110, Dec. 2004.
- [2] X. Ma, G. B. Giannakis, and S. Ohno, “Optimal training for block transmissions over doubly-selective wireless fading channels,” *IEEE Trans. on Signal Processing*, vol. 51, pp. 1351–1366, May 2003.
- [3] A. Demir, A. Mehrotra, and J. Roychowdhury, “Phase noise in oscillators: A unifying theory and numerical methods for characterization,” *IEEE Trans. Circuits Syst. I*, vol. 47, pp. 655–674, May 2000.
- [4] G. B. Giannakis and C. Tepedelenlioglu, “Basis Expansion Models and Diversity Techniques for Blind Identification and Equalization of Time-Varying Channels,” *Proc. IEEE*, vol. 86, pp. 1969–1986, Oct. 1998.
- [5] P. H. Moose, “A technique for orthogonal frequency division multiplexing frequency offset correction,” *IEEE Trans. Commun.*, vol. 42, pp. 2908–2914, Oct. 1994.
- [6] T. Schmidl and D. Cox, “Robust frequency and timing synchronization for OFDM,” *IEEE Trans. Commun.*, vol. 45, Dec. 1997.
- [7] L. Piazzo, P. Mandarini, “Analysis of Phase Noise Effects in OFDM Modems,” *IEEE Trans. Communications*, vol. 50, no. 10, pp. 1696–1705, Oct. 2002.
- [8] H. Liu, and G. B. Giannakis, “Deterministic Approaches for Blind Equalization

of Time-Varying Channels with Antenna Arrays,” *IEEE Trans. Signal Processing*, vol. 46, pp. 3003-3013, Nov. 1998.

[9] G. Leus and M. Moonen, “Deterministic subspace based blind channel estimation for doubly-selective channels,” *Proc. IEEE Workshop Signal Process. Adv. Wireless Commun.*, pp. 210-214, Jun.. 2003

[10] S. Haykin, *Communication systems*. 4th ed., New York: Wiley, 2001

[11] P. Schniter, “Low-complexity equalization of OFDM in doubly-selective channels,” *IEEE Trans. Signal Process.*, vol. 52, no. 4, pp. 1002-1011, Apr. 2004.

[12] R. H. Clark, “A statistical theory of mobile radio reception,” *Bell Labs Syst. Tech. J.*, vol. 47, pp. 957-1000, Jul.–Aug. 1968.

[13] W. C. Jake, *Microwave Mobile Communications*, New York, Wiley, 1974

[14] A.H. Sayed, *Fundamentals of Adaptive Filtering*. New York, NJ: Wiley, 2003.

[15] R. C. Cannizzaro, P. Banelli, and G. Leus, “Adaptive channel estimation for OFDM systems with Doppler spread,” *Proc. IEEE Workshop on Signal Processing Advances in Wireless Communications*, 2006.

[16] H. Kim and JK Tugnait, “Recursive least-squares decision-directed tracking of doubly-selective channels using exponential basis models,” *ICASSP 2009. IEEE International Conference*, pp. 2689-2692, Apr. 2009.

[17] X. Zhao, J. Kivinen, P. Vainikainen, and K. Skog, “Characterization of Doppler spectra for mobile communications at 5.3 GHz,” *IEEE Transactions on Vehicular Technology*, vol. 52, no. 1, pp. 14–23, Jan. 2003.

[18] J. J. van de Beek, O. Edfors, M. Sandell, S. K. Wilson, and P. O. Brjesson, “On channel estimation in OFDM systems,” *Proc. IEEE Vehicular Technology Conf. Chicago, IL*, vol. 2, pp. 815-819, Jul. 1995.

[19] O. Edfors, M. Sandell, J.-J. van de Beek, S. K. Wilson, and P. O. Brjesson, “OFDM channel estimation by singular value decomposition,” *IEEE Trans. Commun.*, vol. 46, no. 7, pp. 931–939, Jul. 1998.

- [20] S. Coleri, M. Ergen, A. Puri, and A. Bahai, "Channel estimation techniques based on pilot arrangement in OFDM systems," *IEEE Trans. Broadcast.*, vol. 48, no. 3, pp. 223-229, Sept. 2002.
- [21] A. R. S. Bahai and B. R. Saltzberg, *Multi-Carrier Digital Communications: Theory and Applications of OFDM*: Kluwer Academic/Plenum, 1999.
- [22] D. Slepian, "Prolate spheroidal wave functions, Fourier analysis, and uncertainty - V: The discrete case", *Bell Syst. Technical Journal*, vol.57, no. 5, pp. 1371-1430, May-Jun. 1978.
- [23] T. Zemen, and C. F. Mecklenbräuer, "Time-variant channel estimation using discrete prolate spheroidal sequences", *IEEE Trans. Signal Process.*, vol. 53, no. 9, pp. 3597-3607, Sep. 2005.
- [24] O. Lugo, A.G. Parra-Michel, R. McLernon, D.C. Kontorovitch, V.Y., "Enhancing the performance of the CR blind channel estimation algorithm using the Karhunen-Loeve Expansion", *Acoustics, Speech, and Signal Processing, 2002. Proceedings. (ICASSP '02). IEEE International Conference*, Vol.3, no. 3, pp.2653-2656, May 2002.
- [25] I. Barhumi, G. Leus, and M. Moonen, "Time-domain and frequency-domain per-tone equalization for OFDM in doubly-selective channels," *Signal Process.*, vol.84, no.11, pp.2055–2066, Nov. 2004.
- [26] G.H. Golub and C.F. Van Loan, *Matrix Computations*. John Hopkins Press, 1996
- [27] H. Schmidt, V. Kuhn, K.D. Kammeyer, R. Rueckriem and S. Fechtel, "Channel tracking in wireless OFDM systems," *SCI*, 22-25 Jul. 2001.
- [28] S. Coleri, M. Ergen, A. Puri, A. Bahai, "A study of channel estimation in OFDM systems," *IEEE Vehicular Technology Conf.*, Vancouver, Canada, pp. 894-898, Sep. 2002.
- [29] T. Pollet, M. Van Bladel, and M. Moeneclaey, "BER sensitivity of OFDM systems to carrier frequency offset and Weiner phase noise," *IEEE Trans. Commun.*, pt. 1, vol. 43, pp. 191-193, Feb.–Apr. 1995

[30] J. van de Beek, M. Sandell, and P. Börjesson, "ML estimation of time and frequency offset in OFDM systems," *IEEE Trans. Signal Processing*, vol. 45, pp. 1800–1805, Jul. 1997.

[31] S. Ohno "Maximum likelihood inter-carrier interference suppression for wireless OFDM with null subcarriers," *Int.Conf. Acoust., Speech, Signal Process. (ICASSP)*, vol. 3, p. 849. Mar. 2005,

[32] G.B. Giannakis and C. Tepedelenlioglu, "Basis expansion models and diversity techniques for blind equation of time-varying channels," *Proc. IEEE*, vol. 86, pp. 1969-1986. Oct. 1998,

[33] D. K. Borah and B. D. Hart, "Frequency-selective fading channel estimation with a polynomial time-varying channel model," *IEEE Trans. Commun.*, vol. 47, no. 6, pp. 862-873, Jun. 1999.

[34] S. He and J.K. Tugnait, "Doubly-selective channel estimation using exponential basis models and subblock tracking," *IEEE GLOBECOM-07, Washington, DC*, Nov. 2007.

[35] M. K. Tsatsanis and G. B. Giannakis, "Modeling and equalization of rapidly fading channels," *Int. J. Adapt. Control Signal Process.*, vol. 10, pp. 159–176, Mar. 1996.

[36] M. Visintin, "Karhunen-Loeve expansion of a fast Rayleigh fading process," *IEEE Electron. Lett.*, vol. 32, no. 8, pp. 1712–1713, Aug.1996.

[37] S. Haykin, *Adaptive Filter Theory*. Englewood Cliffs, NJ: Prentice-Hall, 1996.

[38] K. D. Teo and S. Ohno, "Optimal MMSE finite parameter model for doubly-selective channels," *Proc. IEEE Global Telecommun. Conf. (GLOBECOM)*, pp. 3503–3507, 2005.

[39] H. A. Cirpan and M. K. Tsatsanis, "Maximum likelihood blind channel estimation in the presence of Doppler shifts," *IEEE Trans. Signal Process.*, vol. 47, no. 6, pp. 1559–1569, Jun. 1999.

- [40] M. Guillaud and D. T. M. Slock, "Channel modeling and associated inter-carrier interference equalization for OFDM systems with high Doppler spread," *Int. Conf. Acoust., Speech, Signal Process. (ICASSP)*, vol. IV, pp. 237–240, Apr. 2003.
- [41] G. Leus and M. Moonen, "Deterministic subspace based blind channel estimation for doubly-selective channels," *Proc. IEEE Signal Process. Workshop Signal Process. Adv. Wireless Commun. (SPAWC)*, pp. 210–214, Jun. 2003.
- [42] A. P. Kannu and P. Schniter, "MSE-optimal training for linear timevarying channels," *Proc. IEEE Int. Conf. Acoust., Speech, Signal Process. (ICASSP)*, pp. iii/789–iii/792, Mar. 2005.
- [43] G. L. Stüber, "Broadband MIMO-OFDM Wireless Communications," *Proc. IEEE*, vol. 92, no. 2, pp. 271-294, Feb. 2004.
- [44] S. H. Han and J. H. Lee, "An Overview of Peak-to-Average Power Ratio Reduction Techniques for Multicarrier Transmission," *IEEE Wireless Commun.*, vol. 12, no. 2, pp. 56–65, April 2005.
- [45] T. M. Schmidl and D. C. Cox, "Robust frequency and timing synchronization for OFDM," *IEEE Trans. Commun.*, vol. 45, pp. 1613-1621, Dec. 1997.
- [46] T. Michel and G. Wunder, "Optimal and low complexity suboptimal transmission schemes for MIMO-OFDM broadcast channels," *Proc. IEEE Int. Conf. on Communications (ICC)*, May 2005.
- [47] S. Olmos, L. Sörnmo, and P. Laguna, "Block adaptive filters with deterministic reference inputs for event-related signals: BLMS and BRLS," *IEEE Transactions on Signal Processing*, vol. 50, no. 5, pp. 1102–1112, May 2002.
- [48] S. Makino, Y. Kaneda, N. Koizumi, "Exponentially weighted step-size NLMS adaptive filter based on the statistics of a room impulse response," *IEEE Trans. Speech Audio Process.* vol. 1, no.1, pp. 101-108, Jan. 1993.
- [49] T. Rappaport, *Wireless Communications - Principles & Practice*. Upper Saddle River (NJ), USA: Prentice Hall, 1996.
- [50] O. Rousseaux, G. Leus, P. Stoica, and M. Moonen, "Generalized training based

channel identification,” *Proc. IEEE Global Conf. Communications (GLOBECOM)*, San Francisco, CA, pp. 2432–2436, Dec. 2003

[51] O. Rousseaux, G. Leus, P. Stoica, and M. Moonen, “Gaussian maximum likelihood channel estimation with short training sequences,” *IEEE Trans. Wireless Commun.*, vol. 4, no. 6, pp. 2945–2955, Nov. 2005.

[52] A. Sampath and J. M. Holtzman, “Estimation of maximum Doppler frequency for handoff decisions,” *Proc. IEEE Vehicular Technology Conf.*, pp. 859–862, 1993,.

[53] Bamler, R., “Doppler frequency estimation and the Cramer-Rao bound,” *IEEE. Trans. on Geoscience and Remote Sensing*, Vol. 29, No. 3, May 1991.

